c.1

AN IMPROVED UPPER LIMIT FOR MUONIUM CONVERSION TO ANTIMUONIUM

by

GLEN MURRAY MARSHALL
B.Sc., McGill University, 1974
M.Sc., University of British Columbia, 1977

A THESIS SUBMITTED IN PARTIAL FULFILLMENT OF
THE REQUIREMENTS FOR THE DEGREE OF
DOCTOR OF PHILOSOPHY

in

THE FACULTY OF GRADUATE STUDIES
(Physics)

We accept this thesis as conforming
to the required standard

THE UNIVERSITY OF BRITISH COLUMBIA
February, 1981

In presenting this thesis in partial fulfilment of the requirements for an advanced degree at the University of British Columbia, I agree that the Library shall make it freely available for reference and study. I further agree that permission for extensive copying of this thesis for scholarly purposes may be granted by the head of my department or by his or her representatives. It is understood that copying or publication of this thesis for financial gain shall not be allowed without my written permission.

Department of Physics

The University of British Columbia
2075 Wesbrook Place
Vancouver, Canada
V6T 1W5

Date 10 March 1981

ABSTRACT

An experiment resulting in the reduction of the upper limit for muonium (μ^+e^-) conversion to antimuonium (μ^-e^+) is described. The limit obtained for the effective four fermion coupling constant is $G < 42G_F$ (95% confidence level). The muon in a system initially formed as muonium and evolving under the most favorable conditions will thus be identifiable as a negative particle in less than 4% of the observed decays. The results improve by over one order of magnitude the best previous limit obtained from a search for $e^-e^- \rightarrow \mu^-\mu^-$ interactions. Neither process is expected to exist if an additive conservation law is obeyed by muon number.

The present status of the theory of electroweak interactions, as it pertains to muonium conversion, is reviewed. It is shown that muon number nonconservation can be accommodated in a variety of ways, some of which might allow a value for G of $0.1G_F$. The steps that were taken to make the present experiment as sensitive as possible are detailed. The major improvement over previous conversion experiments is the use of fine silica powder in carefully arranged layers to allow muonium to exist for a large fraction of its lifetime in vacuum, where conversion is not highly suppressed. Another important facet of the technique, which is described in detail, is the use of an intense beam of surface muons with a stopping density previously unattainable. A chapter on the analysis of the data contains a quantitative discussion of the processes which must occur for

conversion to be detected. The numbers derived there are essential to the establishment of a realistic limit on the coupling of muonium to antimuonium.

TABLE OF CONTENTS

LIST OF FIGURES

LIST OF TABLES

ACKNOWLEDGMENT

It is a pleasure to express my gratitude to the many people whose encouragement and assistance were essential to the research described herein. My thesis supervisor, Dr. John B. Warren, did not tire of reassuring me of the worth of the experiment; he is also responsible for the conception of using fine powder targets for producing muonium in vacuum. Dr. Jess H. Brewer has been a patient and excellent source of advice, ideas, and experimental expertise, particularly in the area of muon spin rotation. For the smoothe, orderly progress of the experiment I am especially indebted to Dr. Chris J. Oram, Mr. Robert F. Kiefl, and Mr. George S. Clark, without whose assistance it would not have been successfully completed. Dr. David M. Garner kindly supplied and supported several computer routines used in the analysis, and played a dynamic role in the original establishment of muonium in vacuum. The apparatus was constructed with the extremely capable technical assistance of Mr. Alan Morgan, Mr. Chris Stevens, and Mr. Brian Smith, who, along with the operators and staff of TRIUMF, deserve my sincere thanks.

I wish to acknowledge several persons not involved in the experiment for their friendship and support. Dr. Pamela A. Maher survived the ordeal of living with the odd hours of a TRIUMF graduate student most amiably and admirably. Mr. H. Dean Rolfson was the first to demonstrate to me the order and logic that is the magic of physics. My brother, Gregory, was also responsible for my earliest academic aspirations, while my

father, Gerald, provided the encouragement and opportunity to attain them. But the lessons that I value most are not those of physics, but of people, of right and wrong, and of the need to be in every sense an individual; for these and many other things I thank my mother, the late Grace Elizabeth Marshall, to whom this thesis is dedicated.

G.M.M.

1. INTRODUCTION

Physics in the twentieth century can be distinguished from the other sciences partly by its concern not only with interactions whose effects are evident in everyday life, namely those of electromagnetic and gravitational origin, but the so-called strong and weak phenomena as well. The latter play no established role in other natural or life sciences except possibly as tools which have been developed through an understanding of the physics. Consideration of the apparent classification of nature's processes into four divisions has been a common occupation of modern physicists, who would seek some reason or connection within what seems (or seemed, until recently) a rather arbitrary scheme. We are not satisfied to think of nature as arbitrary.

An advance toward the ideal of a unified approach to two or more of the fundamental processes was made possible by the development of gauge field theories. It now appears that there is an inherent connection between the weak and electromagnetic forces, to the extent that they are now considered separate manifestations of something known as the electroweak interaction. The analogy between the elementary particles which do not take part in the strong interaction, the leptons, with those physically elusive but widely accepted hadron constituents, the quarks, inspire the hope that the strong interaction can be solidly integrated with the electroweak by

further development of the gauge field approach.

Many, many problems have yet to be solved before it can be said that even the electroweak sector is understood. Progress is made partly by searching for processes allowed (but not necessarily demanded) by a unified theory. In many cases these processes are rare, and one measure of progress has been the ability of the experimenter to establish just how rare they must be[1], so that at least a few versions of the theory can be definitely overruled. One of the byproducts of this situation is the endless challenge it offers to the wiles of the experimenter.

The subject of this thesis is the improvement of the limit on muonium (μ^+e^-) conversion to antimuonium (μ^-e^+). The history of interest in this reaction predates the acceptance of gauge field theories because of an ambiguity in the form of muon number conservation. Recent evidence has done much to resolve the ambiguity, but it will be demonstrated in this thesis that the latitude of the theory still justifies the cost and effort of attempting to reduce the upper limit for conversion. The outstanding problem in a conversion experiment has been, for reasons which will be discussed, the difficulty in producing ample muonium in an environment conducive to conversion: the success of the present experiment is largely due to the discovery of a method by which this may be accomplished. Another important factor has been the development in the past five years, largely at TRIUMF, of muon beams with intensities

---

[1]The concept of "never" is rare in itself, since it is an impossible limit to attain experimentally.

and stopping densities which make a conversion search practicable. The other facets of the experiment might be described as conventional. Some suggestions will be made in the concluding chapter for improvements which may in future allow the limit on muonium conversion to be reduced still further.

1.1. Muon Number Conservation

The first suggestion that muonium might spontaneously convert to antimuonium was made by Pontecorvo (Pontecorvo, 1957), who considered the process as an analogue to the weak neutral kaon-antikaon mixing. There had previously been discussed (Konopinski and Mahmoud, 1953) the possibility of an additive law governing the conservation of a lepton number L, which in one form did not disallow muonium conversion (see Table 1.1.1). In another form, favored by the authors at that time,

Particle	e^-,ν_e	$e^+,\bar{\nu}_e$	μ^-,ν_μ	$\mu^+,\bar{\nu}_\mu$	others
L	+1	-1	+1	-1	0

Table 1.1.1. Original lepton number assignments, with the positive muon considered as an antiparticle. Reactions must conserve ΣL.

it did disallow conversion because the negative muon was considered as an antiparticle rather than a particle, and the lepton numbers for the muonic particles were of the opposite sign. Parenthetically it is interesting that this particular form is the only one, even today, within which the nomenclature of muonium and antimuonium makes sense. If the positive muon is an antiparticle, the μ^+e^- system should be known as antimuonium, contrary to popular usage. At any rate, almost concurrent with Pontecorvo's suggestion were the first (Nishijima, 1957; Schwinger, 1957) proposals that there might be a further quantum number, a muon number L_μ (see Table 1.1.2), that also must be conserved. If it were, processes such as

Particle	e^-,ν_e	$e^+,\bar{\nu}_e$	μ^-,ν_μ	$\mu^+,\bar{\nu}_\mu$	others
L_μ	0	0	+1	-1	0

Table 1.1.2. Muon number assignments. Reactions must conserve ΣL_μ (Nishijima, 1957; Schwinger, 1957)in an additive scheme, or $(-1)^{\Sigma L_\mu}$ in a multiplicative scheme (Feinberg and Weinberg, 1961a).

$\mu \rightarrow e\gamma$, $\mu \rightarrow eee$, and $\mu^-p \rightarrow e^-p$, which involve a muon converting to an electron without neutrino emission or absorption, would not take place; they had not been observed (and still haven't) in experiments sensitive to rates below those otherwise expected. Consistency of the muon number concept in this form also demanded the acceptance of a second type of neutrino, the muon neutrino, which is distinguishable

from its electron counterpart by its muon number.

Several years later another scheme was proposed (Feinberg and Weinberg, 1961a), based on ideas which will be elaborated upon in section 2.1.1, in which muon number was conserved not as the sum ΣL_μ but as the product $(-1)^{\Sigma L_\mu}$, along with the usual additive lepton conservation. Obviously any process conserving ΣL_μ, thus satisfying the additive scheme, would also satisfy the multiplicative scheme, but the converse is not true. The multiplicative scheme also demanded a distinguishable muon neutrino; its existence was proven in an experiment using neutrinos from pion decay (mostly produced in association with positive muons) interacting with neutrons. The absence of electron production signified the "muonness" of the neutrinos, and also supported some form of the muon conservation law.

No real resolution to the ambiguity in the form of muon conservation occurred for more than one and a half decades. Only recently have experimental data been obtained which tend to discount the multiplicative approach. A test must be made by searching for interactions for which ΣL_μ changes by at least two units between initial and final states, while satisfying other conservation laws for charge and lepton number. Candidates for the test are the reactions $\mu^+ \rightarrow e^+ \bar{\nu}_e \nu_\mu$, $e^- e^- \rightarrow \mu^- \mu^-$, and $\mu^+ e^- \rightarrow \mu^- e^+$. The first, a charged current interaction, has recently been searched for (Willis et al., 1980), and its nonobservation strongly favors the additive assignment. The latter two, both mediated by a neutral current interaction, have also been searched for (Barber et al.,1969; Amato et al., 1968, and this work) but the sensitivity is too low and the results are inconclusive for a determination of the

character of muon number conservation.

1.2. Incorporation of the Third Lepton Generation

Any modern discussion of lepton interactions must include some mention of the newest generation, the tau particle or tauon, and its neutrino (Perl et al., 1975). The same is true here, for its existence and decay modes must be accounted for by the conservation laws. All evidence is compatible with the sequential lepton model, in which each type of lepton-neutrino pair (electron, muon, tauon, and possibly heavier undiscovered generations) is associated with a distinct lepton number, as in Table 1.1.3 (see Perl, 1978, for a review). Note that this is

Particle	e^-,ν_e	$e^+,\bar{\nu}_e$	μ^-,ν_μ	$\mu^+,\bar{\nu}_\mu$	τ^-,ν_τ	$\tau^+,\bar{\nu}_\tau$	others
L_e	+1	-1	0	0	0	0	0
L_μ	0	0	+1	-1	0	0	0
L_τ	0	0	0	0	+1	-1	0

Table 1.2.1. Sequential lepton number assignments. Reactions must conserve ΣL_e, ΣL_μ, and ΣL_τ separately, in the additive scheme.

equivalent for muons and electrons to the numbers already

assigned, since in an additive scheme any linear combination of quantum numbers (such that the transformation matrix has nonzero determinant) will give equivalent selection rules ($L = L_e + L_\mu$); the multiplicative law needs only to be accompanied by the condition that $\Sigma(L_e + L_\mu)$ (i.e., particles minus antiparticles in the lepton sector) must be conserved, to obtain the previous selection rules. A reformulation of the multiplicative scheme to include the tauon might, in an ad hoc manner, without recourse to theoretical justifications, demand separate conservation of $\Sigma(L_e + L_\mu + L_\tau)$, $(-1)^{\Sigma L_\mu}$, and either $(-1)^{\Sigma L_\tau}$ or the more stringent ΣL . On the other hand, the multiplicative law is the result of an assumed invariance under permutation of primitive leptons (see section 2.1.1). Maintaining and extending that approach has led to a theory (Derman, 1978) which requires, given the nonexistence of $\mu \rightarrow e\gamma$, the conservation $\Sigma(L_e + L_\mu + L_\tau)$ and $(-1)^{\Sigma(L_\mu + L_\tau)}$ only; the decay $\tau \rightarrow e\gamma$ may take place, albeit at a reduced rate, well below present limits. Muonium may also convert to antimuonium.

A more detailed explanation of muon number and muonium conversion will be given in the second chapter, in which the aim is to convince the reader of a solid justification for an improvement of existing limits. The experiment performed at TRIUMF to achieve this goal will be described in the third chapter, with further reference to the experiments which have gone before. The analysis of the data, along with a quantitative description of the processes which must be understood for the reduction of the numbers obtained into the form of a limit for muonium conversion, comprise the fourth chapter. The fifth chapter contains the final result, and a

brief discussion of the influence of various experimental factors on the sensitivity achieved.

2. THEORY OF THE MUONIUM-ANTIMUONIUM INTERACTION

A partially successful theory of weak interactions was first developed by Fermi (Fermi, 1934) to describe the beta decay of nuclei. The proposed interaction was vector alone, allowing transitions between nuclear states of equal angular momentum. Shortly thereafter a more general interaction was proposed (Gamow and Teller, 1936) which was a linear combination of vector as well as scalar, pseudoscalar, axial vector, and tensor terms, and could couple nuclear states differing by one unit of angular momentum. Nuclear beta decay was studied from this foundation until the middle fifties, when the tacit assumption of parity conservation in the interaction was questioned and found to be incorrect (Wu et al., 1957). Further experiments were consistent with an interaction Hamiltonian with both vector and axial vector parts, which now forms the basis of the so-called vector minus axial vector (V-A) theory of weak interactions. This theory was still not perfect because of the unphysical high energy behavior; it is now generally regarded as a phenomenologically correct description of the low energy limit of a class of more widely applicable formulations, known generically as gauge theories. They describe the observed weak force in terms of massive exchange particles, the W and Z bosons. Before getting into more details of these latest approaches, however, it is useful to provide a framework for muonium-antimuonium conversion based on a simple V-A interaction

Hamiltonian.

2.1. The Theory Before 1967

The calculations in this section follow those described in an early paper on the subject (Feinberg and Weinberg, 1961b), when a muonium-antimuonium conversion experiment was less than a gleam in the experimenter's eye. That reference stressed the severe influence exerted by the atom's environment on any observable muonium conversion rate. Included here is some theoretical background which will prove useful in the analysis of the experiment performed at TRIUMF.

2.1.1. The Four Fermion Current-Current Interaction

Low energy weak interactions have been well described by an interaction Hamiltonian of the form

$$H_w(x) = 2^{-(1/2)}\, G_F\, J^{\lambda}(x) J^{\dagger}_{\lambda}(x) \ , \qquad 2.1.1.1$$

where summation over repeated Greek indices is assumed. $J^{\lambda}(x)$ is the weak four-current, a function of the spacetime variable $x = (x^0=t,\vec{x})$. G_F is the weak coupling constant, with an experimentally determined value of $1.03 \times 10^{-5}\ m_p^{-2}$ (m_p = proton

mass) or 1.4×10^{-49} erg•cm^3 in cgs units. The most general four-current is a sum of leptonic and hadronic parts; however, for the following discussion, the hadronic part will be ignored. In purely leptonic processes such as muon decay or neutrino scattering on electrons, complications due to strong interactions do not arise.

According to the V-A theory, the leptonic current has the form

$$J_\ell^\lambda(x) = \overline{\Psi}_{\nu_\ell} \gamma^\lambda (1 - \gamma^5) \Psi_\ell , \qquad 2.1.1.2$$

where the Ψ's are field operators for the particles concerned (ℓ = e or μ). For the moment, the third tau lepton generation will not be considered, since it played no part in theoretical developments at this stage. Equation 2.1.1.2 denotes the charged current of a lepton and its neutrino. There also exist neutral current weak interactions, such as muon neutrino inelastic scattering on protons (Barish et al., 1974; this of course involves hadrons) and muon antineutrino elastic scattering on electrons (Hasert et al., 1973). All processes so far observed, whether charged or neutral, obey a muon number conservation law.

The assumed form of the leptonic current, containing only fields of one type or generation of leptons (muon or electron), leads to the prediction of an additive conservation of muon number. This can be formalized as follows (see Bailin, 1977). For the lepton number assignments of the first chapter and the fields as defined in appendix A1, the lepton numbers of a state are the eigenvalues of an operator $\tilde{L}_\ell$, which then satisfies the

commutation relations

$$[\tilde{L}_\ell, \psi_{\ell,\nu_\ell}(x)] = -\psi_{\ell,\nu_\ell}(x) \qquad 2.1.1.3a$$

$$[\tilde{L}_\ell, \bar{\psi}_{\ell,\nu_\ell}(x)] = +\bar{\psi}_{\ell,\nu_\ell}(x) \qquad 2.1.1.3b$$

and commutes with other field operators (i.e., those of other lepton generations). The result is that

$$[\tilde{L}_\ell, J_\ell^\lambda(x)] = 0, \qquad 2.1.1.4$$

so that $\tilde{L}_\ell$ also commutes with the weak Hamiltonian (equation 2.1.1.1). Similarly, $\tilde{L}_\ell$ commutes with the free field and electromagnetic field Hamiltonians, and thus with the full Hamiltonian. It is then apparent that the eigenvalue L_ℓ is conserved in transitions between physical eigenstates of $\tilde{L}_\ell$.

If we do not restrict the form of the current, such an additive scheme does not necessarily prevail, and a more general multiplicative one will account for physical observations. A multiplicative muon number follows, for instance, from assuming invariance of nature under the permutation of two primitive leptons, say, e' and μ' (Feinberg and Weinberg, 1961a; see also Cabibbo and Gatto, 1960) which can transform into each other, and will manifest themselves physically as linear combinations $e = (\mu' + e')/2^{(1/2)}$ and $\mu = (\mu' - e')/2^{(1/2)}$ of different mass. The e'-μ' permutation invariance under weak interactions requires two kinds of neutrinos, ν_e and ν_μ, which of course are now known to exist (Danby et al., 1962), and implies only a multiplicative selection rule (but does not rule out a stronger additive law).

It was not until relatively recently that experimental information became available which permitted some choice between the two schemes. An experiment to determine the type of electron neutrino in positive muon decay showed that the ratio of $\bar{\nu}_e$ to ν_e was less than 0.25 with 90% confidence (Eichten et al., 1973). An additive law predicts exactly zero, whereas a multiplicative law predicts 0.5 . A more sensitive experiment (Willis et al., 1980) measured the same ratio to be less than 0.098 with 90% confidence. Therefore, any universal muon number conservation law is unlikely to be multiplicative.

The questions that must now be asked about the fundamental interactions are quite different from those of 1961, because of the successes of unification theories (see section 2.2). The present emphasis is on whether there is a universal muon (or lepton, or baryon) conservation law at all. Assuming that there is not, it is then important to determine the level at which it is violated in order to draw further conclusions about the proper formulation of the theory.

For the case of muonium-antimuonium conversion (and e^-e^- to $\mu^-\mu^-$ scattering) the point of contact between theory and experiment is an effective coupling constant G, usually expressed in terms of G_F, for the interaction Hamiltonian density,

$$H_w(x) = 2^{-(1/2)}\, G(\bar{\psi}_\mu \gamma^\lambda(1-\gamma^5)\psi_e)(\bar{\psi}_\mu \gamma^\lambda(1-\gamma^5)\psi_e). \qquad 2.1.1.5$$

This has the current-current form of equation 2.1.1.1, and the

currents are V-A, but otherwise the nature of the expression is quite different from equation 2.1.1.2. No neutrino fields are present, and the currents do not change the charge but rather the generation (muon or electron) of the particle. Each current changes muon number by +1 and electron number by -1, so that the overall changes for the interaction are +2 and -2 respectively. This means that $\sum(L_e+L_\mu)$ and $(-1)^{\sum L_\mu}$ are conserved, and a multiplicative muon number conservation is satisfied, whereas an additive one is not.

It is shown in appendix A1 that the matrix element for conversion from 1S muonium ($|Mu\rangle$) to 1S antimuonium ($|\overline{Mu}\rangle$) states is

$$\langle\overline{Mu}|\ H_w(x)\ |Mu\rangle = \delta/2\ . \qquad 2.1.1.6$$

Disregarding spin selection rules and an unimportant sign,

$$\delta = 16G/(2^{(1/2)}\pi a_o^3) = 2.1 \times 10^{-12}\ (G/G_F)\ \text{eV}, \qquad 2.1.1.7$$

where a_o is the Bohr radius of 1S muonium . A universal (i.e., to all orders of perturbation theory) additive law corresponds to $G = 0$, whereas the existence of a first order interaction, described by equation 2.1.1.6 and unsuppressed by any additive muon conservation, might imply $G \sim G_F$.

2.1.2. Vacuum Eigenstates of the Muonium-Antimuonium System

If $G \neq 0$, muonium and antimuonium are not energy eigenstates of the full (that is, including H_W) Hamiltonian, H.

Let H include a term of electromagnetic origin which causes the partial Hamiltonian, $H - H_W$, to have nondegenerate eigenvalues for the states $|Mu\rangle$ and $|\overline{Mu}\rangle$. If the difference of eigenvalues is Δ, then the full Hamiltonian H can be represented by a 2x2 matrix of the form (taking δ to be real)

$$H = H_o + H_I, \text{ with} \qquad 2.1.2.1$$

$$H = (E_o/2) \begin{bmatrix} 1 & 0 \\ 0 & 1 \end{bmatrix}, \text{ and} \qquad 2.1.2.2$$

$$H = 1/2 \begin{bmatrix} \Delta & \delta \\ \delta & -\Delta \end{bmatrix} = H_{EM} + H_W \qquad 2.1.2.3$$

acting on the states $|Mu\rangle = \begin{bmatrix} 1 \\ 0 \end{bmatrix}$ and $|\overline{Mu}\rangle = \begin{bmatrix} 0 \\ 1 \end{bmatrix}$. H_o, with eigenvalue E_o, includes all terms in H describing the energy of the atom which are the same for muonium and antimuonium. The eigenvalues E_1 and E_2 of H differ by $W = (\delta^2 + \Delta^2)^{(1/2)}$, and the normalized eigenvectors become:

$$|M_1\rangle = (2W(W - \Delta))^{-(1/2)} \; (+\delta|Mu\rangle + (W - \Delta)|\overline{Mu}\rangle),$$

$$|M_2\rangle = (2W(W + \Delta))^{-(1/2)} \; (-\delta|Mu\rangle + (W + \Delta)|\overline{Mu}\rangle). \qquad 2.1.2.4$$

These reduce, for $\Delta \ll \delta$, to:

$$|M_1\rangle = 2^{-(1/2)}(+|Mu\rangle + |\overline{Mu}\rangle),$$
$$|M_2\rangle = 2^{-(1/2)}(-|Mu\rangle + |\overline{Mu}\rangle). \qquad 2.1.2.5$$

2.1.3. Evolution of Antimuonium from Muonium

A nonzero value of δ leads to energy eigenstates which are orthogonal linear combinations of muonium and antimuonium states. The consequence is that a state $|\Psi(t)\rangle$, in the Schroedinger picture, evolving from a state $|\Psi(0)\rangle = |Mu\rangle$ at time zero, has a nonvanishing probability of being identified as $|\overline{Mu}\rangle$ at some later time.

The probability that the state will be identified as antimuonium rather than muonium (for these are states which will be observed via electromagnetic scattering or weak muon decay processes) at time t is

$$P_{\overline{Mu}}(t) = |\langle\overline{Mu}|\Psi(t)\rangle|^2. \qquad 2.1.3.1$$

Expanding the state $|\Psi(t)\rangle = \exp(-iHt)|Mu\rangle$ in terms of the energy eigenstates $|M_j\rangle$ of eigenvalue E_j gives:

$$\langle\overline{Mu}|\Psi(t)\rangle = \sum_{j=1}^{2} \langle\overline{Mu}|M_j\rangle \exp(-iE_j t) \langle M_j|Mu\rangle$$
$$= i \exp(-i(E_1+E_2)t/2) (\delta/W) \sin(Wt/2) . \qquad 2.1.3.2$$

A part of the full Hamiltonian H involves the weak muon decay for both $|Mu\rangle$ and $|\overline{Mu}\rangle$. This can be accounted for by considering H to have complex eigenvalues. Putting $Im(E_\sigma) = \lambda$, the muon decay rate, the imaginary parts of E_1 and E_2 are $\lambda/2$, and equation 2.1.3.1 becomes

$$P_{\overline{Mu}}(t) = \exp(-\lambda t)\ (\delta/W)^2\ \sin^2(Wt/2)\ . \qquad 2.1.3.3$$

For $W << \lambda$, the domain for which $P_{\overline{Mu}}(t)$ is greatest satisfies $Wt << 1$, so

$$P_{\overline{Mu}}(t) \sim \exp(-\lambda t)\ (\delta t/2)^2\ . \qquad 2.1.3.4$$

If an experiment were performed which detected conversion by means of the observation of a fast electron from negative muon decay, an expression for the probability of the muon decaying as μ^- would be required. Multiplying equation 2.1.3.3 by the decay rate λ, and integrating over all time yields

$$P_{\mu^-} = \delta^2\ /\ 2(\delta^2 + \Delta^2 + \lambda^2)\ , \qquad 2.1.3.5$$

which is approximately $\delta^2/2\lambda^2 = 2.5 \times 10^{-5} \bullet (G/G_F)^2$ for $\Delta << \lambda$.

If, however, a muonic X-ray were used for the signature, the relevant expression would be 2.1.3.3 evaluated at the time of collision of antimuonium with the atom producing the X-ray. The right hand side of equation 2.1.3.3 has a maximum at $t = 2/\lambda$, or 4.4×10^{-6} s, of $6.6 \times 10^{-6}\ (G/G_F)^2$ in the approximation of 2.1.3.4. This will be applied in the fourth chapter in order to estimate the expected rate of the TRIUMF

muonium-antimuonium experiment in terms of (G/G_F).

2.1.4. The Effect of Electromagnetic Fields on Conversion

Little has been said up to this point about the origin or value of Δ; one might wonder whether it is important, or under what circumstances the approximation $\Delta << \lambda$ might be valid.

Such questions were addressed in the first detailed publication on muonium-antimuonium conversion, from which most of this chapter has been derived (Feinberg and Weinberg, 1961b). For the case of muonium in vacuum, Δ arises from the macroscopic electromagnetic fields present. Two points should be kept in mind:

1. Not all fields or field derivatives contribute to Δ.
2. Not all of the 1S muonium hyperfine states are affected in the same way.

The first point is exemplified by considering possible contributions to Δ from a uniform electric field. For a state of particular angular momentum (an axial vector) the only scalars upon which can depend ($\vec{E}\bullet\vec{E}$ and $(\vec{J}\bullet\vec{E})^2$) are even in the electric field and are the same for muonium and antimuonium. Since the energy shift is, by definition (equation 2.1.2.3), positive for muonium and negative for antimuonium , it cannot depend on a uniform electric field. If there is also a uniform magnetic field (another axial vector) present, further scalars can be formed, but only those containing $\vec{H}\bullet\vec{J}$ are not even in

both $\vec{E}$ and $\vec{H}$.

This serves to illustrate the second point; $\vec{H}\bullet\vec{J}$ is zero for the two hyperfine states of $\vec{J} = \vec{S}_\mu + \vec{S}_e$ for which m_J, the projection of $\vec{J}$ along $\vec{H}$, is zero. These two states are conventionally labelled $(J,m_J) = (1,0)$ and $(0,0)$. A naive but useful picture of the source of Δ can be gleaned from a Breit-Rabi diagram for the energies of the hyperfine states of muonium in a magnetic field, and the reflection of the diagram through the H=0 axis (see Figure 2.1.4.1). It must be remembered that,

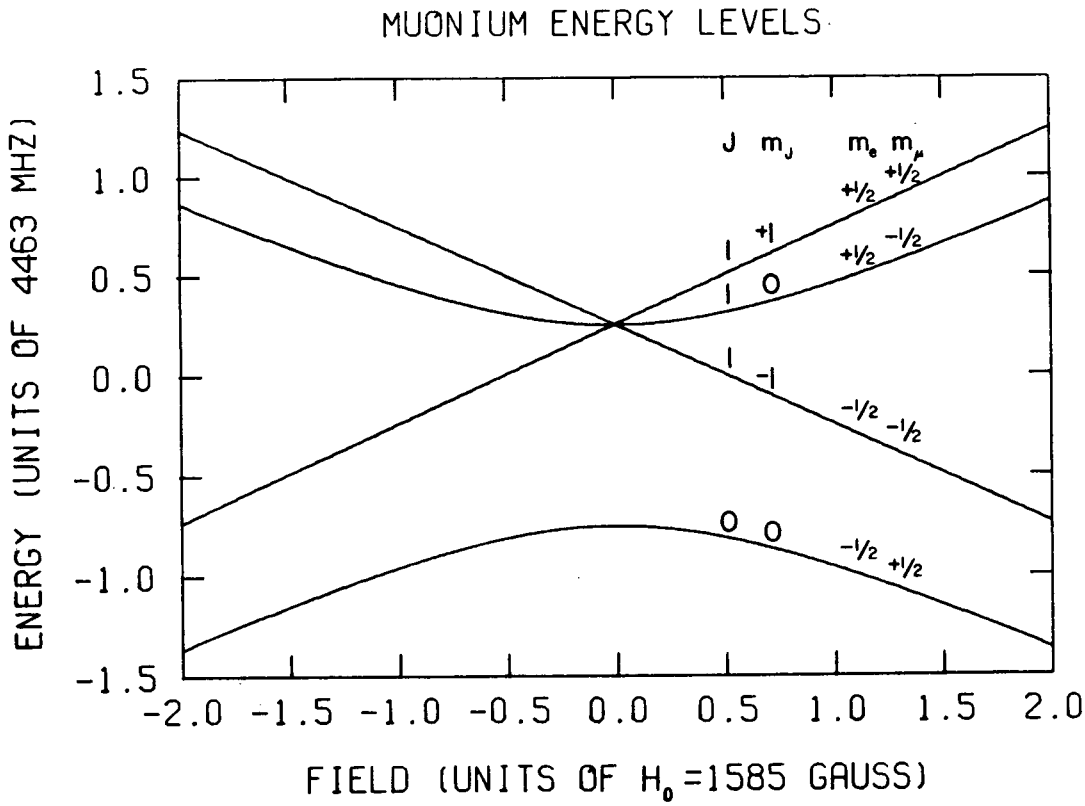

Figure 2.1.4.1. Splitting of $m_J=\pm1$ states of muonium and antimuonium in a magnetic field.

for $\delta \neq 0$, these are not the eigenstates of the full Hamiltonian

(see Morgan, 1967, for a more correct and complete treatment). Switching the sign of H has the same effect on a given level as switching the signs of the magnetic moments (i.e., charges) of the muon and the electron, as happens in muonium to antimuonium conversion. The nondegeneracy of the $(1,\pm1)$ states of muonium and antimuonium results. The value of Δ one obtains is eH/m, where m is the electron mass. Thus $\Delta \sim 1.2 \times 10^{-8} \times H$ eV, if H is in gauss. Comparing this to λ,

$$\Delta/\lambda \sim 40\ H\ , \qquad 2.1.4.1$$

and the conclusion is that H must be kept well below 0.025 gauss in order for conversion of these states to be unsuppressed.

Estimates of contributions to Δ from electric field gradients have also been made (Feinberg and Weinberg, 1961b). These can be ignored for the case of muonium in vacuum.

2.1.5. Muonium in the Presence of Matter

It is not easy to obtain abundant muonium in vacuum, so the possibility of observing the conversion in gases and solids has been carefully investigated (Feinberg and Weinberg, 1961b). The conclusion reached was that such experiments would not be very sensitive because of the large values of Δ encountered in the interactions of muonium with the target substance.

In a gas, collisions of the muonium-antimuonium system with the surrounding atoms involve Coulomb processes and the

associated large ($\Delta >> \lambda$) energy differences. During a collision the energy eigenstates approach:

$$|M_1> = (\delta^2(1 + \delta^2/4\Delta^2))^{-(1/2)} (\delta|Mu> + \delta^2/2\Delta|\overline{Mu}>)$$
$$\sim |Mu> \text{ , and}$$

$$|M_2> = (\delta^2 + 4\Delta^2)^{-(1/2)} (-\delta|Mu> + 2\Delta|\overline{Mu}>)$$
$$\sim |\overline{Mu}> \text{ .} \qquad 2.1.5.1$$

The $|M_1>$ component will scatter from, say, an argon atom like $|Mu>$, that is, elastically, but the $|M_2>$ component has a high probability for scattering inelastically like $|\overline{Mu}>$, forming a muonic argon atom and a free positron or positronium atom (Morgan, 1967). During the collision any $|M_2>$ component is in effect removed, and when Δ is switched off as the scattering process ends, the system is in the $|Mu>$ state as it was at t=0, the time of muonium formation. In effect, the collision inhibits the coherent growth of the $|\overline{Mu}>$ component (somewhat in analogy with the regeneration of the short-lived component of a neutral kaon beam as it passes through matter).

The net result is that the probability of the muon decaying as μ^- (equation 2.1.3.5) is reduced by a factor of 1/N, where N is the mean number of collisions during the muon lifetime. For argon gas at normal temperature and pressure, N is of the order of 10^5.

In solids the situation is more complicated still. Contributions to Δ arise from the overlap of the muonium wave function with those of the atoms of a molecular crystal, or from

high electric fields and gradients within an ionic crystal. Depending on the nature of the material, the probability of the muon in muonium decaying as μ^- is 10^{-14} to 10^{-20} times its value in vacuum (equation 2.1.3.5; see Feinberg and Weinberg, 1961b). It has been suggested by B. Bergersen that this may be overly pessimistic. For example, in a metal the electron density at the positive muon is nearly as large as for a muonium atom, even though no single electron is correlated for long with the muon. The energy band of the conduction electrons might provide a way around the problem of non-degeneracy of initial and final states: for any initial-state energy, there will be a band of nearly degenerate final state energies. The conversion rate then depends upon the local density of states. These ramifications are not simple to calculate, so the use of a metal target to establish an acceptable upper limit for G is not appealing. Moreover, the density of states is likely not large enough that an experimental advantage would accrue.

It is therefore desirable, if difficult, to allow the muonium-antimuonium system to evolve in vacuum or a rarefied gas after muonium formation. A technique for accomplishing this is described in sections 3.2.2 and 4.2.2.

2.2. Unified Gauge Theories and Muonium-Antimuonium Conversion

The forces of nature are usually subdivided into the strong, electromagnetic, weak, and gravitational interactions, each with unique attributes. Attempts to unify two or more of these, that is, to characterize them by common strength and symmetry properties, has been a major goal of physicists in this century.

The Fermi theory of beta decay (Fermi, 1934) was an early example in which the vector nature of electromagnetism was adapted to the weak lepton-hadron interaction through a change in coupling constant. Some further development in the Fermi theory, leading to the successful V-A interpretation of some low energy weak processes, was mentioned in section 2.1.1. Of course the discovery that weak interactions were not pure vector blighted the apparent analogy with electromagnetism.

There were other problems with the four fermion interaction. Even before the V-A form was assumed, divergences existed in the calculation of some weak processes such as neutrino-lepton scattering. When expanding the scattering operator S in the usual perturbation series in G_F, shown diagrammatically in Figure 2.2.1, one hopes that the first order term will dominate because of the weakness of the interaction. However, the propagator for the intermediate leptons from the second order term, containing insufficient inverse powers of the lepton momenta, diverges in the momentum integral, so truncation of the series is only possible by inserting an ad hoc cutoff Λ.

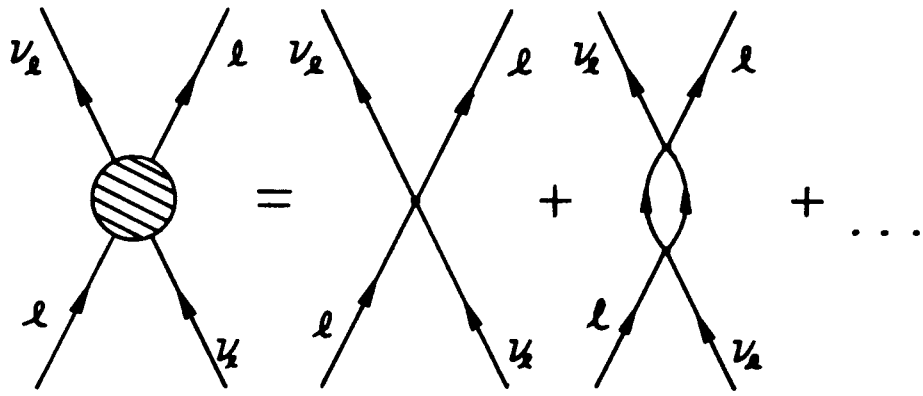

Figure 2.2.1. Diagrammatic expansion of the neutrino-lepton scattering operator

The second order term then becomes proportional to $G_F(G_F\Lambda^2)$ and the dimensionality of the extra factor G_F is balanced by Λ. Renormalization of the masses and the coupling constant are not possible as in quantum electrodynamics.

The inclusion of an intermediate exchange boson W improves the situation with respect to the unitarity violation. Renormalization is still a problem. If the elementary coupling of the lepton current is to a massive spin one boson, the analogy with QED is closer. Assume, for the moment, a weak coupling of about the same strength as for electromagnetic interactions (the boson mass must then satisfy $G_F \sim e^2/m_W^2$, so $m_W \sim 30$ GeV). Then, for the e^4 (four vertices) contributions to lepton-lepton scattering (figure 2.2.2), the weak boson propagator has terms proportional to $k_\alpha k_\beta/m_W^2$, from longitudinal degrees of freedom, which do not contribute in the photon propagators of QED due to gauge invariance. These terms dominate at higher energies, and the "extra" convergence guaranteed by the gauge invariance in QED is absent from the weak process. Perturbation theory thus breaks down.

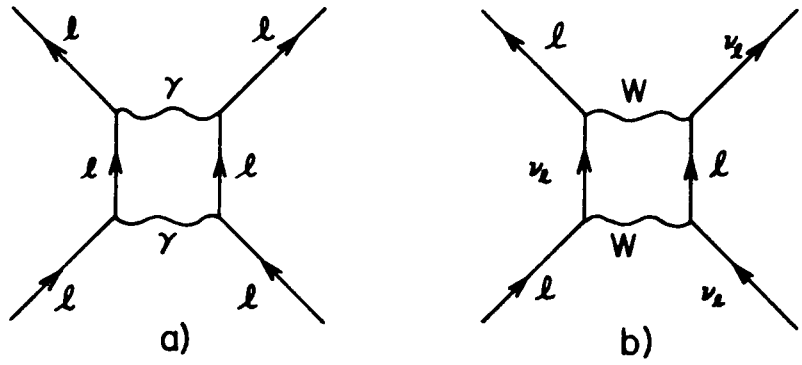

Figure 2.2.2. Order e^4 (or G_F^2) lepton-lepton scattering in (a) QED, and (b) weak interactions.

A remedy for these outstanding deficiencies of the old approach was proposed in 1967, in the form of a gauge theory unifying weak and electromagnetic interactions.

2.2.1. Gauge Theories of Weak and Electromagnetic Interactions

Since 1967 there have appeared numerous publications which have attempted to explain the nature of the unified gauge model for weak and electromagnetic interactions, now known as the Weinberg-Salam (WS) theory (Weinberg, 1967; Salam, 1968). In addition to the original references, source material for this section includes textbooks (Bailin, 1977; Taylor, 1976) and several fine review articles (Weinberg, 1974 and 1977; Abers and Lee, 1973; Bernstein, 1974). Only a brief introductory explanation of the theory will be given here.

The suggestion of the previous section is that a convergent theory might be based on a gauge invariant Lagrangian, as is

QED, but involving a charged vector field. This is accomplished by the WS model in the following way, considering for the moment only first generation (i.e., electron-type) leptons.

The fermion fields appear in the Lagrangian as left-handed doublets and right-handed singlets,

$$L = 1/2\ (1 - \gamma^5) \begin{bmatrix} \nu_e \\ e \end{bmatrix}$$

$$R = 1/2\ (1 + \gamma^5) \begin{bmatrix} e \end{bmatrix}\ , \qquad 2.2.1.1$$

where ν_e and e are neutrino and electron fields (analogous to ψ_{ν_e} and ψ_e of appendix A1). If τ_i (i=1,2,3) are the Pauli matrices for SU(2) leptonic isospin $\vec{T} = \vec{\tau}/2$, and $\tau_\pm = 1/2\ (\tau_1 \pm \tau_2)$, then

$$\tau_+ L = 1/2\ (1 - \gamma^5) \begin{bmatrix} e \\ 0 \end{bmatrix} \qquad 2.2.1.2$$

and the charged currents can be written

$$1/2\ \bar{\nu}_e\ \gamma^\mu (1 - \gamma^5) e = \bar{L} \gamma^\mu \tau_+ L, \text{ and}$$
$$1/2\ \bar{e}\ \gamma^\mu (1 - \gamma^5) \nu_e = \bar{L} \gamma^\mu \tau_- L. \qquad 2.2.1.3$$

To complete the group of which these currents are members (usually known as SU(2) leptonic isospin) one needs

$$1/2\ [\bar{\nu}_e \gamma^\mu (1 - \gamma^5) \nu_e\ - \bar{e} \gamma^\mu (1 - \gamma^5) e]$$
$$= \bar{L} \gamma^\mu \tau_3 L\ . \qquad 2.2.1.4$$

A major success of the theory was the experimental confirmation

of its prediction of neutral currents as described by this last expression.

The electromagnetic current can be included in the usual form:

$$\bar{e}\gamma^{\mu}e = -1/2\ \bar{L}\gamma^{\mu}\tau_3 L + 1/2\ \bar{L}\gamma^{\mu}L + \bar{R}\gamma^{\mu}R\ . \qquad 2.2.1.5$$

The last two terms on the right hand side conserve leptonic hypercharge $Y \equiv N_L/2 + N_R$, the N's referring to the eigenvalues of a number operator for leptons of the indicated helicity. In this way the group U(1) of leptonic hypercharge enters the theory, and a Lagrangian can be written down which is invariant under $SU(2)_L \times U(1)$ infinitesimal local gauge transformations. The transformations are

$$\begin{aligned} L \rightarrow L' &= (1+ig\vec{\Lambda}(x)\bullet\vec{T}+i(g'/2)\Lambda(x))\ L\ , \text{ and} \\ R \rightarrow R' &= (1+ig'\Lambda(x))R\ , \end{aligned} \qquad 2.2.1.6$$

where g and g' are constants and $\vec{\Lambda}(x)$ and $\Lambda(x)$ are gauge functions. The inclusion of g' in this particular way insures that the hypercharge-conserving terms of equation 2.2.1.5 couple to the gauge field B associated with U(1). The gauge fields for $SU(2)_L$ and U(1) transform as

$$\begin{aligned} \vec{A}_\mu \rightarrow \vec{A}'_\mu &= \vec{A}_\mu + \partial_\mu\vec{\Lambda} - g\vec{\Lambda}x\vec{A}_\mu \\ B_\mu \rightarrow B'_\mu &= B_\mu + \partial_\mu\Lambda \end{aligned} \qquad 2.2.1.7$$

and the renormalizable Lagrangian is (in the notation and phase convention of Weinberg, 1967)

$$\mathcal{L}_0 = -1/4\ (\partial_\mu \vec{A}_\nu - \partial_\nu \vec{A}_\mu + g\vec{A}_\mu x \vec{A}_\nu)^2 - 1/4\ (\partial_\mu B_\nu - \partial_\nu B_\mu)^2$$
$$-\bar{R}\gamma^\mu(\partial_\mu - ig' B_\mu)R \qquad 2.2.1.8$$
$$-\bar{L}\gamma^\mu(\partial_\mu - ig\vec{T}\cdot\vec{A}_\mu - (i/2)g' B_\mu)L \quad .$$

There are more terms in Weinberg's Lagrangian, but these serve to illustrate some points of the model, if the physical leptons are inserted according to equations 2.2.1.1:

1. The normalized neutral vector field coupling to the $\bar{\nu}_e \nu_e$ current is

$$Z_\mu = (g^2+g'^2)^{-(1/2)}\ (gA_{\mu 3} + g' B_\mu) \quad . \qquad 2.2.1.9$$

2. The field orthogonal to Z_μ is

$$A_\mu = (g^2+g'^2)^{-(1/2)}\ (-g' A_{\mu 3} + gB_\mu) \quad , \qquad 2.2.1.10$$

which couples only to the $\bar{e}e$ current (the A_μ used here is not to be confused with $\vec{A}_\mu$ as used in equations 2.2.1.7 and 2.2.1.8).

3. The coefficient of $i\bar{e}\gamma^\mu e A_\mu$, which is to be identified with electrodynamic coupling, is $gg'/(g^2+g'^2)^{(1/2)}$, and is equal to the electronic charge e.

4. The charged vector field associated with $\bar{e}\nu_e$ and $\bar{\nu}_e e$ terms appears as

$$W_\mu = 2^{-(1/2)}\ (A_{\mu 1} + iA_{\mu 2}) \quad . \qquad 2.2.1.11$$

Note that it has become common to define a mixing angle θ_w (the

Weinberg angle) as $\tan\theta_w = g'/g$ (Weinberg, 1972), and to write the fields and couplings in terms of this angle.

The concept of isotopic local gauge invariance represented by the SU(2) character of equation 2.2.1.8 was not a new invention in WS; it had been formulated much earlier (Yang and Mills, 1954) but convergence of the theory demanded unphysical massless quanta of the SU(2) gauge field. The new feature was that explicit mass terms (and non-renormalizability) could be avoided by introducing a scalar meson doublet whose vacuum expectation value broke the symmetry of the Lagrangian under $\vec{T}$ and Y (a process referred to as the Higgs-Kibble mechanism, after Higgs, 1964 and Kibble, 1967). There is no experimental guide to the exact structure of the Higgs scalar mesons that are introduced, but the so-called minimal structure of the original 1967 model is a doublet of the form

$$\phi = \begin{bmatrix} \phi^+ \\ \phi^\circ \end{bmatrix} \qquad 2.2.1.12$$

where the vacuum expectation value $\langle\phi^\circ\rangle$ of ϕ° is λ (ϕ^+ retains a zero value); this λ is not to be confused with the muon decay rate of section 2.1. The Lagrangian of equation 2.2.1.8 becomes

$$\begin{aligned} \mathcal{L} &= \mathcal{L}_o + \mathcal{L}_H \\ &= \mathcal{L}_o - 1/2 \bullet |\partial_\mu \phi - ig\vec{A}_\mu \bullet \vec{T}\phi + (i/2)g' B_\mu \phi|^2 \\ &\quad -G_e(\bar{L}\phi R + \bar{R}\phi^\dagger L) - M_1^{\,2}|\phi|^2 + h|\phi|^4 \,. \end{aligned} \qquad 2.2.1.13$$

Replacing by its vacuum expectation value will lead to the masses

$$m_e = \lambda G_e,$$
$$m_W = \lambda g/2, \text{ and} \qquad 2.2.1.14$$
$$m_Z = (g^2 + g'^2)^{(1/2)} \bullet (2^{-(3/2)} \lambda) ,$$

with the photon remaining massless. The low energy limit of the electron-neutrino current coupling via W exchange must be that of the V-A theory, so

$$g^2/8m_W^2 = 1/4\lambda^2$$
$$= G_F/2^{(1/2)} . \qquad 2.2.1.15$$

The model can be extended to second and higher (i.e., μ and τ) generations of leptons by the addition of appropriate terms containing $L_{\mu,\tau}$ and $R_{\mu,\tau}$ fields to expressions 2.2.1.8 and 2.2.1.13. The parameters G_μ and G_τ must be chosen such that $G_{\mu,\tau}/G_e = m_{\mu,\tau}/m_e$.

The WS theory in this form has survived all the tests to which it has been subjected with presently available techniques. There are features, however, which lack aesthetic appeal (e.g., the need to include the Higgs bosons and adjust their couplings by hand to give correct lepton masses). It is safer to regard $SU(2)_L \times U(1)$ as a subgroup of the true electroweak gauge group, whose further properties might not be clearly revealed by present knowledge. Much effort is being channelled into so-called grand unification schemes, gauge theories unifying strong, electromagnetic, and weak interactions with correspondingly larger gauge groups such as SU(5) and SO(10).

2.2.2. Muon Number Violation and Muonium Conversion in Extended Theories

The WS theory in its simplest form (sometimes referred to as the standard model), as defined by the leptonic electroweak Lagrangian of equation 2.2.1.13 with extension to μ and τ fields, does not allow a violation of muon number. This is apparent from the observation that the fermion currents coupling to gauge vector or Higgs scalar bosons do not change lepton flavor. The conservation is not really built in to the theory, but is a consequence of the assumptions made from the outset.

In the first place, the neutral left-handed leptons (neutrinos) were assumed massless. If this were not so, and if the muon neutrino and electron neutrino masses were not degenerate, their weak eigenstates would not be mass eigenstates, and a situation much like the Cabibbo mixing of the quark sector would occur. A GIM mechanism (Glashow, Iliopoulos, and Maiani, 1970) could lead to lepton flavor-changing weak neutral couplings suppressed by a factor of the order of $G_F \sin\theta \cos\theta \, (m_1^2 - m_2^2)$ (becoming second order in G_F), where m_1 and m_2 are the neutrino masses and θ a mixing angle. For the largest mass difference allowed by current direct measurements of the muon neutrino mass of about 0.5 MeV (Daum et al., 1980), the suppression is of the order of 10^{-12}. Using a more stringent estimate of $(m_1^2 - m_2^2) = 25\ eV^2$ (Mann and Primakoff, 1977), based on cosmological arguments, the suppression would be more like 10^{-22}. In some sense, then, approximate muon number conservation can be regarded as due to the near degeneracy of

neutrino masses, compared with other typical masses. If there

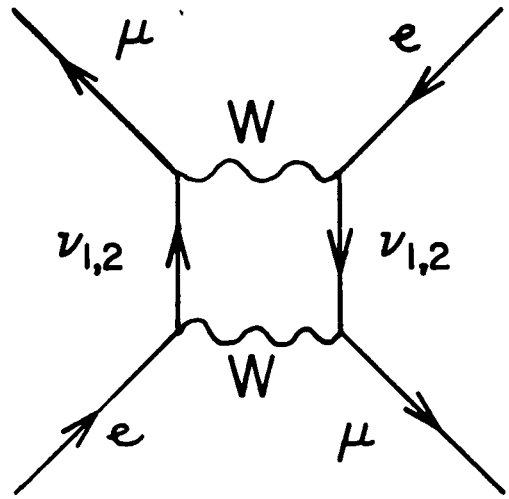

Figure 2.2.2.1. Conversion process via non-degenerate neutrinos.

is no other, more dominant mechanism for conversion, the muonium-antimuonium effective coupling as described by Figure 2.2.2.1 should satisfy

$$G/G_F < 10^{-14} \qquad 2.2.2.1$$

for a mass difference of 1 MeV. Very recently, a reactor neutrino experiment has shown some evidence for neutrino instability or mixing (Reines et al., 1980), and the lower limit on the squared mass difference is about 0.3 eV^2. There is at this writing much controversy regarding several neutrino mass or mass difference experiments, and no result has as yet been widely accepted.

Secondly, the Higgs boson content of the theory is minimal.

The single Higgs doublet was introduced in the simplest way possible to account for the observed mass structure, and also predicts the relative strength of charged and neutral currents. A slightly more general set of Higgs doublets was considered (Bjorken and Weinberg, 1977) on the strength of a rumour of the observation of the decay $\mu \rightarrow e\gamma$ (which, though later shown to be unfounded, caused much activity among theorists postulating mechanisms for muon number violation). The electron and muon mass terms in a generalization of $\mathcal{L}_H$ of equation 2.2.1.13, $-G_e(\bar{L}_e \phi R_e) - G_\mu(\bar{L}_\mu \phi R_\mu)$, become

$$-g_1 \bar{L}_\mu \phi_1 R_\mu - g_2 \bar{L}_e \phi_2 R_\mu - g_3 \bar{L}_\mu \phi_3 R_e - g_4 \bar{L}_e \phi_4 R_e . \qquad 2.2.2.2$$

Assuming $\phi_2 = \phi_3$, and $g_2 = g_3$ is the same order as g_1 ($m_\mu G_F^{(1/2)}$ for $<\phi_1^0> \sim G_F^{-(1/2)}$), it is possible that

$$G/G_F \sim m_\mu^2/m_H^2 \sim 10^{-4} \qquad 2.2.2.3$$

for $m_H \sim 10$ GeV (see Figure 2.2.2.2). There is, however, little basis for such assumptions. Note that expression 2.2.2.2 can be extended to include the tau generation, in which the muon mass in equation 2.2.2.3 would be replaced by the tau mass, and the ratio of coupling constants might approach 10^{-1}.

A third extension of the standard model postulates a modification of the fermion fields to include right-handed doublets and associated V+A currents involving massive neutral right-handed fermions $N_{1,2}$ (Cheng and Li, 1977). One prediction of this extension is that the electronic neutral current is purely vector, with no axial part as in the standard model.

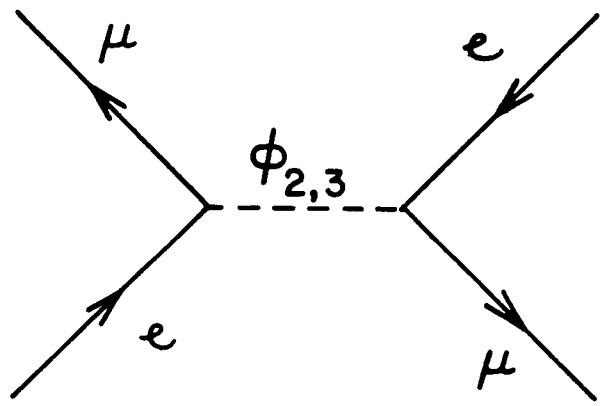

Figure 2.2.2.2. Conversion via non-minimal Higgs coupling.

Some early experiments on atomic parity violation by neutral currents in heavy atoms did not agree with V-A predictions (for a review, see Bouchiat, 1977), but more recent meaurements with systems more easily understood show the expected parity violations, and the model with V+A currents is not supported. The diagram for possible muonium-antimuonium conversion in this extension is that of Figure 2.2.2.1, with $\nu_{1,2}$ replaced by the heavy fermions $N_{1,2}$. The GIM mechanism is still applicable, but the mass difference is not necessarily small. Cheng and Li obtain

$$G/G_F = (G_F/16\pi^2)\ \sin^2\theta\cos^2\theta\ (m_1^2 - m_2^2) \qquad 2.2.2.4$$

when $m_1 >> m_2$. For the maximal mixing angle and a mass squared difference of 1 GeV², one obtains $G/G_F \sim 10^{-8}$. Note that since right-handed currents are participating, the axial parts of the effective Hamiltonian (equation 2.1.1.5) must change sign, (1 -

γ^5) to $(1 + \gamma^5)$. This has no effect on the final result for of appendix A1.

The last extension of the standard model which will be mentioned did not result from speculation on the rumoured $\mu \rightarrow e\gamma$ decay, but rather from the discovery of the third tau generation of leptons (Perl et al., 1975). The conversion scheme is based on the proposition (Derman, 1978 and 1979) of invariance of the Lagrangian under permutation of the three lepton labels, e, μ, and τ, a symmetry spontaneously broken by the Higgs-Kibble mechanism by which the leptons acquire their grossly dissimilar masses. Permutation invariance requires a minimum of three Higgs doublets; the demand of mass non-degeneracy of the charged leptons leads to the conclusion that some of the Higgs particles carry lepton flavor, leading to a non-conservation of additive muon (or tauon) number. Instead, a multiplicative parity-like conservation law is implied, the τ and one of μ or e possessing a positive parity, the other (e or μ) a negative one. This particular assignment insures the apparent absence of $\mu \rightarrow e\gamma$. The theory makes some specific predictions on decay phenomena which might be observed, but as usual the Higgs masses often appear in matrix elements, making estimates of rates rather imprecise. It is important to note that, while the Higgs particles of the positive lepton parity are required to be very massive to reproduce known phenomena, those of negative parity could be of the order of 10 GeV. Diagrams similar to figure 2.2.2.2 could then result in G/G_F as large as 0.1, essentially the same as for the Bjorken and Weinberg model extended to third generation leptons. It is also possible, within this model, that charged current interactions

may exhibit a multiplicative conservation law at a much lower level than neutral current ones, making muonium conversion an interesting test.

The purpose of this section has been to show that modern theories of weak and electromagnetic interactions can at present encompass a broad range of possibilities; variations on the WS theme are diverse and manifold, because experimental results can not yet differentiate among several of the possibilities. The attitude of the particle physics community must then be that efforts toward an improvement in our knowledge of the electroweak phenomenology, toward an increase in the level of confidence in (or demonstration of the breakdown of) laws such as that of muon number conservation, are worthwhile.

3. DETAILS OF THE CONVERSION EXPERIMENT

The principle of the muonium-antimuonium conversion experiment is quite simple; one needs only to observe muonium and determine whether it does or does not convert to antimuonium. In practice there are several problems of varying severity making this determination difficult. The muon is not stable, so that observations must be made during its lifetime, and the probability of conversion is reduced because of the competing process of muon decay. The environment of muonium can drastically influence the interaction rate, as explained in section 2.1. Detection of possible conversion events must be achieved with reasonably high efficiency while maintaining a low background rate.

The formation of muonium atoms from a beam of muons will take place during the passage through and energy loss in some moderator (solid, liquid, or gas). The electron capture and loss processes involved are analogous to those of protons slowing in matter, and formation of a neutral atom is thought to be most likely when the muon (or proton) has a velocity comparable to that of the valence atomic electrons (see, for example, Tawara and Russek, 1973). After further energy loss, muonium states may persist or disappear, depending upon the moderator. In some materials, the precession of the spins of polarized muonium atoms may be observed after thermalization is complete, and limits on the amount of muonium formed are easily

obtained (Brewer et al., 1975) by the methods of muon and muonium spin rotation.

The moderator, necessary for muonium formation in a conversion experiment, subsequently inhibits conversion by interacting electromagnetically with the charges and magnetic moments of muonium. Herein lies the reason that very sensitive searches for muonium-antimuonium conversion have not yet occurred; muonium formation and conversion cannot take place at their respective optimum rates in any one environment, and compromises must be made.

Detection of the conversion is a relatively less difficult problem. There are two ways to approach it. One can search either for a fast negative electron resulting from the normal decay of the muon in antimuonium, or for a characteristic muonic X-ray from the capture of the negative muon in an atomic orbital about a nucleus from the target environment.

Presented in this chapter will be the details of the methods used to optimize the probability of detecting muonium conversion in the experiment at TRIUMF . In order to put this most recent effort in perspective, it is worthwhile to comment on previous muonium-antimuonium conversion experiments, both successful and unsuccessful, as well as on some related investigations regarding the multiplicative muon number conservation scheme.

3.1. A Review of Related Experiments

3.1.1. Other Muonium-Antimuonium Experiments

The only reliable limit which has been set by a conversion experiment on the coupling constant G of equation 2.1.1.5 is due to a Yale group working at the Nevis synchrocyclotron (Amato et al., 1968). A conventional beam of muons from pion decay in flight was degraded so that some muons would stop in an argon gas target at one atmosphere pressure. Various plastic scintillators completely surrounded the gas region for the identification of stopping muons. The scintillators also detected subsequent decay electrons. Two sodium iodide scintillation counters, sensitive to argon muonic 2P-1S X-rays at 644 keV, were used to identify the conversion. To reduce background, accepted events included only those photon counts following a muon stop for which no electron of either charge was detected. This meant that some real conversion events could be rejected due to negative muon decay from the 1S atomic state in argon (as opposed to nuclear muon capture), but the loss was more than offset by the resultant background reduction. However, the effect of the argon environment on the muonium produced was such that the best upper limit obtainable was $G \leq 5800 G_F$.

The assignment of this limit relied upon several numbers,

one of which was the muonium formation probability in argon gas at one atmosphere. This was taken to be unity, consistent with calculations and observations at the time of the experiment. More recent measurements have shown this probability to be somewhat lower at 0.63 ± 0.07 (Mikula et al., 1979; see also Barnett et al., 1975). Much effort was directed toward the calculation of the probability that a muonium atom in the target would lead to an argon muonic atom (Morgan, 1967), a result crucial in the interpretation of the data. This probability, stated here for future reference, is $(1.0 \pm 0.2) \times 10^{-10}(G/G_F)^2$, including the effect of muonium-argon collisions which drastically reduce the conversion rate. For comparison, the conversion probability in vacuum (see section 2.1.3) is $2.5 \times 10^{-5}(G/G_F)^2$.

An attempt was made by a University of Arizona group, working at the Berkeley 184" cyclotron, to use a target of thin, hot metal foils in vacuum. An inhomogeneous target was used in order to reduce the effect of the moderator on the conversion rate. One component of the target was to serve as an electron donor, the other as a region where the conversion probability was high (the vacuum). It was expected that muons might diffuse in the foils quickly enough to reach the surface, where they could pick up an electron to form muonium before entering the vacuum between foils. Some indirect evidence for muonium formation was obtained (Bowen et al., unpublished; see also Kendall, 1972) from muon spin relaxation measurements, but no direct muonium spin rotation signal was observed. Detection of a possible muonium-antimuonium conversion was to be by helical scintillator telescopes in a magnetic field such that only fast

negative electrons from antimuonium decay would be observed. One very important aspect of this experiment was the associated development of a high stopping density beam of low momentum (~29 MeV/c) "Arizona" muons, now usually referred to as surface muons because of their origin from pions stopped in the surface of a production target (Pifer et al., 1976). The use of such beams is now common for stopped positive muon experiments at meson facilities, and is essential to the conversion experiment at TRIUMF (see section 3.2.1).

Another unique type of muon beam has been used in an investigation of muonium formation in low pressure ($\sim 10^{-2}$ mm Hg) argon gas. Positive pions of 39.5 MeV/c momentum will, upon decay in flight, produce some muons of energy less than 10 keV from decay in the direction opposite the pion momentum. In a subsequent collision with the gas, muonium could be formed. A group from the University of Berne, working at CERN, attempted to detect the formation by applying a magnetic field along the incident beam, to trap the charged particles, while searching for muons decaying at some distance from the beam axis (Hofer et al., 1972). Muons emitted in pion decay with a velocity transverse to the applied field would spiral until forming muonium, when they would be able to escape the magnetic field to be detected in a ring concentric with the incident beam. No signal attributable to muonium formation was detected.

The most recent idea for forming muonium useful for a conversion experiment is that of a Virginia-Maryland group working at SREL (Barnett et al., 1977), using a target similar to that of the Arizona experiment and the original Arizona beamline transported from Berkeley. In this case, a stack of

200 (unheated) gold foils, each of 10^{-5} cm thickness, was used. Muonium spin rotation indicated that the stopped muons formed muonium in vacuum with a claimed probability of 0.28 ± 0.05. Although this result indicated that a vast improvement in muonium conversion experiments was immediately possible, it could not be reproduced at LAMPF (Beer et al., 1979) or SIN (Arnold et al., 1979a), where similar experiments of higher sensitivity were undertaken; no effects attributable to muonium formation in vacuum were observed in either instance. A target consisting of collodion films with gold evaporated onto the surfaces was studied at TRIUMF, but it also showed no measurable muonium formation. Thus it seems probable that this method is not workable.

This completes the list of prior attempts, mostly unsuccessful, to lay a foundation upon which a sensitive muonium-antimuonium conversion experiment could be based. As an aside, the production of muonium in vacuum is also a prerequisite for some sensitive tests of quantum electrodynamic effects in muonium (e.g., in measurements of the fine structure, Lamb shift, and hyperfine structure of the n=2 excited state) (Hughes, 1979).

3.1.2. Experiments with Other Systems

A non-zero value for the coupling constant G of equation 2.1.1.5 will result in processes other than muonium conversion. In particular, a collision of two energetic negative electrons

could result in two negative muons by the same interaction. Using this fact, an experiment at the Princeton-Stanford electron storage rings has set a limit of $G \leq 610G_F$ (Barber et al., 1969), nearly an order of magnitude better than the Yale-Nevis muonium-antimuonium upper limit.

In addition to this, a recent experiment on neutrinos from positive muon decay has searched for electron antineutrinos, which would be allowed only if muon conservation obeyed at most a multiplicative law (Willis et al., 1980). The result strongly disfavors the multiplicative scheme, in that the ratio of "wrong" muon decays to all decays is measured to be $R \leq 0.098$, whereas $R = 0.5$ might be expected from the multiplicative rule. The interaction which could lead to a nonzero value of R, however, is not the neutral current one of equation 2.1.1.5, but rather involves charged currents and the associated exchange bosons. For this reason, the limit on the ratio R cannot be used to calculate a limit on the ratio G/G_F without recourse to a specific model to determine the elementary couplings, exchange particles, and their interrelationships. For instance, in the model of Derman discussed in section 2.2.2, the masses of the charged and neutral Higgs particles would determine the respective ratios, and there is no a priori reason to assume that the masses are equal. The upper limit on "wrong" muon decay, therefore, does not absolutely rule out muonium-antimuonium conversion with a stronger coupling. On the other hand, it is convincing evidence that a muon conservation law, if it does exist at all, is additive in nature.

With the knowledge of the history of muonium conversion experiments and the related multiplicative law research, the

outstanding problems become more clearly defined. The attempt at TRIUMF to find solutions to these will be the subject of the following section.

3.2. The Apparatus and Techniques Used

An attempt was made at TRIUMF to design an apparatus which would maximize the sensitivity to muonium conversion. This effort, initiated in 1975, largely concerned the muonium production target itself, but precise magnetic field control and a simple, efficient scheme for detection were also sought. Within the limitations thus imposed, it was imperative that a beamline with a well defined, high luminosity, high stopping density muon beam be available.

3.2.1. M13 and Surface Muons

Such a beamline was built and commissioned at TRIUMF by the spring of 1979. It was a low energy channel, designed to be as short as possible (9.4 m) so that pions down to about 10 MeV (with a mean decay length of about three metres) might survive passage through it. The optical and beam control (via slits and jaws) properties also make it excellent for surface muons, especially since the muon source, the primary production target,

can be made small.

The origins of surface muons, both historically and physically (Pifer et al., 1976), were mentioned briefly in the preceding section. When 500 MeV protons interact with nucleons of a target such as carbon, positive pions will be produced. The energy distribution of these pions, only recently determined (Crawford et al., 1980) down to the low regime important for surface muon production, makes it possible for some to come to rest close to the surface of the production target (a 13 MeV pion has a range close to 1.0 $g \cdot cm^{-2}$). These pions may arise from proton interactions anywhere in the target, as long as the pion energy corresponds to a range which is the amount of target material which must be traversed in order that it just reaches the surface. One does not want the target to be much larger than the proton beam profile, then, because the surface muon rate depends on the solid angle subtended by the surface averaged over the proton interaction region (neglecting any anisotropy in the pion production angles).

There are two other reasons that small production targets are desirable. The first is obvious; a smaller muon source will lead to a smaller muon beam spot in a channel with reasonable optics. The second involves contamination of the beam by positrons. Below a momentum of 52.8 MeV/c, the maximum positron energy from muon decay at rest, the positrons in the beam come both from conversion of gammas from neutral pion decay and from muons decaying in the production target. The former are much reduced by the use of small, low Z targets since conversion of gammas is less likely. The latter may be dealt with by beam separation techniques.

One such separation technique which has been applied for surface muons (Reist et al., 1978; Arnold et al., 1979b) is the use of a few $mg \cdot cm^{-2}$ of degrader material at an appropriate focus before the final bend in the beamline. Since the muons lose more energy in this degrader than do positrons, the two components of the beam will be spatially separated after the next bending element. This technique has been observed at TRIUMF to have some adverse effect on final muon beam spot sizes.

A schematic diagram of the M13 channel is shown in Figure 3.2.1.1. Viewing the primary production target at an angle of

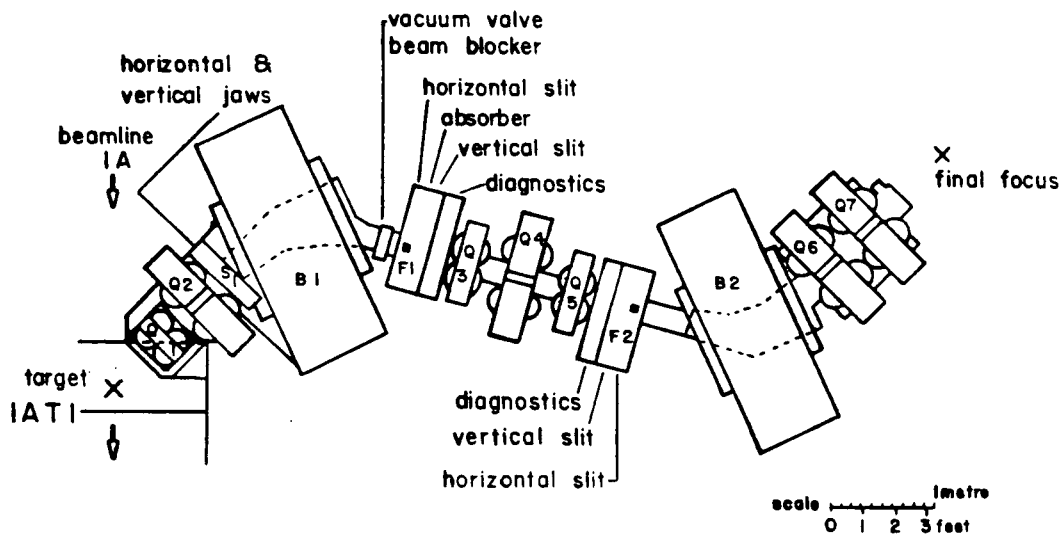

Figure 3.2.1.1. The M13 pion/muon channel at TRIUMF .

135° to the 500 MeV proton beam, it consists of nine magnetic elements; two quadrupoles, a 60° right bending dipole, three more quadrupoles, the second 60° left bending dipole, and the final two quadrupoles. A vacuum box with remotely controllable

vertical and horizontal jaws, to define the beamline acceptance and determine flux, is positioned between Q2 and B1. Between B1 and Q3 is the first dispersed focus, F1. Horizontal slits determine the segment of the dispersion plane to be used, thereby allowing control of the momentum acceptance, while vertical jaws can be used for flux limitation and the reduction of scattered beam particles. Two four-position wheels, supporting various thicknesses of polyethylene sheet, are also near F1, and can be used to reduce contamination by unwanted particles (positrons in a surface muon beam, or protons in a pion beam). An equivalent (by the symmetry of the channel) dispersed focus F2, between Q5 and B2, is equipped with another set of vertical jaws and horizontal slits. Though to some extent redundant, this set can reduce the tails of the final beam profile arising from particles scattered in the beam tube further upstream. All magnet power supplies (except B2, at this writing) as well as slits, jaws, and absorber are controlled via microcomputer through CAMAC interfaces or through the remote controls system maintained by TRIUMF .

Figure 3.2.1.2 shows the particle fluxes measured from a 1.45 mm graphite target available when the channel was first commissioned. Note the dramatic surface muon peak at 29 MeV/c. The low electron contamination is obtained by the use of thin, bare, production targets, with no extraneous surrounding materials. Presently available targets (used in the conversion experiment) include 2.0 mm and 10.0 mm graphite pieces, and scaling of muon fluxes with target thickness is in this case reliable. Figures 3.2.1.3 and 3.2.1.4 show the effect of horizontal slits and jaws on particle flux and beam spot

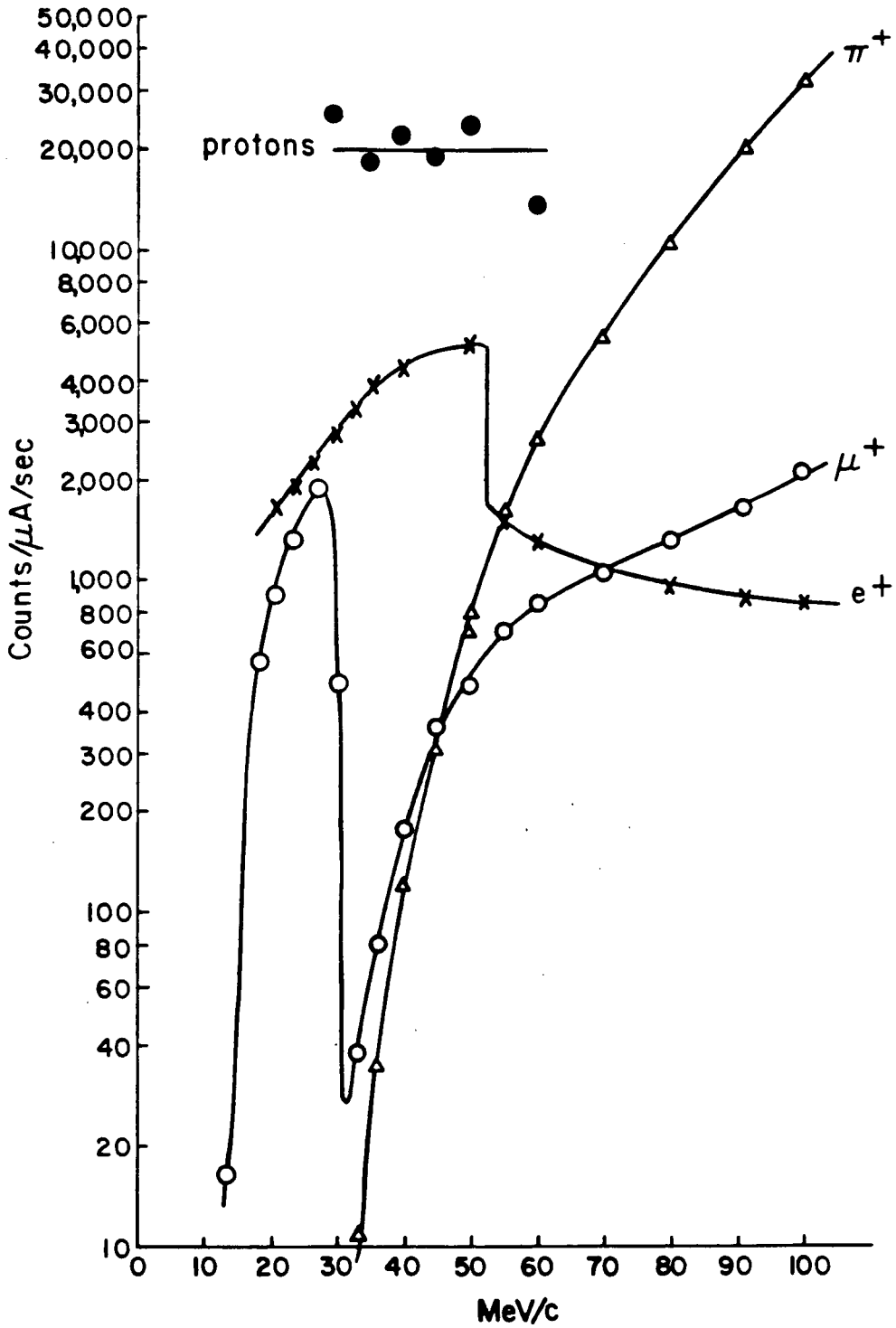

Figure 3.2.1.2. M13 positive particle fluxes from a 1.45 mm graphite target.

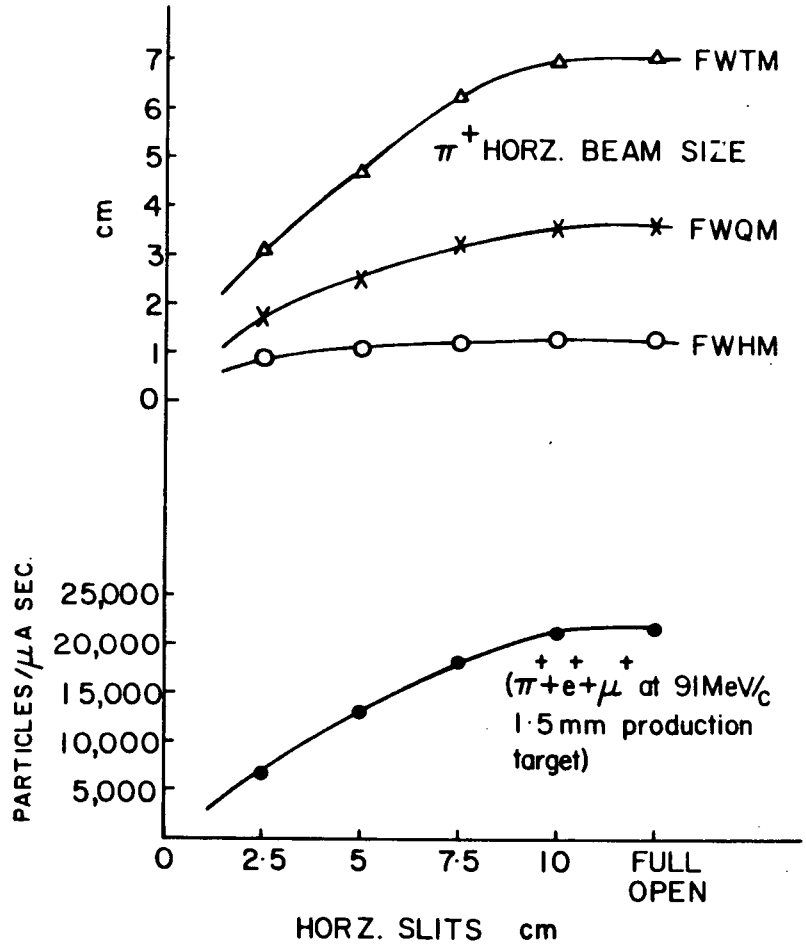

Figure 3.2.1.3. Effect of horizontal slits on M13 particle flux and beam spot dimension.

dimension, in terms of full width at half, quarter, and tenth maximum. Finally, the effect on surface muon rates of the positioning of the primary proton beam on the production target is shown in Figure 3.2.1.5, along with a curve estimated by C. J. Oram based on simple assumptions on the mechanism of surface muon production; specifically, the probability that a pion originating at any point in the target stops in a surface layer is taken to be proportional to the product of the solid angle subtended by, and the length of the pion track in, the

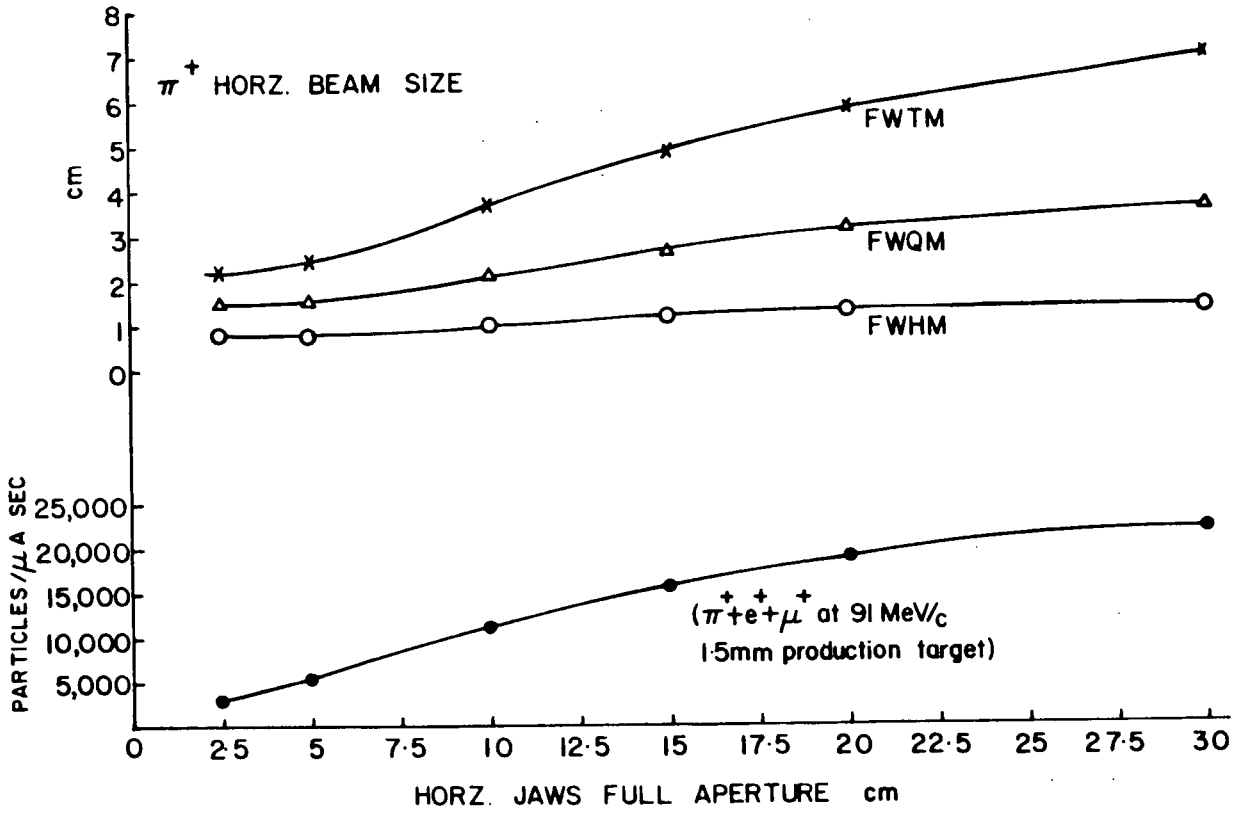

Figure 3.2.1.4. Effect of horizontal jaws on M13 particle flux and beam spot dimension.

layer. The width of the proton beam was realistically assumed to be 1.0 mm (FWHM). The gross features of the data are reproduced surprisingly well. Further details on procedures used in tuning the channel and measuring the beam properties have been published (Oram et al., 1980).

The beam tube is held under vacuum by pumps on the primary proton beam line, which in turn is contiguous with the main cyclotron vacuum. No windows exist between the primary production target and the end of the beam tube. The end consisted, for this experiment, of a 0.127 mm (0.005") Mylar window of 7.6 cm (3.0") diameter, through which surface muons

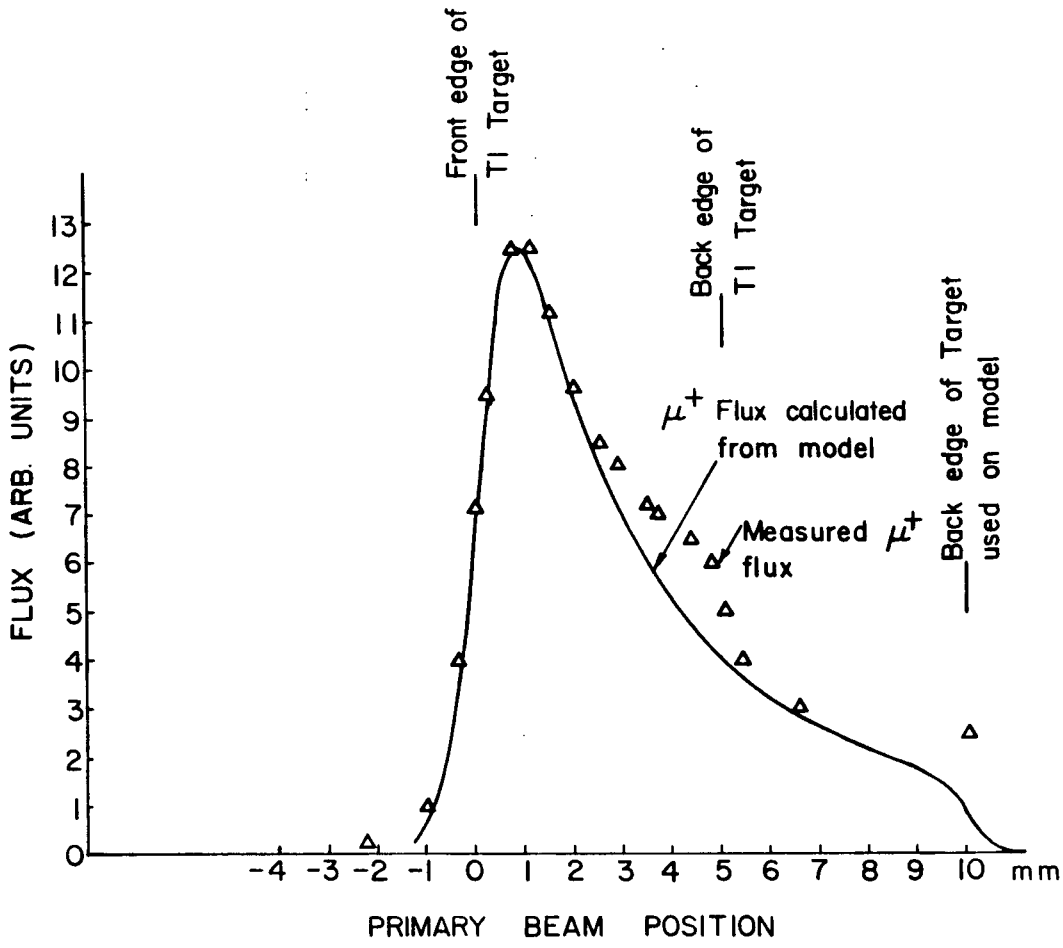

Figure 3.2.1.5. Surface muon rate versus proton beam position on the production target.

will easily pass.

Although a flux of 10^6 surface muons per second could be obtained for 100 μA proton current incident on a one centimeter production target, the experiment was run at about 10^5 s^{-1}. The reduction was due to a lower proton current and/or the use of a 2.0 mm production target, as well as a slight closure of the horizontal jaws to reduce the positrons in the tails of the beam profile. The range of the muons (figure 3.2.1.6) was 135 $mg \cdot cm^{-2}$ Mylar, with an apparent range spread of about 25 $mg \cdot cm^{-2}$

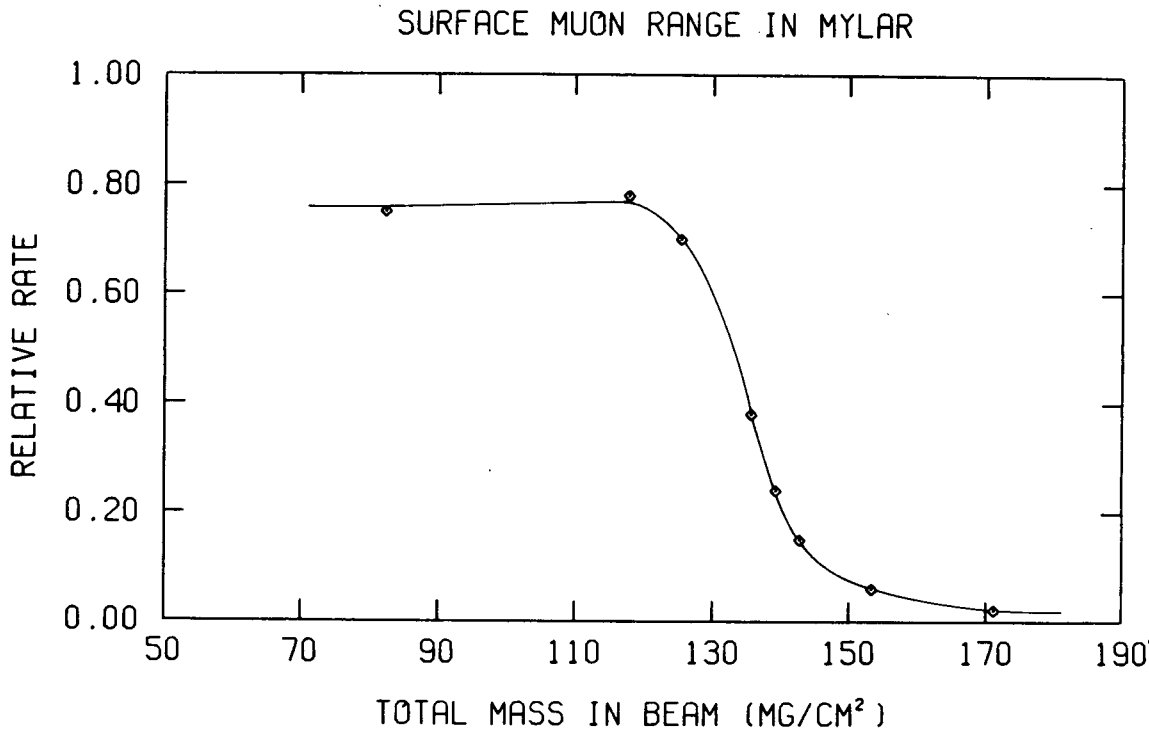

Figure 3.2.1.6. Surface muon integral range curve.

(FWHM).

3.2.2. The Target: Production of Muonium in Vacuum

It has been pointed out that a sensitive conversion experiment cannot be performed without the production of muonium in vacuum. It is the purpose of this section to describe the target and indicate, in a qualitative way, how muonium may be produced in vacuum. More detailed rate estimates can be found in section 4.2.2, with reference to appendices A2 and A3.

The target consisted of a sloping stack of seventeen identical elliptical expanded polystyrene frames supporting thin collodion films. Each film in turn supported, on the upper downstream surface, a thin fluffy layer of silica powder for muonium production. The lower, upstream surface was coated with calcium oxide in which antimuonium could give rise to an easily recognizeable muonic X-ray (see Figures 3.2.2.1 and 3.2.2.2).

Each frame was a ring, 3 mm thick by 8 to 10 mm wide, of

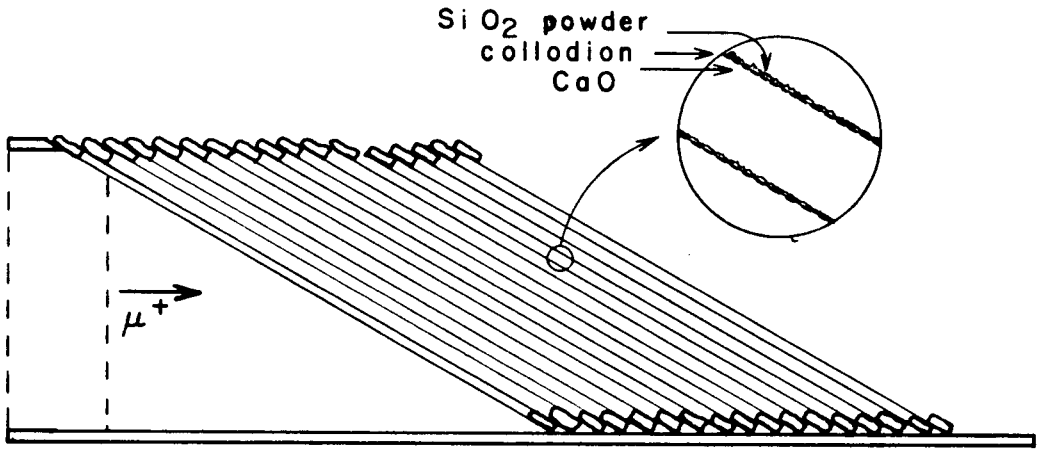

Figure 3.2.2.1. Illustration of the target used for muonium production in vacuum.

roughly elliptical shape (20 cm major by 10 cm minor axis lengths). The frames were heat treated for strength and vacuum compatibility. The collodion film was created by first dissolving a chip of collodion (cellulose nitrate, trade name Parlodion, from Mallinckrodt Chemical) in amyl acetate to produce a three to five per cent solution, then floating a milliliter of solution on a clean water surface, allowing the amyl acetate to evaporate. The residual collodion film could

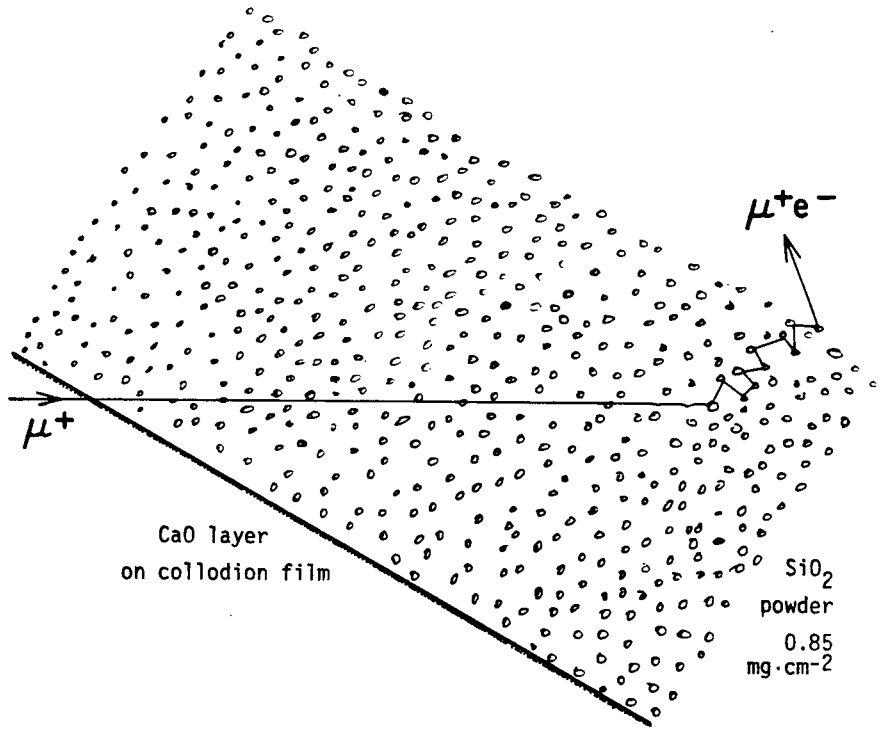

Figure 3.2.2.2. A single layer of the target, illustrating the mechanism of muonium production in vacuum.

then be picked up by sliding the frame in the water beneath the film and gently removing it from the water surface with film attached. The mean weight of collodion attached to a frame was 17 ± 6 mg, corresponding to an average film thickness of 0.11 mg•cm^{-2}.

The only function of the collodion was to support the active constituents of the target, the silica and the calcium oxide. The silica, in the form of a very fine (particle diameter 7 x 10^{-7} cm, density 0.032 g•cm^{-3}, or 0.015 times that of bulk silica) powder, is known to produce muonium copiously in the intergranular voids (Marshall et al., 1978; Kiefl et al.,

1979). However, the estimated thermal muonium collision rate with powder particles, about 2×10^{10} s^{-1}, makes the powder itself unsuitable for antimuonium conversion. By using a thin layer of powder, there is some chance that muonium can escape the voids into a true empty vacuum (the actual probability of escape will be calculated in the fourth chapter). The target employing the collodion substrate was constructed to take advantage of this.

The reason for the slope of the target is twofold. In the first place, it means that the silica powder can rest on the surface without falling off; the alternatives would be to use a vertical muon beam, placing the layers horizontally, or to stick the silica to the collodion by other means, possibly destroying its muonium production properties. Neither seemed practical. The second reason is that it doubles the length of material per layer in the beam direction for a given layer thickness, thereby stopping more muons near the layer surface.

Prior to the application of the powder layer and final assembly of the target stack, two things were done. First, the individual foils were lightly moistened on one surface with a spray of an acetone-water mixture and dusted with silica powder. Only a tiny amount (0.04 ± 0.02 $mg \cdot cm^{-2}$) of the silica adhered to the collodion after the liquid evaporated, but it served to roughen the surface considerably. This was important for reasons which will soon become apparent. Secondly, a thin coating of calcium metal was evaporated onto the other surface and allowed to oxidize in a dry atmosphere. The resulting calcium oxide film was estimated to average five to six micrograms per square centimeter, but precise weighing was

difficult since the heat from evaporation of the calcium metal tended to drive moisture from the collodion film, while the oxide would convert to hydroxide and/or carbonate in a period of minutes during weighing. Comparisons of weights before and after evaporation were thus only approximate. The conversion reaction of the oxide was eliminated by keeping the target foils in a dry, inert environment until insertion into the evacuated target region at the end of the M13 beam line.

The final step was the building of the stack with powder lightly dusted on one surface of each foil. The first frame was mounted, on an expanded polystyrene support structure, with the major axis making a 30° angle with the horizontal, calcium oxide side down. On the upper, roughened surface was sprinkled (with the aid of fine mesh screen) silica powder. A second frame was similarly placed adjacent to the first and lightly glued in place, then sprinkled with more powder. This procedure was continued until all seventeen foils were in place, each supporting approximately 0.85 $mg \bullet cm^{-2}$ of silica. The final foil was not sprinkled. The roughness of the collodion film, after the treatment mentioned previously, made the powder stable to small vibrations; it would not slide on the 30° incline when carefully handled.

The average perpendicular distance between films was measured to be 4.4 mm, while the physical thickness of the powder layer was 0.3 mm. With this information, and reasonable assumptions about the motion of muonium within the powder layer, an estimate can be made of the probability of muonium conversion to antimuonium. This will be calculated in section 4.2.2, using the formulae derived in appendix A3. It is sufficient at this

point to have a more general idea of the mechanism. Muons thermalizing in a target consisting of layers of evacuated silica powder (as used on the collodion films) form muonium atoms in the intergranular void with high probability. The muonium atoms are free to move at thermal velocity among the grains, undergoing collisions and migrating macroscopic distances in the 2.2×10^{-6} s muon lifetime. A fraction of the atoms, especially those formed near the surface of a layer, actually leave the vicinity of the powder and travel without collision across the gap between films. The transit times approach the mean muon lifetime for spacings of the order of one centimeter. For this small fraction of the incident muons, the opportunity for conversion is nearly maximized. Moreover, any atom that does convert to antimuonium can be torn apart on collision with the atoms or molecules on the facing surface (calcium oxide, in this case), which can in turn lead to a muonic 2P-1S X-ray, the signature of a conversion event.

3.2.3. Magnetic Field Measurement and Control

A factor of two in the sensitivity of the experiment is gained by forming muonium in a region where magnetic fields are of the order of ten milligauss or less (see equation 2.1.4.1 and Figure 2.1.4.1). This was accomplished at TRIUMF by the use of three mutually perpendicular Helmholtz pairs and a sensor which controlled their power supplies to compensate automatically for changes in the ambient field.

The problem of creating a uniform magnetic field (or gradient) can be approached from several points of view. The most elegant and efficient procedure is the construction of a geometrically correct array of current loops, creating a central field free of undesired gradients to the required order (Garrett, 1967). Consider pairs of circular coaxial current loops above and below a plane of symmetry, such that the current in each member of a pair travels in the same sense (for the creation of a gradient, the current would be in the opposite sense). The currents will create an axial field at the intersection of the plane of symmetry and the axis, which, by the symmetry, has no first or higher odd derivative along the axis. With only one pair, the separation of the coils can be specified to null the second derivative, and the Helmholtz condition results. Further pairs with different separations and/or currents can be added to null fourth, sixth, etc., derivatives, provided that problems in computation of the correct parameters can be overcome.

If one can tolerate a sacrifice in efficiency, in terms of field produced per kilowatt of power consumed, amount of materials needed, and overall size, a large volume of uniform field can also be produced by making the initial Helmholtz pair large, with no nulling of higher derivatives. An advantage of this approach, for a practical system within which an experiment can be erected, is that the region of uniformity is well away from the coil winding, so that large detectors can be accommodated entirely within the structure quite easily. Since the liquid nitrogen reservoir dewars on the germanium crystals used were bulky, and a large field was not required, it was

decided to opt for a large Helmholtz assembly.

The three mutually perpendicular pairs which were built were square rather than circular, to make fabrication more simple. The x, y, and z coils measured 189, 196, and 204 cm on a side, respectively. Blocks enabled attachment of one pair to each of the other two at the twenty-four points (four on each face of the cube) of proximity of the frames. For square coil geometry, the Helmholtz condition is that the separation should be 0.855 times the dimension of the square.

By far the largest field component that had to be eliminated was due to the cyclotron fringe field, approximately three gauss in the vertical (z) direction. Moreover, it was at some times desireable to apply a vertical field for muonium spin rotation tests on various samples, including the conversion target. Therefore, allowance was made for a ±10 gauss range vertically and a ±1 gauss range both in the beam direction (+x) and perpendicular to it (y). The z coils consisted of 2 x 260 turns of AWG 12 copper conductor, capable of sustained operation at 140 V and 5 A. The x and y coils were each 2 x 52 turns of AWG 14, operating at up to 36 V and 5 A.

The coils were wound on frames of kiln-dried oak. The reason that metallic forms were not used is that the currents induced in them by variations in the coil current at up to 200 Hz would restrict the frequency bandwidth for the production of a.c. magnetic fields. The aim was for the system to be capable of eliminating at least 60 Hz variations in the ambient field, when used in conjunction with the magnetometer controller and feedback system.

The coils were powered by Kepco bipolar operational power

supplies. A 36 V, 5 A supply was used for each of the x and y pairs, and two 72 V, 5 A units energized the z coils. The outputs were governed by a Schonstedt HCM-3 triaxial magnetic field control unit, which also constantly monitored the three magnetic field components produced at a triaxial magnetometer probe placed on the z axis near the center of the Helmholtz array. In this manner, the controller, power supplies, coils, and magnetometer probe formed a loop such that variations in the ambient magnetic field components were automatically measured and compensated for.

Although most accelerator-oriented physicists have a working knowledge of the principles of measurement of higher magnetic fields (e.g., NMR, Hall effect), the operation of the saturable inductor magnetometer, a device useful at zero and very low fields, may be less familiar. If a magnetic field is induced in an easily saturable material with a sinusoidal driving current of frequency f through a solenoidal primary coil, that field can be sensed by a secondary coil. In zero ambient magnetic field, the output of the secondary will be a sine function with flat tops and bottoms corresponding to the saturation of the material. A Fourier decomposition of the function will include frequencies 3f, 5f, and so on. If a nonzero field component exists along the solenoid axis, the waveform on the secondary coil will flatten at points on the sine curve which are displaced from the zero field values by an amount corresponding to the applied field component (see Figure 3.2.3.1). The Fourier spectrum will then also contain harmonic terms of the even frequency multiples 2f, 4f, and so on. Circuitry to sense one of these frequencies can be made to cause

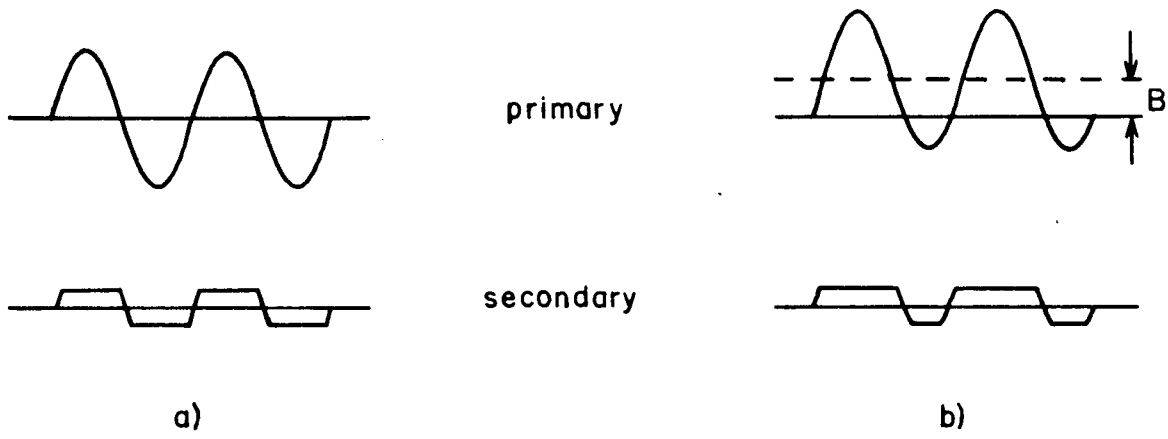

Figure 3.2.3.1. Saturable inductor magnetometer waveforms
(a) in zero ambient field.
(b) with a nonzero field component B.

a d.c. current through the primary coil (in addition to the sinusoidal driving current) such that the even components are eliminated; the value of the required d.c. current is then proportional to the ambient field component along the solenoid axis. With fundamental frequencies in the kHz range, slowly varying (i.e., up to 200 Hz) a.c. magnetic fields can also be measured.

Setting the three field components to zero was accomplished via an independent, uniaxial saturable inductor magnetometer (Hewlett Packard model 3529A probe and 428BR controller). The zeroing of this probe was in turn accomplished by insuring that accurate rotations of the probe by 180° caused equal but opposite field measurements. After some iterations, each of the three field components at the coil centre could be reduced to one milligauss or less, well within the tolerance of an antimuonium conversion experiment.

Field gradients, however, presented another problem. Since the target was approximately 10 cm long, a gradient of only two milligauss cm^{-1} was sufficient to exceed the criterion of less than ten milligauss in the stopping region. Although the theoretical applied field uniformity satisfied this demand, the ambient field uniformity did not. It was thus difficult (and pointless) to determine whether the coils were operating at the designed field homogeneity. The lowest maximum gradient that could be obtained under beam conditions, using iron blocks external to the coils for trimming purposes, was four milligauss cm^{-1}. The solution to the gradient problem was a sheet of mumetal, 0.25 mm thick and 35 cm long, wrapped around the vacuum pipe containing the target (see Figure 3.2.4.1). With this in place, along with the compensation provided by the coils, the maximum gradient was reduced to less than one milligauss cm^{-1}, and field surveys at the beginning and end of the data taking showed no component in excess of 3 ± 1 milligauss over the entire target region.

3.2.4. Detectors and Hardware in the Target Region

The gamma rays from a myriad of processes in the target region (and elsewhere) were detected via two independent germanium detectors on either side of the target enclosure, approximately 8 cm from its centre. A diagram of the layout comprises Figure 3.2.4.1.

Both detectors were large, high efficiency, coaxial,

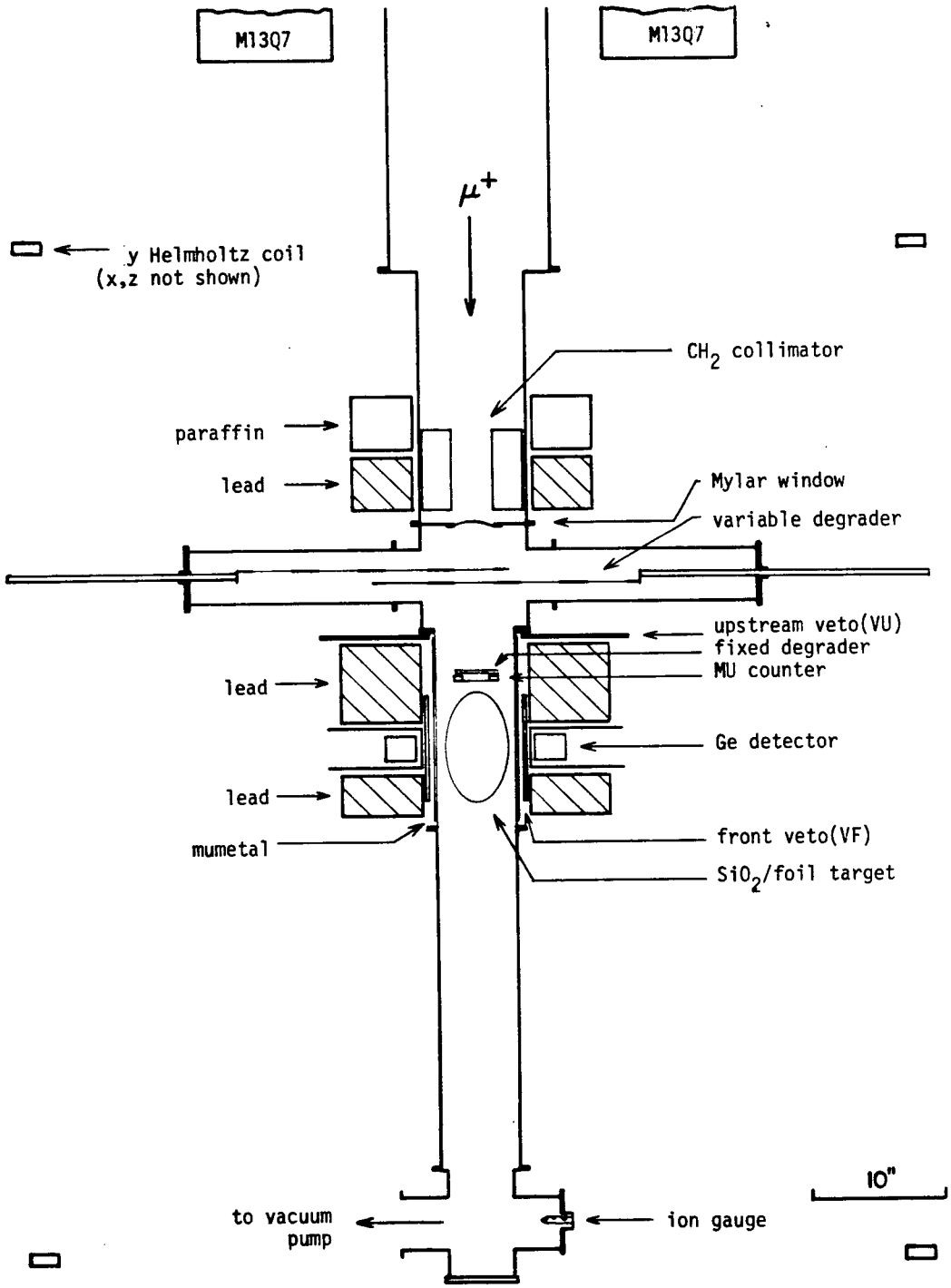

Figure 3.2.4.1. Schematic of muonium conversion apparatus.

cooled-FET germanium devices, but were otherwise dissimilar. One was an Ortec lithium-drifted crystal of 51.55 mm diameter by 55.5 mm length (active volume 103.2 cm^3) while the other, an intrinsic germanium detector of 48.53 mm diameter by 40 mm depth (active volume 71.5 cm^3), was manufactured by Aptec. Curves representing the photopeak efficiencies of each detector, as a function of photon energy, are displayed in Figure 3.2.4.2. The

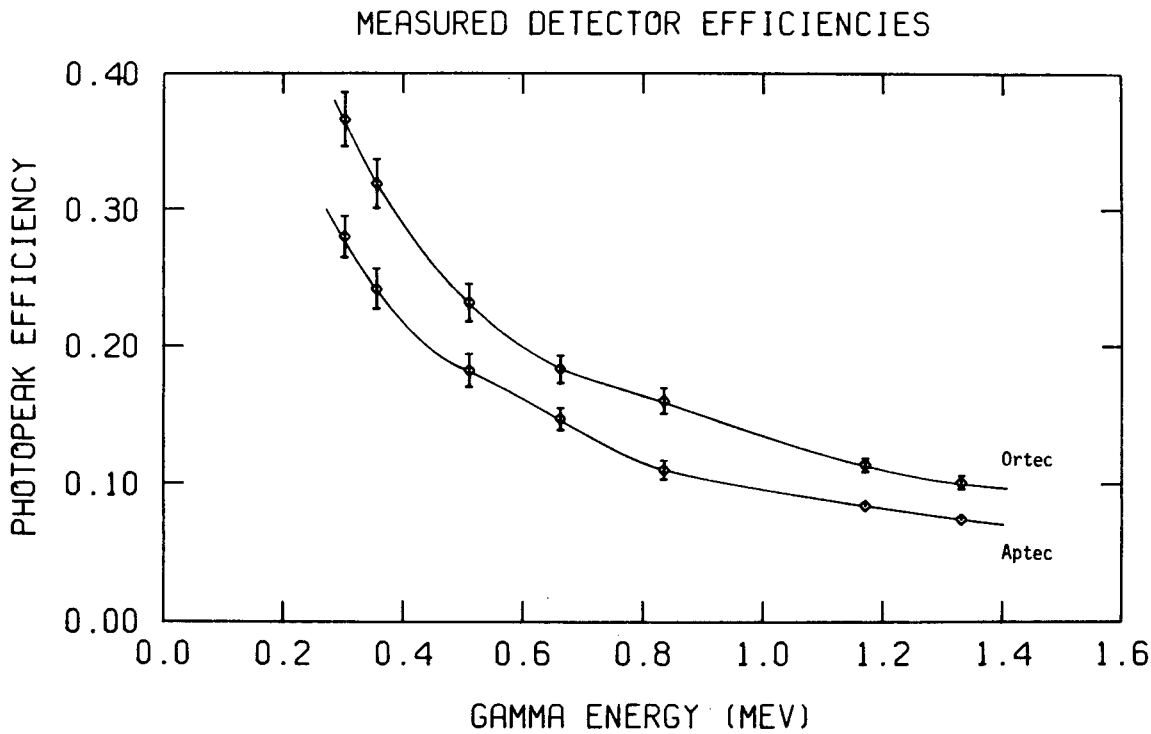

Figure 3.2.4.2. Photopeak efficiencies versus energy for the two detectors used.

curves will be referred to in the analysis presented in the next chapter. Both detectors were warranted for a resolution of better than 1.9 keV (FWHM) at 1.33 MeV, and in practice

surpassed that figure. Other features of the target region may be noted from figure 3.2.4.1. For instance, a 0.25 mm scintillation counter (MU) of 5 cm diameter identified incoming muons, distinguished by pulse height from the positron contamination in the beam. A surface muon will deposit more than six times the energy in a thin scintillator that a beam electron will (Trower, 1966). With good light collection, the pulse height difference makes for easy discrimination between the two particles. Immediately upstream of this counter, a 0.20 mm fixed Mylar degrader ranged the muons to stop in the silica/collodion target. Fine range adjustments were made by selecting appropriate additional thicknesses of Mylar from several mounted on two frames which could be adjusted by mechanical vacuum feedthroughs. In addition to a 0.12 mm (7.5 cm diameter) Mylar window separating target from beamline vacuum systems, a further 0.15 mm was required to maximize the stopped muon rate.

Two veto scintillation counters (VF) detected charged particles approaching the germanium detectors. Muons decaying to positrons of up to 52.8 MeV were one inevitable source of background radiation problems which could be alleviated by the veto counters. Further suppression of undesirable radiation in the germanium crystals was accomplished by shielding with polyethylene, paraffin, and lead. An explanation of the background problems encountered is contained in the following section.

3.3. Data Acquisition

Data were collected in a very simple fashion. Most of the procedures employed originated in pionic and muonic X-ray experiments. This is not to say that no particular problems emerged; on the contrary, the operation of large germanium detectors in close proximity to a stopping beam of over 10^5 muons per second required some special tactics. In this section, a description of the sources of radiation entering the detectors will be given. The steps taken to minimize the impact of background sources on the data are also discussed. The hardwired processing of information from counters and detectors is described in detail, with an explanation of the logic of the electronics used. Finally, a subsection is devoted to a summary of the conditions under which the data were accumulated and stored, including experimental parameters such as rates.

3.3.1. Primary Sources of Background and Their Minimization

The sensitivity of the TRIUMF experiment to a possible muonium-antimuonium coupling depends in part on the likelihood of processes resulting in background gamma radiation of similar energy to the muonic X-ray processes of interest. The rule of thumb states that the square root of the number of background gammas, accumulated within the full width at half maximum (FWHM) of the expected X-ray, determines the minimum number of

foreground events necessary for observing an effect of one standard deviation (68% confidence level). Therefore an understanding of the backgrounds present and the procedures for their reduction is of some importance.

The sources of the radiations of interest may be categorized as follows:

1. Muon decay positrons: It is essentially certain that a positive muon will decay to a positron with an energy following the Michel spectrum, up to a maximum of 52.8 MeV. Bremsstrahlung energy losses of the positrons result in a continuum of gamma rays, up to the full energy. Some gammas are within the muonic X-ray energy region (either initially or after subsequent Compton scattering). The positrons eventually annihilate with electrons, giving mostly two 0.511 MeV photons per annihilation. The positrons themselves can enter the detector, depositing energy directly by radiation and ionization: most such particles leave more than a few MeV in the germanium crystal (unlike the gammas of interest) since the radiation length is about 2.2 cm (or 12 $g \cdot cm^{-2}$; see Particle Data Group, 1976).

2. Beam positrons: Approximately one half to two thirds of the beam entering the target is positrons, the sources of which were explained in section 3.2.1. Like the muon decay positrons, they can radiate and produce the troublesome bremsstrahlung background. On the other hand, they tend to remain a beam, passing through the very light target and out of the apparatus

where they do little harm. A very small number undergo large angle scattering, creating problems similar to those caused by decay positrons.

3. Other sources: Included in this category are the induced nuclear gammas from material in the vicinity of the detectors, direct neutron activation of the detectors, and cosmic rays. Some energy structure is of course present in this background; most notably, a 0.835 MeV ^{54}Mn line appeared close to the 0.784 MeV calcium muonic 2P-1S line which was searched for as a conversion signal. Rather than presenting a problem, this line proved to be a valuable calibration during the analysis.

The decay positron background was the most severe and the most difficult to deal with. This fact had been anticipated; several features were incorporated into the apparatus to mitigate the problem.

First of all, it was apparent that muons stopping near or in the target, but not in the active regions, should be eliminated. The low thickness and stopping power of the collodion films was important for this reason. Control of the muon beam spot size via M13 jaws was an asset, especially as it reduced the flux in the tails of the beam distribution. The degrader (including the defining scintillator) necessary for ranging muons into the target was as close to it as possible. This was found to be crucial because of the large multiple scattering suffered by the slow muons. Without the collodion target in place, the muons stop mostly in the walls of the vacuum tube in the target region or slightly downstream of it,

so the background due to decay positrons was not much reduced by its removal.

The second feature built into the apparatus initially was a length of aluminum tube spun to a wall thickness of 1 mm, which constituted the vacuum pipe in which the target would be placed. It was expected that this would minimize the radiative energy loss by the positrons in the vacuum tube wall, and hence the bremsstrahlung entering the detector (similar reasoning led to the use of expanded polystyrene as a support material for the collodion). However, the spun aluminum tube was abandoned for a pipe of 3 mm wall thickness, after a measurement of gamma count rates in the energy range of interest, as a function of the amount of aluminum between target and detector, revealed a difference of less than five per cent. It should also be noted that this was performed before extensive shielding of the detectors was undertaken, and other sources of (positron independent) background were dominant. The experimenters were not unhappy at the change, since many precautions had to be observed in using the thin tube: an identical one had buckled while being used under vacuum by another group at TRIUMF! In addition, a flange could be welded on the thicker pipe which allowed the final degrader and defining scintillator to be installed much closer to the target, further reducing the beam loss due to multiple scattering.

Thirdly, scintillation veto counters were installed. These could be used in fast coincidence (see section 3.3.2 following) with pulses from the crystals to veto events associated with charged particles in and near it. Initially a set of three scintillators covered all but the rear face of each detector.

This arrangement was modified when a high background, uncorrelated with beam in M13 (i.e., "other sources"), necessitated more extensive lead shielding surrounding the detectors and thus conflicting with the scintillators physically. Eventually a large, 20 x 20 cm^2 counter, 0.65 cm thick, was used in front of each detector. The large counter size aided the reduction of background events due to the bremsstrahlung of positrons in the lead shielding.

As an aside, the choice of a calcium oxide coating for the production of possible muonic X-rays was also motivated partially by background considerations. The 2P-1S energy of 0.784 MeV (Engfer et al., 1974) is above the positron annihilation background yet still low enough to be detected with reasonable efficiency. Another reason for the choice is the low evaporation temperature of Ca, which the fragile collodion films can at least sometimes withstand (many were ruptured during preparation).

The procedures adopted because of muon decay positron background were often also effective for the minimization of beam positron effects. Some further effort in this direction included the trimming of slits and jaws to reduce the beam halo. Positrons, light particles that they are, can undergo large deviations during Coulomb scattering from a nucleus. This takes place along the length of the beam line, causing those not ordinarily within its momentum and coordinate acceptance to emerge in a broad smear. By closing otherwise unnecessary slits and jaws to the point just short of reducing the muon flux, some of the smear was removed. In addition, paraffin and polyethylene shielding immediately upstream of the muon target

removed some of the halo with minimal radiation release, which was in turn dealt with by substantial lead shielding (see section 3.2.4).

By remotely inserting a small amount (about 30 mg•cm^{-2} CH_2) of degrader at F1, one could displace the muon beam at the end of M13 such that it did not pass the upstream polyethylene collimation. The beam positrons still remained more or less undeviated, so it was quite easy to see their contribution to the gamma spectrum. It turned out to be much smaller than that due to decay positrons, as was expected.

The background due to sources other than decay or beam positrons was initially larger than expected. It was not clear at the outset whether optimum sensitivity would be achieved with or without extensive lead shielding of the detectors; in some cases, especially with relativistic electrons or positrons present, it can act as a gamma source because of shower production. By testing the effect of shielding, it was determined that, at the moderate rates used, about half of the gamma background was not beam related and could be drastically reduced by careful placement of lead blocks. Neutrons were part of the problem, partially alleviated by the construction of a concrete and paraffin wall at the maze entrance to the proton beam tunnel adjacent to M13, where some neutrons seemed to originate. Characteristic neutron lines (Bunting and Kraushaar, 1974) were observed in the gamma spectra. One line came very close in energy to the 0.784 MeV calcium line(more discussion on this will appear in section 4.1). A substantial positron annihilation peak was observed even with M13 shut off, probably from primary proton interactions such as neutral pion gamma

conversion in the production target. Some further lines were identifiable, but only the aforementioned ^{54}Mn line was close in energy to the region of interest.

It suffices to say that the background problem was dealt with mostly by trial and error. By changing various parameters, one could determine the best method of lessening a particular background rate. Several different aspects of the apparatus were at this stage designed, tested, or altered. This evolution was paralleled by similar development of the electronic hardware arrangement, the subject of the forthcoming section.

3.3.2. Electronics Configuration Used

The function of the data acquisition system was to obtain energy information about the spectrum of gamma rays below approximately 1.0 MeV, originating in the target. The task of the electronics was to ensure that the events obtained satisfied some simple criteria. Apart from the suppression of background events, the most important aspect of this selection related to the maintenance of the high resolution capability of the germanium spectrometer. The sensitivity of the experiment depended on, among other things, the resolution obtainable.

A detailed diagram of the circuitry that was used in taking data is shown in Figure 3.3.2.1. Some units, denoted by an x, are duplicated in the actual system to handle two detectors. An attempt will be made to explain, in the remainder of this section, the logical arrangement of the important components.

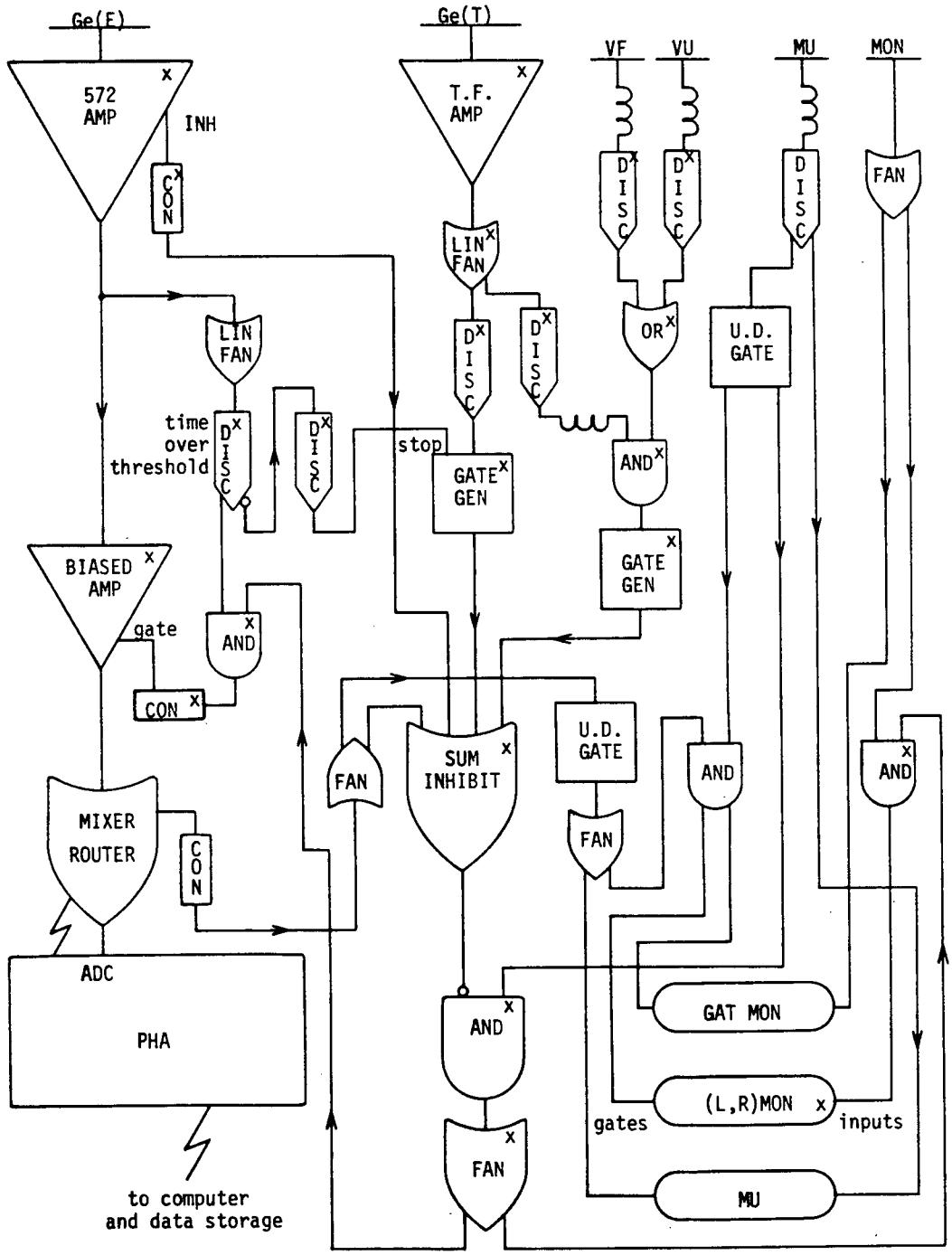

Figure 3.3.2.1. Electronics diagram for circuit used (see text).

The electron-hole pairs, created in the germanium crystal by the passage of ionizing radiation, cause a sharp (~50 ns) change in the voltage output of the charge sensitive preamplifier on the detector. This signal, denoted as Ge(E) in the figure, is shaped and amplified further, so that the peak voltage (something less than 10 V) is proportional to the energy deposited in the germanium, for the energy range of interest. The BIASED AMPlifier further amplifies a selected range of the analog signal, if a logical gating pulse has been properly applied. From there, the signal is fed through a MIXER ROUTER into a pulse height analyzer (PHA). It is digitized by that unit's analog to digital converter (ADC) and the appropriate channel of one of the two 2048 channel histograms is incremented, depending upon which detector saw the event.

The amplifier output also feeds a linear fan-in fan-out (LIN FAN) which inverts the positive analog pulse for input into a NIM discriminator (DISC) operating in the time-over-threshold mode. This unit performs two functions, the first being to pulse the GATE input of the BIASED AMP if several gating conditions have been met. The second is to define the end of the analog pulse. The trailing edge serves to fire a further DISCriminator which in turn stops a GATE GENerator that eventually inhibits gating of the BIASED AMP .[1]

This second function is an important one. It was found that the large energy deposited in a germanium crystal by the fast electrons could saturate the preamplifier, causing the

---

[1]The author is grateful to J. A. Macdonald for suggestions regarding this particular point.

amplifier to "hang up" at a non-quiescent value of about eight volts for varying periods of up to 40 μs. This was a real source of dead time, especially for the Aptec intrinsic germanium detector whose preamplifier was not as capable of handling the highly ionizing energetic positrons. Furthermore, a certain loss of energy resolution and photopeak symmetry was a consequence of the poor baseline definition in the long pulse tails. The circuit deals with this in the following way. Whenever a large pulse occurs, it is amplified (by the T.F. AMP) to fire a discriminator, starting a GATE GENerator that inhibits gating of the BIASED AMP. The inhibit is removed only when a quiescent (less than about 50 mV) level is sensed by the time-over-threshold DISCriminator.

Three other signals serve to inhibit gating of the BIASED AMP, each fanning in to the SUM INHIBIT unit. One is derived from the BUSY signal of the PHA through the MIXER ROUTER, while another (INH) comes from special pile-up circuitry of the main amplifier (572 AMP). The latter maintains resolution at the expense of accepted rate for high count rates. Both must pass through a TTL-NIM level converter (CON). The third inhibit occurs when either veto scintillator, front (VF) or upstream (VU), fires in fast (i.e., within about 40 ns) coincidence with the amplified timing output (Ge(T)) of the detector. As mentioned in the previous section, this serves to reduce counts due to showers from charged particles in the lead shielding around each detector. Constant fraction discrimination (CFD) is used on detector timing signals. Other timing in the circuit is slow, and gate lengths are in the microsecond range.

The SUM INHIBIT fan blanks any output from an AND gate

enabled by an updating 12 μs gate (U.D. GATE) in turn initiated by an incident muon firing the defining counter (MU). At the rates used in the experiment, the 12 μs gate was on virtually whenever the beam was on, and there was a reasonably high probability of two muons being in the target at one time. The major function of this gating is to protect the spectrum from background occurring during occasional cyclotron trips of anywhere from a fraction of a second to several hours duration.

Most of the remainder of the circuitry measures numbers vital to the analysis of the experiment, the total muons incident and the fractional live time. Incident muons are identified by pulses from the MU defining counter, and are counted in a scaler enabled whenever the PHA is collecting events.

The live time measurement is slightly more complex. One scaler measures a quantity labelled gated monitor (GAT MON), which is accumulated when the PHA is collecting events and the updating muon gate (U.D. GATE) is on (necessary for an event to be gated through the BIASED AMP and measured by the PHA). A second and third scaler (only one of which is shown in the diagram) measure left (LGM) and right (RGM) counts. These require the same gating as GAT MON, but are inhibited by SUM INHIBIT, which also inhibits gating of the BIASED AMP, that is, the measurement of an event. The fractional live time for a particular detector is just the ratio of the corresponding left or right gated monitor to GAT MON. The monitor used in the experiment consisted of periodic pulses derived from a pulse generator.

This completes the description of the operation of the

electronic hardware; the remaining section will deal with the actual procedure of data accumulation using the described system.

3.3.3. Accumulation and Storage of Data

With all the equipment set up, the magnetic field adjusted to zero, and the target quickly and carefully transferred from its dry storage to the vacuum (5×10^{-7} mm Hg) of the target tube, the surface muon beam was allowed into the target region. The first task was to adjust the degrader for a maximum stopping rate in the foil target. This was accomplished by scaling the energetic positron events in the detectors in coincidence with the front veto (VFL and VFR) scintillators, and maximizing the rate. After a short calibration run using sources with the beam on, the first of ten runs of actual data taking began. The incident muon rate was typically about 1.7×10^{5} s^{-1}, using 25 μA of proton current carefully steered onto a graphite production target of 10 mm thickness. Several hours of accumulation time, corresponding to a few billion incident muons, made up each run, after which the data were recorded, along with the relevant scaler totals. Interspersed with these were calibration runs (using mostly ^{137}Cs and ^{54}Mn sources) to check for possible gain shifts, plus some negative muon normalization checks, the results of which will be used in the forthcoming chapter on analysis.

The gamma spectra were transferred via B.C. Telephone

lines to temporary disk storage on the U.B.C. Amdahl 470 V/6 computer for subsequent analysis and permanent storage on magnetic tape. A program specifically for the transfer, PHARUN (Clark, unpublished), created a data file on the disk, copied the information in easily usable character format, and checked that the data were successfully stored. During the time required to write the contents of 4096 channels to the file, any necessary changes in the experimental parameters were made, and the vacuum was checked. When this had been completed, the spectrum was erased and the cumulative scalers zeroed.

This concludes the description of the muonium to antimuonium conversion experiment performed at TRIUMF . The information thus obtained must be used in conjunction with that from some peripheral experiments, in order that a meaningful upper limit for the process can be determined. The actual results of all of these, the methods by which they are deduced, and the way in which they can be combined to calculate a value for G, are the subjects of the next chapter.

4. ANALYSIS AND INTERPRETATION OF THE DATA

There are two basic steps which must be taken, after the data have been collected, to derive a result for muonium to antimuonium conversion in the form of a value (or limit) on the coupling constant G defined by equation 2.1.1.5.

The first consists of applying a well-understood statistical procedure to the energy spectrum of gamma rays obtained. The fruit of this effort, and the goal of the first section of this chapter, will be the determination of a number and its associated uncertainty representing the counts in a (possibly nonexistent) photopeak in the spectrum from a calcium 2P-1S muonic X-ray transition.

The second step is more complex. An estimate must be made for the probability that a muon, upon entering the target region, will eventually lead to detection of the full energy of the muonic X-ray after conversion has taken place. Each step in the sequence of events required for the successful counting of the X-ray must be understood and assigned a probability, in order that the only unmeasurable or incalculable quantity in the overall probablility is the coupling constant G. There is also an uncertainty in the probability which should be estimated. Since there are several independent steps between muon incidence and event detection, the overall probability will be the product of probabilities or efficiencies for the individual processes. Some factors are easily measured, some must be computed, while

others may be more accurately evaluated as a subproduct with other terms. The meaning of this will become more clear in the second section of this chapter, which deals with the calculation of the experimental sensitivity in terms of G.

Meanwhile, the time is ripe for presentation of the data upon which this thesis depends.

4.1. The Results: Determination of a Limit on the Number of Events Observed

Ten pulse height spectra for each of the two germanium detectors comprise the results of the search for the negative muonic X-ray in the calcium constituent of the target. The accumulation times for each spectrum were typically three to five hours, corresponding to two or three billion incident muons.

Figure 4.1.1 shows the sums of each set of ten spectra, from 0.55 to 1.0 MeV. The data correspond to a total of 2.32×10^{10} incident muons. The fractional live times for the Aptec and Ortec spectra were 0.82 and 0.92 respectively.

Because of slight long term drifts in the gain and offset (causing shifts of ±0.6 keV maximum, at 0.835 MeV) among the spectra, the resolution obtained by a simple summation is not optimal. One can, however, ameliorate the situation for a particular region of interest by calculating the effective drift

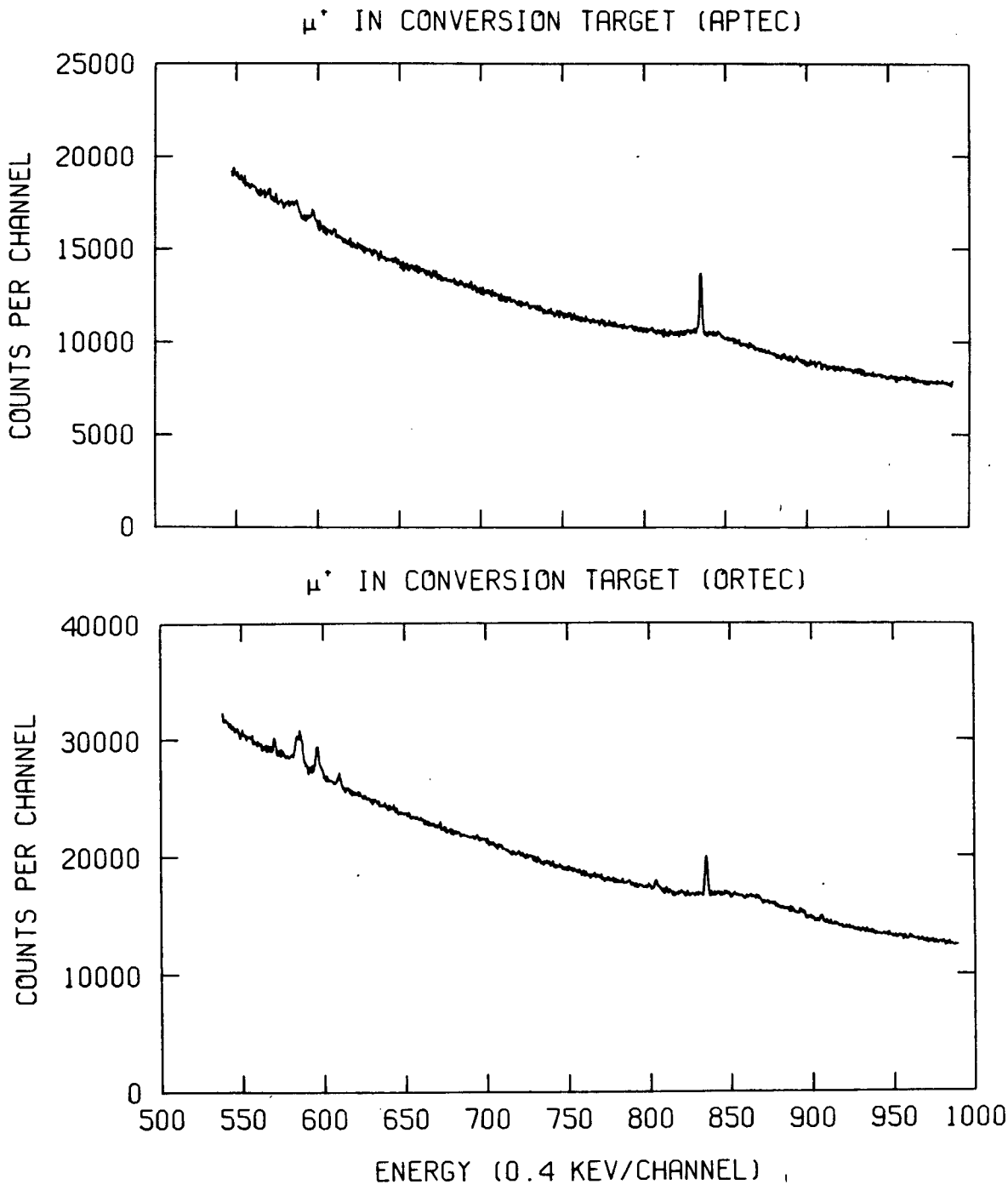

Figure 4.1.1. Gamma spectra from simple summation of all data.

in offset using known lines and adjusting the channel numbers accordingly before addition of the spectra. If the gain (as opposed to offset) drifts are small, this procedure will restore much of the short term resolution over limited regions of interest.

The adjustment of channel numbers was accomplished in the following way. The large (Doppler broadened) annihilation peak at 0.511 MeV (not shown in the figures) and the small background ^{54}Mn peak at 0.835 MeV in each of the twenty histograms were fitted to a gaussian form to determine the channel numbers of the centroids (gamma photopeak energies were obtained from Marion, 1968). From this calibration, the channel numbers for the 0.7837 MeV calcium X-ray were deduced, and the spectra were summed over a region encompassing the peak such that the calculated positions, to the nearest channel, should coincide. The results of the summation are shown in Figure 4.1.2.

The features to note from the histograms are:

1. the prominent ^{54}Mn peak at 0.8348 MeV. It is possible that a 0.8345 MeV line from neutron activation of ^{72}Ge is also present (Bunting and Kraushaar, 1974), but the likelihood of the manganese assignment was shown to be correct during background runs with the cyclotron off. Moreover, the peak shape is not consistent with that of a neutron induced line. The intensity of the line relative to the smooth background differs for the two spectra presumably because of the geometry.

2. a resolved peak at 0.804 MeV, of unknown origin. Although the shape of the peak in the Aptec data is

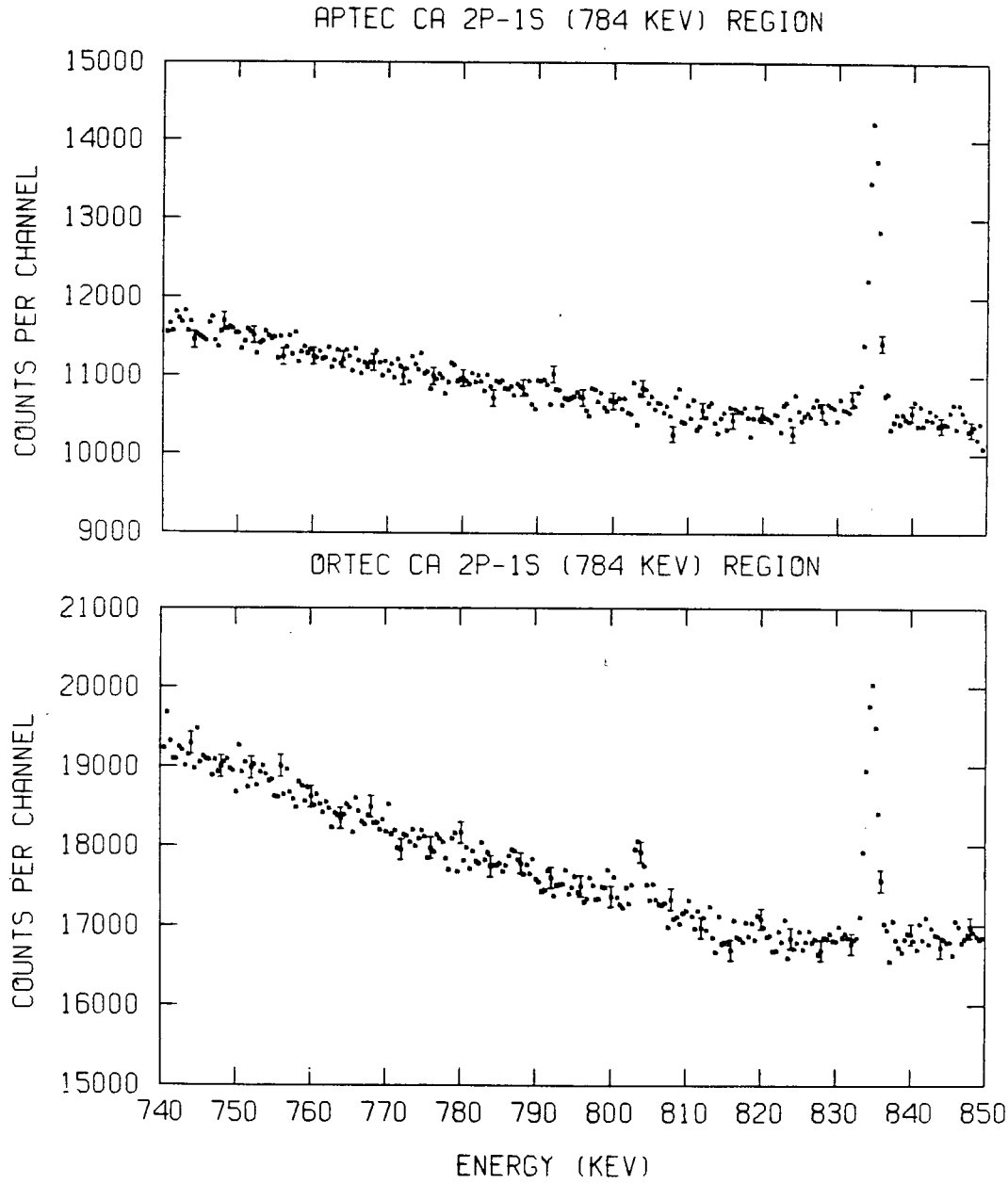

Figure 4.1.2. Summation of shifted spectra in the Ca X-ray region. Note suppression of the zero of the y axis.

not well determined, it looks to be skewed for the Ortec spectrum toward higher energies, a well established property of neutron induced lines resulting from a variable fraction of the nuclear recoil energy being converted to electron-hole pairs in germanium (ibid).

3. definite neutron induced peaks at 0.569, 0.585, 0.596, and 0.609 MeV (figure 4.1.1 only), which were also observed by Bunting and Kraushaar. They were able to attribute the latter two to neutron inelastic scattering on ^{74}Ge, but could not specify the origin of the lower energy pair.

4. a rather featureless region near the 0.784 MeV calcium muonic 2P-1S energy. This is convincing graphic evidence that no muonium conversion to antimuonium has been observed in the present experiment.

As a preliminary check of the apparatus and detection systems, some data were also acquired from an argon gas target at room temperature and one atmosphere pressure, similar to that used in the previous search for muonium conversion (Amato et al., 1968). They are shown in Figure 4.1.3. The corresponding number of incident muons was 3.4 x 10^9. An analysis of this information allows some comparison of target techniques, which appears in the final chapter.

Quantitative limits on the number of events that could be present in a calcium photopeak were derived as follows. From a gaussian fit to the summed ^{54}Mn peaks of Figure 4.1.2, an experimental resolution for each detector in terms of full width

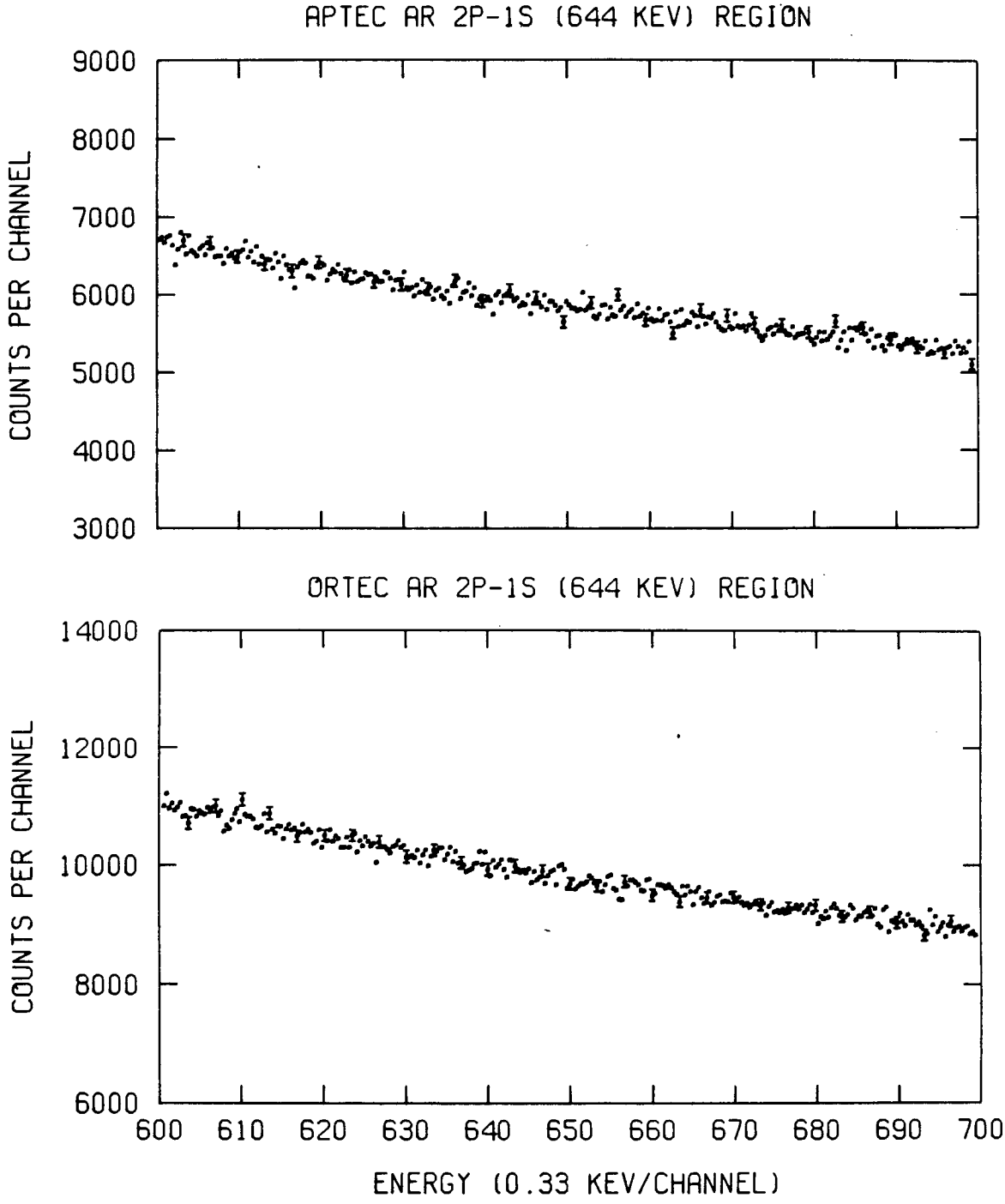

Figure 4.1.3. X-ray data for positive muons in argon gas target at room temperature and one atmosphere.

at half maximum (1.67 ± 0.05 keV for Aptec, 1.73 ± 0.07 keV for Ortec) was obtained at 0.835 MeV. The expected line width was calculated for the lower calcium energy by assuming that it scales with the square root of the energy, which holds when the statistical fluctations in the number of electron-hole pairs dominates the contributions to the width; in any case, the correction is only about 3%, similar in magnitude to the uncertainty in the FWHM. The widths at 0.784 MeV were taken as 1.62 keV (Aptec) and 1.68 keV (Ortec).

A gaussian function of the form

$$N = 0.939(N_o/FWHM)\exp[-(1/2)\bullet\{(E-E_o)/(0.425\bullet FWHM)\}^2] + A + B(E) \qquad 4.1.1$$

was used to fit a range of data over a region centred on the 0.7837 MeV energy. The same form was used to fit ^{54}Mn peaks, with good success. When fitting annihilation lines, which were well defined statistically, it could not reproduce the wings of the peaks. This was not a problem since an accurate determination of the area (N_o) was not required. In this expression, N_o is the number of counts in, E_o the centre, and FWHM the width of, the peak. The constants arise from a conversion of the standard deviation of the peak into FWHM, along with factors usually seen in a normalized gaussian expression. The numbers A and B represent the constant and linear (in energy) terms for the background, respectively. The multiparameter minimization routine MINUIT (James and Roos, 1971) was used to minimize χ^2 and assess from the shape of the hypersurface the values and uncertainties of the parameters.

For the normalization, determinations of uncertainties (which determine in turn the final limit on the number of events observed) were accomplished with the MINUIT subroutine MINOS, which searches the χ^2 hypersurface for the change in the value of the parameter (both positive and negative) for which that statistic is increased by one, thus defining a one standard deviation uncertainty.

Fits to a possible calcium line were obtained by fixing E and FWHM to the calculated values and allowing N_o, A and B to vary. Since A and B are highly correlated and therefore not independently well defined over small energy regions, preliminary estimates based on linear fits of the data from 0.740 to 0.800 MeV were used as initial input, in order that realistic minima could be found. N_o was initially set to zero. The values obtained were quite insensitive to the value of E_o in a range ±1.2 keV from the expected peak position. However, the answers obtained for N_o and its uncertainty did depend on the range of channels around the 0.784 MeV position that were used for the fit, as shown in Table 4.1.1.

The source of this dependence is the statistical improvement in the determination of the continuous background as a broader energy range is included. The value of χ^2 (per degree of freedom) is rather small unless more data is included on either side of a peak. It is especially true for the Aptec results, where the number of events per channel is only about 60% of that of the Ortec spectrum.

The one standard deviation limits on N_o can be taken to be 277 (Aptec) and 371 (Ortec). The last entries from Table 4.1.1 are used since they should in theory be more representative of

Energy Range Analyzed (keV)	Degrees of Freedom	Aptec		Ortec	
		$N_0 + \sigma$ (counts)	χ^2	$N_0 + \sigma$ (counts)	χ^2
±3	12	-249+333	7.04	+186+141	7.34
±4	17	-182+310	8.50	+17+406	21.4
±5	22	-206+296	11.2	-134+389	24.4
±6	27	-146+289	23.7	-51+378	34.7
±7	32	-159+284	32.9	-44+371	35.5
±8	37	-153+277	42.4		

Table 4.1.1. Values obtained by MINUIT for different ranges of data analyzed.

an accurate estimate; by including a larger segment of the spectrum in the fit, the background underneath a possible photopeak is better defined, and χ^2 is more reasonable. The standard deviation in the sum of N_0 from the two detectors is obtained by adding the variances, giving an upper limit of 463.

4.2. Relationship of Events Observed to the Upper Limit for Conversion

With a limit on the number of events observed in hand, it remains to translate that number into a limit on the coupling constant G of the four fermion Hamiltonian of equation 2.1.1.5, which could describe muonium-antimuonium conversion.

To this end, a number P can be defined for each detector such that the relation between the number of observed events,

N_o, is the product of P and the total number of incident muons, N, within the live time of that detector, i.e.,

$$N_o = PN \quad . \qquad 4.2.1$$

P is just the probability that, given a positive muon entering the target, the calcium 2P-1S muonic X-ray following its conversion to antimuonium will contribute to the photopeak at 0.784 MeV in the detector under consideration. P, of course, depends on G.

Values for P can be derived by first writing it as a product of the probabilities, fractions, or efficiencies of each member of the series of processes which must occur for the detection of the X-ray. These numbers and their respective definitions are listed below, in the order in which they take place:

1. F(foils): the fraction of muons which, having passed through the thin MU counter, eventually stop in the active silica component of the sloping target stack. It will be assumed in section 4.2.5 that this number does not depend on whether the muons are positive or negative, in order to facilitate calculations.
2. F(Mu): the fraction of positive muons which, having stopped in the silica powder component, form muonium.
3. F(vac): the fraction of muonium atoms formed in the powder grains which reach the intergranular voids before decaying. It depends on, among other things, the grain size, and has been measured by muonium spin

rotation techniques.

4. F(gap): the fraction of those muonium atoms in the intergranular voids in a silica powder layer which migrate by a random walk among the grains and eventually into the gap on the upper, downstream side of the layer. This fraction is a function of the layer thickness.

5. $P(\overline{Mu})$: the probability that a thermal muonium atom leaving one side of the gap between target layers will have converted to antimuonium by the time it reaches opposite side. This number contains the value of G (or more precisely, G^2).

6. P(capt): the probability that an antimuonium atom impinging on a calcium oxide surface will result in the inelastic scattering process whereby the negative muon is captured by the atoms of the molecule (either calcium or oxygen).

7. E: the overall detection efficiency, defined as the probability that a negative muon from antimuonium in calcium oxide will result in a calcium 2P-1S X-ray which deposits its full 0.784 MeV energy in the germanium detector under consideration. Two values will be derived, E(Apt) and E(Ort), for use in the calculations.

The determination of each of these numbers (or in one case, a subproduct F(foils)•E) will allow the calculation of P:

$$P = F(foils)\bullet F(Mu)\bullet F(vac)\bullet F(gap)\bullet P(\overline{Mu})\bullet P(capt)\bullet E \ . \qquad 4.2.2$$

The following sections will deal with the terms individually, explaining the basis for the assignment of a value to each.

4.2.1. Muonium Formation

It has been previously mentioned that the choice of silica as a target material was based partially on its penchant for muonium formation. The most careful and systematic measurement of the muonium fraction in the silica powder used in this experiment is that of Kiefl *et al.* (1979), who accounted for muons not stopping in the powder. From a direct observation of muonium spin rotation, the fraction was measured to be

$$F(Mu) = 0.61 \pm 0.03. \qquad 4.2.1.1$$

Muonium spin rotation (for a description of the technique, see, for example, Garner, 1979) was also observed during the conversion experiment in the silica/collodion target, using a small scintillator telescope for positron detection (Figure 4.2.1.1). By normalizing the muonium asymmetry obtained to the muon spin rotation signal in copper (close to 100% muon spin signal), a value of 0.29 ± 0.02 was obtained for the muonium fraction in the entire target region. Since the silica powder was the only substance capable of causing the muonium precession signal, this lower muonium fraction provides a measure of the product $F(foils) \cdot F(Mu)$, and an estimate of

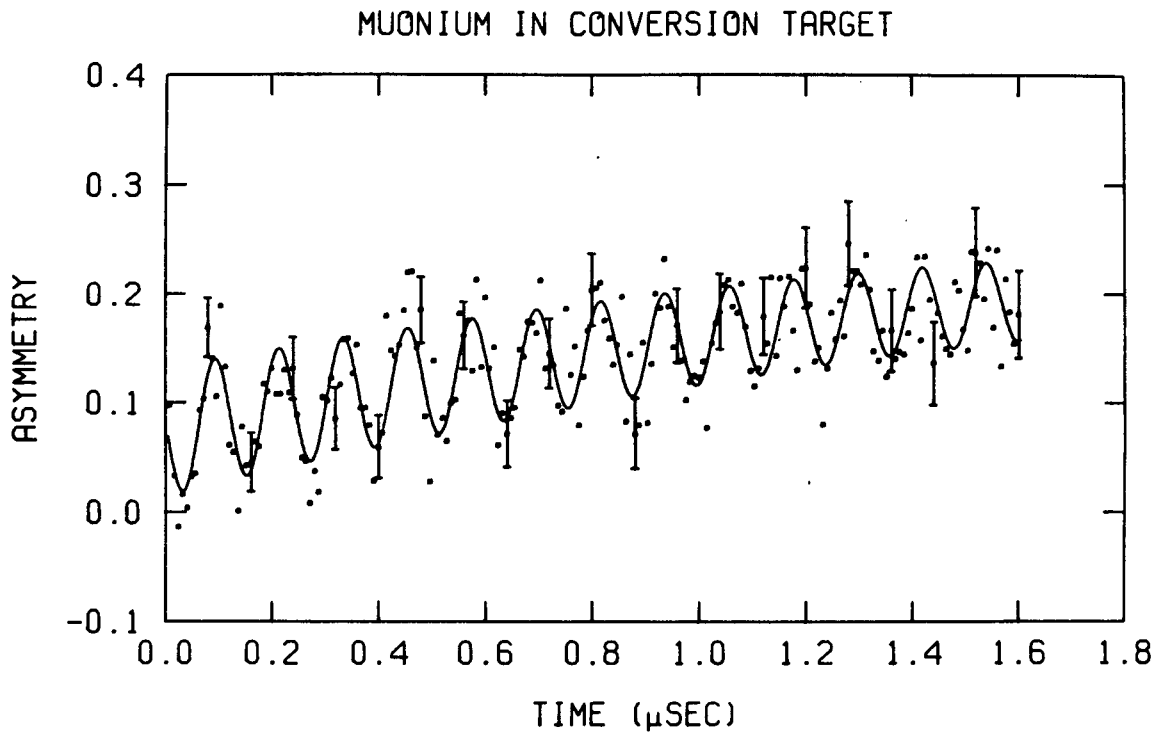

Figure 4.2.1.1. Muonium spin rotation signal in the conversion target.

$$F(\text{foils}) = 0.48 \pm 0.04 \qquad 4.2.1.2$$

results. The apparatus, constructed for muonium conversion rather than spin rotation, was not apt to eliminate systematic errors in muonium formation fractions, and the quoted statistical uncertainty may be misleading. Regardless, the determination of F(foils) is better accomplished by other techniques described in section 4.2.5.

4.2.2. Probability of Ejection into Vacuum; Single Foils

The derivations of values for F(vac) and F(gap) will be the concern of the following discussion. The calculations required are in some cases lengthy, and therefore have been relegated to appendices A2 and A3. Similar techniques can be applied for the estimation of both fractions, with appropriate changes in geometry, muonium velocity, and the distance scale. The major difference in approach to the extraction of the final values is that F(gap) relies solely on reasonable (and possibly pessimistic) conjectures on the motion of muonium among the fine silica particles of the layers in the conversion target. Only sketchy, qualitative experimental evidence could be obtained for the effects to be described; the sensitivity required for a direct, unambiguous measurement of F(gap) could not be reached with the methods employed.

The situation for F(vac) is more clear. The results are on a firm experimental basis, explicable in terms of a model yet largely independent of its validity. It is expected that an energetic positive muon slowing down in a low density silica powder target will behave much the same as in bulk silica, at least insofar as surface effects play no role. That is, electron capture and loss will help to slow the muon, the former dominating at lower energies so that the observed thermalized muonium fraction is large. One expects the atoms to come into thermal equilibrium with the silica grains (although not necessarily at the ambient temperature, since the muon's energy may have caused heating of the grain) in a uniform distribution

throughout the powder grains. Any further thermal motion would cause some of the atoms to reach the grain surfaces and enter the void between particles. Given the size and sphericity of the grains, and the assumption that there exists some barrier inhibiting muonium from re-entering a silica particle, the rate at which muonium reaches the voids can be calculated in terms of a parameter D (henceforth referred to, rightly or wrongly, as a diffusion parameter). An experiment to test the applicability of this approach has been carried out (Marshall et al., 1978) utilizing the spin exchange relaxation of the muonium polarization with oxygen gas to determine the rate of expulsion from the particles and extract values for D. It supported the mechanism just described; moreover, the evidence that muonium does in fact reach the voids and move essentially freely at thermal energies between collisions with grain surfaces seems unshakable (appendix A2 contains more discussion of the techniques and results), whether or not the mechanism is valid. Evidence that muonium in the conversion target is escaping the silica particles to vacuum is provided by Figure 4.2.2.1, where the muonium spin rotation signal of Figure 4.2.1.1 has been removed by the addition of oxygen gas to the target region. The fraction of muonium reaching the voids before decaying, based on the model, is

$$F(vac) = 0.93 \pm 0.01, \qquad 4.2.2.1$$

where the expressions A2.12 and A2.14 have been applied. Assuming no particular model, but using the measured exponential muonium spin relaxation rate in a powder sample with oxygen

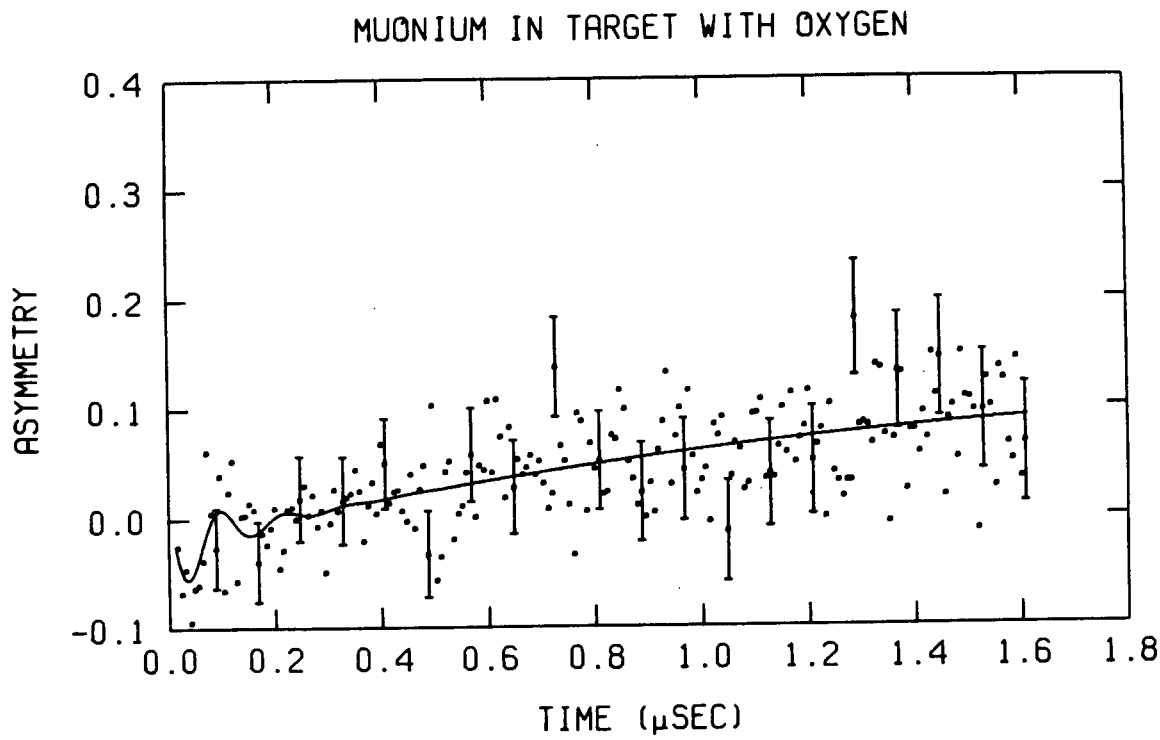

Figure 4.2.2.1. MSR precession signal relaxed by oxygen gas.

present, one gets an estimate for F(vac) of 0.97 ± 0.01 (ibid). Note that this number is derived from a different relaxation spectrum, for a different powder size, than that from which the value of D in A2.14 results. Grain heating (Kiefl, 1981) may be the cause of the discrepancy, since D, a function of temperature, may depend on grain radius. In subsequent calculations, the more pessimistic fraction of 4.2.2.1 will be used.

The estimation of F(gap) can be accomplished via similar mathematical methods, with the major difference being that a value for D (now referring to the diffusion parameter characterizing muonium motion in the voids in a layer consisting

of hard silica spheres surrounded by vacuum, rather than inside a silica sphere) has not been determined by experiment, but must be inferred from simple, reasonable estimates on the properties of the silica layer. This has been carried out in appendix A3 (equation A3.8), assuming a homogeneous distribution of silica particles in a powder such as the one used in the conversion target. The diffusion parameter can then be inserted into equation A3.3 with the muon decay rate $\lambda = (2.2 \times 10^{-6}\ s)^{-1}$ and the average powder layer thickness of 0.3 mm (section 3.2.2) to give an estimate of

$$F(gap) = 0.078 \ . \qquad 4.2.2.2$$

Note that the second (exponential) term in A3.3 is negligible for the large value of the powder layer thickness d, and that F(gap) is then inversely proportional to d. This makes sense; only a small part of the layer, that nearest the gap, is "active", or will emit the muonium that can enter the gap before decay. As d is increased, the probability that a muonium atom will begin its random migration from the "active" portion decreases as d^{-1}, explaining the dependence of F(gap). The point is that a nonuniformity in the value of d over the 150 cm^2 area of the collodion film does not radically change F(gap) calculated from an average value of d, as long as coverage of the surface is complete. Visual examination of the target stack after all runs were completed indicated that coverage was greater than 2/3. Accordingly, the estimate which will be applied for the final analysis is

$$F(gap) > 0.052 \ . \qquad 4.2.2.3$$

F(gap) could not be precisely measured because of the difficulty in determining the whereabouts of muonium atoms near a single collodion foil (or film) supporting a silica layer, similar to the foils making up the target stack. However, a qualitative indication of the presence of muon decays at one centimeter from a single foil was observed.

A plastic detector telescope consisting of two pieces of scintillator material 5 cm long by 0.3 cm wide was arranged so as to detect muon decays within a narrow sheet of about one centimeter thickness. The telescope was aimed at a region one centimeter from and parallel to the upper, downstream face of a silica-covered foil in the evacuated target area of figure 3.2.4.1. The object of the exercise was to observe some enhancement in the muon decay rate, as measured by a time histogram, at times when muonium drifting away from the foil at thermal velocity would pass through the region viewed by the scintillator telescope.

Consider a non-decaying atom of velocity $\vec{v}$ emitted at t=0 isotropically from a surface x=0 into 2π sr. The component of $\vec{v}$ perpendicular to the surface is, by averaging over all directions, v/2, and the number dN in a sheet of thickness dx at a distance x from the surface is

$$dN = \delta(x - (v/2)t)dx \ , \qquad 4.2.2.4$$

where the Dirac delta function has the usual definition. If the exponential decay rate of the atom is λ, the observed decay rate

of the dN atoms in the sheet can be written as

$$-d(dN)/dt = \lambda \exp(-\lambda t) \bullet \delta(x - (v/2)t)dx \ . \qquad 4.2.2.5$$

If a thermal Maxwellian distribution

$$P(v) = 4\pi (m/2\pi kT)^{(3/2)} v^2 \exp(-mv^2/2kT) \qquad 4.2.2.6$$

is assumed, the decay rate must be integrated over v to give

$$-d(dN)/dt = \lambda \exp(-\lambda t)dx \bullet 4\pi (m/2\pi kT)^{(3/2)} (8x^2/t^3) \bullet \exp(-2mx^2/kTt^2) \ . \qquad 4.2.2.7$$

A plot of -d(dN)/dtdx versus t at room temperature for several values of x, notably 1.0 cm, comprises Figure 4.2.2.2.

The data collected from a total of about 3 x 10^9 incident muons (in an elapsed time of about fourteen hours) are shown in Figure 4.2.2.3. An unknown number of the muons (possibly 50% or greater, as estimated from F(foils) in equation 4.2.1.2) were lost from the severe multiple scattering of the beam in the incident detector (MU) and degrader. Of those remaining, only about four per cent would stop in the silica layer, estimated from the layer thickness (1.8 mg$\bullet$cm^{-2}) divided by the FWHM range spread for the surface muon beam (25 mg$\bullet$cm^{-2}). Furthermore, muonium forms with about 61% probability (equation 4.2.1.1). An estimate of the number of muonium atoms formed in the silica during the course of the run is then

$$N(Mu) = 4.6 \times 10^7 \ . \qquad 4.2.2.8$$

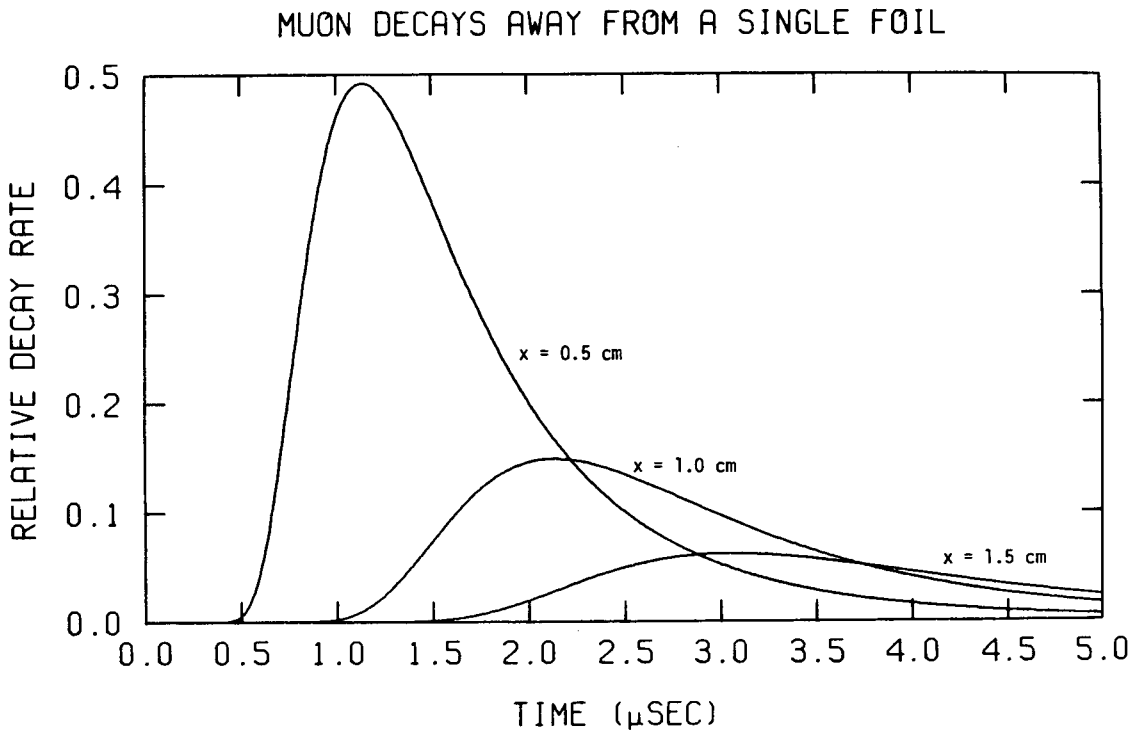

Figure 4.2.2.2. Expected time distribution of decays from muonium drifting thermally in vacuum from a single foil.

The telescope had a geometrical solid angle efficiency of 3.7×10^{-4}. At the incident rates used (6×10^{4} s^{-1}), a fraction of 0.38 of the muon decay events detected were recorded, having passed a criterion of being "alone" in the target (meaning the muon entrance time was both preceded and followed by an eight microsecond interval in which no other muon entered). This cut is necessary to prevent distortion from muon pile-up (Garner, 1979). The detection efficiency for the single foil experiment, E(sf), may be taken roughly as the product of the two, namely

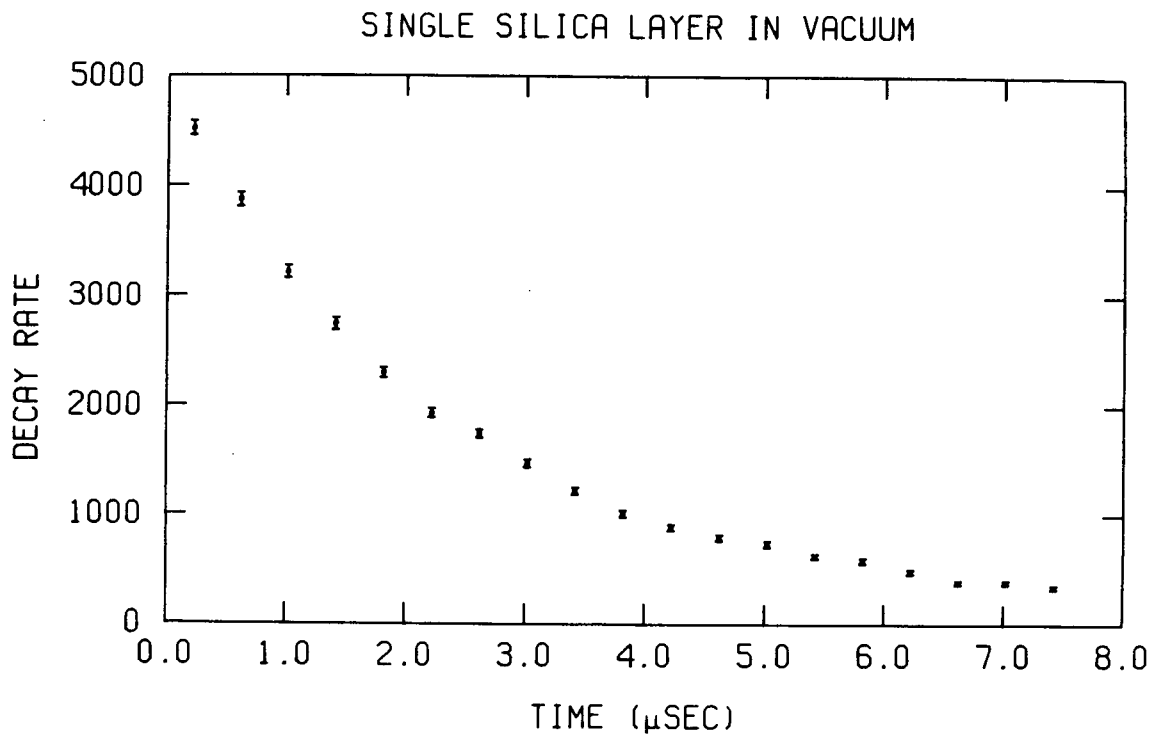

Figure 4.2.2.3. Muon decay curve obtained with narrow telescope centred 1 cm downstream of silica layer.

$$E(sf) = 1.4 \times 10^{-4} \ . \qquad 4.2.2.9$$

The enhancement in the number of events above an exponential background in the muon decay curve should be, if the assumptions made are reasonable,

$$N(enh) = N(Mu) \bullet E(sf) \bullet \exp(-\lambda t) \bullet F(vac) \bullet F(gap) \ . \qquad 4.2.2.10$$

The exponential factor makes allowance for the decay of the atoms before reaching the region of detection.

A five parameter fit to the data of Figure 4.2.2.3 was attempted using the function

$$N(t) = N_0 \exp(-\lambda t) + B + 0.939(N_1/FWHM) \bullet \exp[-(1/2)\{(t - t_0)/(0.425 \bullet FWHM)\}^2] \qquad 4.2.2.11$$

where λ was fixed at the muon exponential decay rate. The gaussian form was assumed for ease of analysis; a more accurate and somewhat intractable functional dependence, derivable from equation 4.2.2.7, was judged unnecessary for the size and statistical signifigance of the enhancement observed. The value of N_1 obtained was +160 with positive and negative standard deviations of 85 and 77 respectively. The center (t_0) and FWHM of the fitted enhancement were 2.8 ± 0.1 and 0.7 ± 0.3 microseconds, so the shape is similar to the 1.0 cm curve of Figure 4.2.2.1. The reduced χ^2 value was 0.845 for 33 degrees of freedom. With N_1 set to zero, the fit obtained had a reduced χ^2 value of 0.913 for 36 degrees of freedom.

The data, then, do show some enhancement at approximately the right position in the decay curve for emission of thermal muonium, although the sensitivity of the method is not adequate for a precise measurement of the rate. A plot of the data and the fit are displayed in Figure 4.2.2.4, where the first two terms of the right hand side of equation 4.2.2.11 have been subtracted. Muonium ejected epithermally from a grain would be expected to thermalize in a few subsequent collisions with neighboring powder particles, before reaching the gap between layers (also indicated by the MSR relaxation rates in oxygen gas, as explained in appendix A2). Taking the value for N_1 as

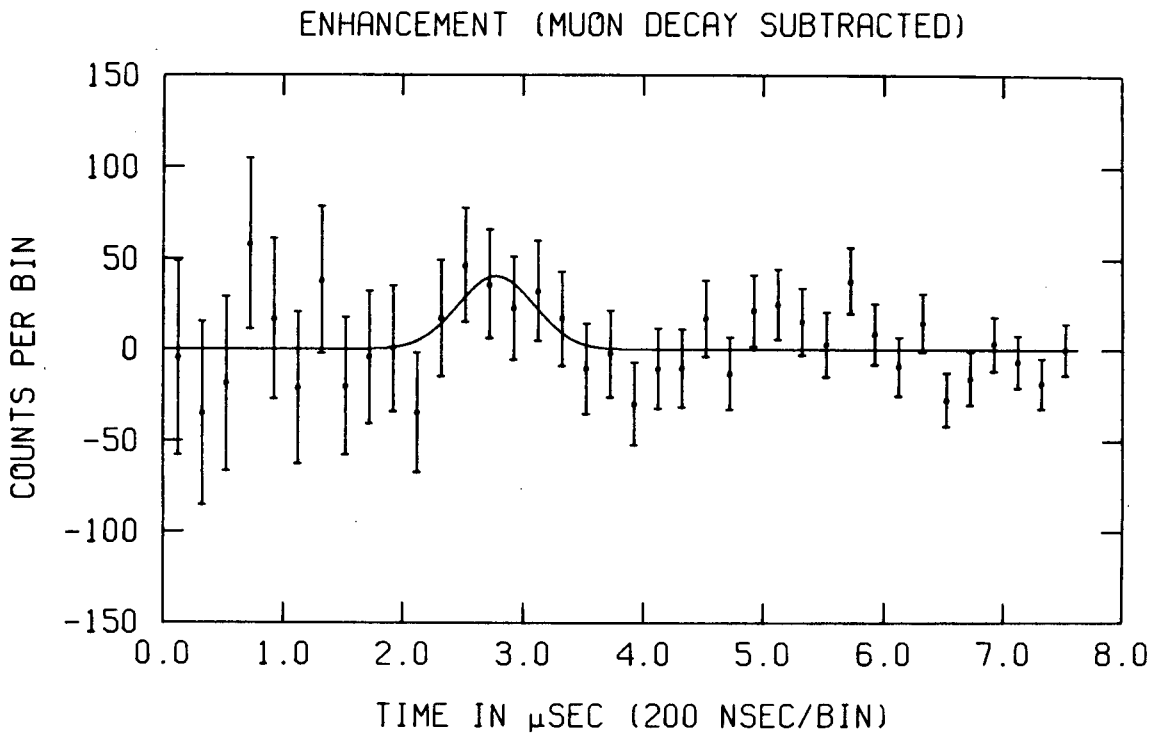

Figure 4.2.2.4. Enhancement in the muon decay spectrum.

an estimate of N(enh) of equation 4.2.2.10, setting $t = 2.8 \times 10^{-6}$ s and F(vac) = 0.93 (equation 4.2.2.1), and solving for F(gap), it is found that

$$F(gap) = 0.095 \qquad 4.2.2.12$$

with a standard deviation of about 50%. Because of the large uncertainty and the difficulty in assessing systematic errors, this result is by no means an unequivocal measurement of F(gap). It is at least not inconsistent with the calculated value of 0.078 of equation 4.2.2.3.

This concludes the discussion of the values which will be

taken for F(vac) and F(gap) in the derivation of a limit on muonium conversion to antimuonium. The next step is to examine what may happen to a muonium atom once it has reached the gap between foils and finds the vacuum environment where conversion is not strongly suppressed.

4.2.3. Conversion Probability

As a muonium atom leaves a flat surface and moves in vacuum toward another flat surface, the split Δ in the muonium and antimuonium energy eigenvalues (introduced in section 2.1.2) is greatly reduced and is no longer detrimental to possible conversion mechanisms. The expression for the probability of conversion as a function of time, equation 2.1.3.4, will hold to a high level of accuracy, so it can be said that

$$P(\overline{Mu};t) = \exp(-\lambda t)(\delta t/2)^2 \ . \qquad 4.2.3.1$$

Assuming a speed v for the atom as it leaves one surface (the silica layer) destined for another surface a distance s away, at an angle θ with the perpendicular, the probability can be expressed in terms of v and θ as

$$P(\overline{Mu};v,\theta) = \{\exp(-\lambda s/v\ \cos\theta)\ \delta^2 s^2\}/4v^2\cos^2\theta \ . \qquad 4.2.3.2$$

An integration over angles can be carried out, assuming

isotropy of the velocity vector in the half space $0 \leq \theta < \pi/2$, to get

$$P(\overline{Mu};v) = (\delta^2/4\lambda^2)\bullet(\lambda s/v)\bullet\exp(-\lambda s/v) \ . \qquad 4.2.3.3$$

Inserting the values of δ and λ, setting $v = 7.4 \times 10^5$ cm$\bullet$s^{-1}, (mean thermal muonium velocity at room temperature, equation A3.8) and s = 0.41 cm (see section 3.2.2), the result is

$$P(\overline{Mu}) = 2.4 \times 10^{-6} \ (G/G_F)^2 \ . \qquad 4.2.3.4$$

A more careful calculation using numerical integration over the velocity distribution (equation 4.2.2.6) will give

$$P(\overline{Mu}) = 2.5 \times 10^{-6} \ (G/G_F)^2, \qquad 4.2.3.5$$

which is the number that will be applied in the evaluation of the right hand side of equation 4.2.2.

Before leaving the topic of $P(\overline{Mu})$, two points should be emphasized:

1. The value derived here is exactly one order of magnitude lower than the time-integrated probability for decay as antimuonium under ideal circumstances (equation 2.1.3.5), and is slightly less than half the maximum of the unintegrated expression 2.1.3.4.
2. $P(\overline{Mu})$ depends on the square of the coupling. Experimentally this means that increasing the sensitivity to G by some factor necessitates reducing

the limit on the number of events observed, or alternatively, increasing the product of factors in the combined detection probability of equation 4.2.2, by the square of that factor. One way of achieving the former is to take more data, but the reduction in the limit of events observed itself depends on the square root of the increase in data. This means that a reduction of the limit on G by a factor of two requires 2^4 or sixteen times as much data, other things being equal. More will be said on this point in the concluding chapter.

The next factor to be evaluated in the expression for P describes the behavior of an antimuonium atom impinging on a surface of calcium oxide and the likelihood of capture of the negative muon into an atomic orbital, a process which must occur for the observation of muonium conversion by the method employed in this experiment.

4.2.4. Negative Muonic X-ray Probability

This section will attempt to present a clue to the solution of the question, "What happens when antimuonium in vacuum interacts with a calcium oxide surface?". Very little theoretical work exists on the interaction of atoms such as antimuonium (a negative nucleus surrounded by a positive electron distribution) with normal matter. Experimentally, it is impossible at this stage to measure the likelihood of

formation of a muonic atom from an initial state containing antimuonium. Although much is known about positronium, which might be thought of as an antimuonium analogue, the equality of mass of the electron and positron makes its atomic properties vastly different; also, because of the exclusion principle, the electron will not be affected by an atomic collision as a negative muon would.

The problem has been approached for the case of antimuonium in atomic hydrogen and inert gases, especially argon, for the analysis of the previous successful muonium conversion experiment described in section 3.1.1 (Amato et al., 1968). The methods employed and the conclusions reached (Morgan, 1967) will be summarized here, insofar as they relate to the problem at hand.

For atomic hydrogen, an interaction potential for the scattering of antimuonium was derived using a perturbation expansion for the ground state eigenvalue of the Schroedinger equation for the system. The procedure is similar to that for deducing the Van der Waals dispersion energy for two hydrogen atoms (Margenau, 1939), but is claimed to be relevant for smaller atomic separations. The result is applicable in the adiabatic approximation where the nuclei (muon and proton) can be considered fixed for the calculation of electron wave functions, and holds for thermal encounters at room temperature. A critical radius, R_c, is defined as that separation of the muon and proton below which the formation of positronium at rest, leaving the muon and proton capable of forming muonic hydrogen, is energetically favored. The assumption is made that this reaction will take place if the muon-proton separation in a

collision of antimuonium with hydrogen is less than R_c. It is then a question of determining the turning point, or distance of closest approach, of an orbit for a given collision and impact parameter, using the interatomic potential. It was found that for a particular collision energy there existed a definite value of impact parameter, R_i', below which the turning point is significantly less than R_c (possible rearrangement of the particles was ignored for the calculation). At thermal collision energies, $R_c \sim 0.5a_o$, $R_i' = 6.5a_o$, and the path length of antimuonium within R_c is about a_o for impact parameters less than R_i' (a_o is the Bohr radius). The electron velocity is about five times the relative muon-proton velocity, so the formation of the lower energy positronium state is a certainty. Moreover, its formation within the volume $r < R_c$ indicates, by the uncertainty principle, that it will escape rapidly, and a reversal of the interaction if the muon-proton separation were again to become greater than R_c is not likely. Subsequent photon emission by muonic hydrogen takes place on a time scale much shorter than the muon lifetime, and the muon will usually decay from the 1S atomic state.

The case for antimuonium scattering by argon is similar except that the accuracy of the determination of the radii R and R_i' is reduced because of a higher uncertainty in the interatomic potential for some separations. The forces tending to break up antimuonium are greater due to the higher charge of the argon core for separations less than R_c. Again, muonic argon formation is a near certainty for impact parameters less than a particular value, calculated to be $7.4a_o$ for the mean thermal collision energy at room temperature. The corresponding

inelastic scattering cross section is

$$\sigma_I = 55.1 \pi a_o^2 \ . \qquad 4.2.4.1$$

An estimation of this quantity by use of an optical model approach, which is not susceptible to error from uncertainty in the interatomic potential, gives

$$\sigma_I = (56.5 \pm 2.3) \pi a_o^2 \qquad 4.2.4.2$$

in close agreement.

A large discrepancy between this cross section and one for another simple atom is not likely (the cross section for atomic hydrogen is calculated to be about $37 \pi a_o^2$). This can provide a clue to the behavior of antimuonium in a collision with a calcium oxide surface. It is very difficult to rigorously calculate a theoretical cross section, and the only recourse is to plausibility arguments. The reduced de Broglie wavelength of thermal antimuonium is $\sim a_o/6$, so the surface can be considered as an array of atoms rather than a continuum. Moreover, a value of the inelastic cross sections of anywhere near the order of magnitude of equation 4.2.4.1, coupled with the thickness of the oxide layer used, insures the certainty that antimuonium encountering the coating will result in the negative muon being captured by either a calcium or an oxygen atom. Thus it is reasonable to set

$$F(\text{capt}) = 1.0 \qquad 4.2.4.3$$

for use in the overall detection probability.

Some assumptions will have to be made regarding the relative capture probabilities for calcium and oxygen. While these can be measured for fast negative muons stopping in oxides, the application of the ratio of probabilities to atomic muon capture from thermal antimuonium requires some justification. As defined in section 4.2, the ratio is contained within the factor E, the detection efficiency, which is the subject of the following section.

4.2.5. Detection Efficiency

It has been stated that the detection efficiency is the probability that a negative muon from antimuonium, when captured in calcium oxide, will result in a calcium X-ray which deposits its full 0.784 MeV in the germanium detector. Two values, one for each detector, will be deduced in this section to account for the difference in response to the radiation. It is more convenient and precise to evaluate the efficiencies in the form of a product with F(foils), the fraction of muons passing through the thin counter which stop in the silica portion of the conversion target. The method of extracting the numbers relies on the use of a beam of negative muons at 29 MeV/c, the momentum of positive surface muons.

Because of the strong absorption of negative pions produced and stopped in the proton target which is viewed by M13, there are none (or very few) which decay to muons in the surface of

the target. Hence, negative surface muons do not exist. Some negative pions, however, escape the target with a velocity that allows their decay into negative muons which satisfy the phase space acceptance of the secondary beamline when it is set up for 29 MeV/c negative particles. Rates are typically (Oram et al., 1980) about 1.5% of the positive surface muon flux, which is low but nonetheless useful for the purposes of this experiment. Because of its high stopping density the slow negative beam should find applications, for instance in muonic X-ray studies of rare targets or low pressure gases, but it has not yet been exploited. One point to note is that the high polarization characterizing the positive beam is reduced to 0.45 ± 0.20 for the negative one (as measured by J.H. Brewer at TRIUMF). No difference in quality (except flux and thus relative contamination) could be distinguished between negative and positive muon beams at 29 MeV/c, nor is one expected when the sharp edge at 29.8 MeV/c of the positive particle momentum distribution is not within the channel acceptance, and the final beam spot size is not determined by the muon source size (multiple scattering is responsible for the enlarged beam at the conversion target, as evidenced by the low value of F(foils) estimated in equation 4.2.1.2). The stopping power for negative and positive beams is the same for energies determining the range and range spread of a 4 MeV muon beam; only at energies comparable to atomic binding potentials does the charge of the beam lead to a difference in the slowing mechanism (atomic capture versus muonium formation). It is therefore accurate to assume that, in the present context, the muon stopping distribution is the same for positive and negative beams. In

particular, the fraction of muons stopping in the active silica component of the target is independent of the charge of the beam.

With this in mind, it is evident that the probability of observing a negative muonic 2P-1S X-ray from silicon at 0.400 MeV (all muonic X-ray energies quoted are from the compilation of Engfer et al., 1974), given that a negative muon has entered the target, is

$$P(Si) = F(foils) \bullet R(Si) \bullet eff(Si) \ . \qquad 4.2.5.1$$

F(foils) has been defined previously, and:

1. R(Si) is the ratio of silicon 2P-1S X-ray intensity to the total muonic K X-ray intensity from silicon and oxygen resulting from muons stopped in the silica powder of the conversion target. It is the relative capture ratio of silicon to oxygen multiplied by the ratio of K_{α} to all K X-rays, and can be measured using a silica powder target.
2. eff(Si) is the efficiency for observing the full energy of a silicon 2P-1S X-ray in a particular detector. Included are the photopeak efficiency at 0.400 MeV, the solid angle, and an attenuation factor for the 0.32 cm aluminum vacuum pipe, mumetal shield, and 0.62 cm front veto scintillator (neglecting the target itself, the scintillator wrapping, and air, which are negligible). The solid angle effect is the only one which cannot be accurately and independently estimated. The efficiency and attenuation depend on

the energy of the X-ray. Both the efficiency and the solid angle will be different for each detector.

The goal of this section is to estimate the quantities E for each detector. From the way in which it has been defined, it is evident that

$$E = R(Ca) \bullet eff(Ca) \ , \qquad 4.2.5.2$$

where the quantities on the right are analogous to those of equation 4.2.5.1, for calcium oxide rather than silicon dioxide. The reader should by now understand the gist of this approach. Multiplying equation 4.2.5.2 by F(foils) and using 4.2.5.1:

$$F(foils) \bullet E = P(Si) \bullet \{R(Ca)/R(Si)\} \bullet \{eff(Ca)/eff(Si)\} \ . \qquad 4.2.5.3$$

P(Si) is measured using the 29 MeV/c negative muon beam and the conversion target, R(Ca) and R(Si) are measured independently with negative muons in silica and calcium oxide targets, and the ratio eff(Ca)/eff(Si) is just the ratio of the detector photopeak efficiencies times the attenuation factors at 0.784 and 0.400 MeV. The factors from F(foils) and the solid angle efficiencies have been absorbed in P(Si) and are thus determined as a product experimentally. This approach should be relatively free of systematic errors, if carried out with care.

The use of R(Ca) is made under the assumption that it is independent of whether the muon is captured from a thermal neutral antimuonium atom or an energetic negative muon beam. The qualitative understanding of muon capture in atoms and

molecules has increased with the growth of activity in mesic chemistry (Schneuwly, 1979; Daniel, 1979), but no theory exists which can accurately predict the effect on R(Ca) of capture from a thermal antimuonium state. A measurement of R(Ca) using thermal antimuonium is not experimentally feasible, but a rough analogy exists with thermal muonic hydrogen. This has been studied in the oxidized surface layers of thin aluminum foils in a hydrogen gas target (Bertin et al., 1978). A reduction of about 40% was observed in the relative 2P-1S aluminum muonic X-ray intensity, presumably because the small size (some 200 times smaller than muonium) and high binding energy allow it to penetrate well within the outer electron orbitals before being torn apart. The negative muon will then populate lower angular momentum states of lower principal quantum number, enhancing nP-1S with respect to 2P-1S transitions. No mention is made of any effect on the relative aluminum and oxygen capture ratios, so it is presumably negligible. The larger, more loosely bound antimuonium atom should behave more like a free negative muon than muonic hydrogen, since it cannot penetrate the atom as easily without breakup. This supports the assumption of the suitability of R(Ca) as derived from negative beam data for capture from the antimuonium state.

The P(Si) are obtainable from data summarized by Figure 4.2.5.1, the spectra fom the two detectors with a negative muon beam in the conversion target. The number of muons entering through the defining (MU) counter was $(2.53 \pm 0.25) \times 10^7$. The large uncertainty results from the high electron contamination (>100 e^- per muon) of the beam, which, although counted with low efficiency in the counter, was responsible for 46 ± 5 per cent

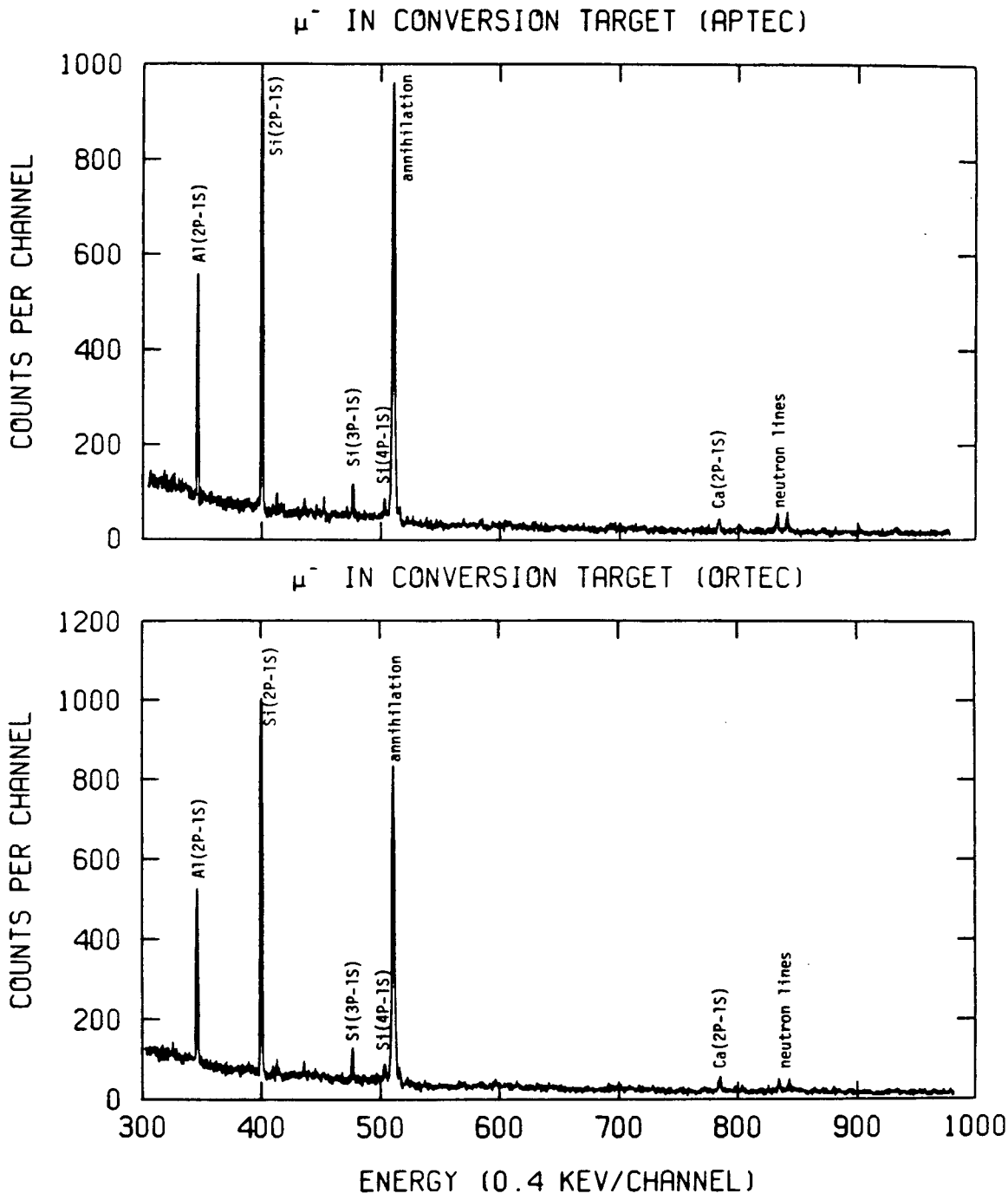

Figure 4.2.5.1. X-ray spectra from negative muons in the conversion target.

of the rate. This number was determined by inserting a thin CH absorber at F1 (see section 3.2.1) which affects the electrons very little but slows the muons such that they have too low a momentum to survive the bend between F2 and F3. The number of counts in the silicon 2P-1S photopeaks (from gaussian fits) were 2961 ± 63 (Aptec) and 3439 ± 68 (Ortec), leading to the assignments

$$P(Si;Apt) = (1.17 \pm 0.13) \times 10^{-4} , \qquad 4.2.5.4a$$

$$P(Si;Ort) = (1.36 \pm 0.15) \times 10^{-4} . \qquad 4.2.5.4b$$

Figures 4.2.5.2 and 4.2.5.3 show muonic spectra from silica powder and calcium oxide targets respectively. The calcium oxide was in the form of a coarse powder and was heated overnight prior to being placed hot in the target chamber vacuum, to insure the absence of hydroxide which will alter the capture ratio. After correcting for detector efficiency and absorption, the line intensities were deduced and summed appropriately. Note the proximity of the oxygen 3P-1S line (158 keV) and the calcium 3D-2P doublet (157 keV, 158 keV). Rather than trying to measure the oxygen line intensity, it was assumed that the relative intensities of the 3P-1S to the 4P- and 5P-1S sums were equal in silica and calcium oxide. The results were

$$R(Si) = 0.17 \pm 0.01 , \qquad \text{and} \qquad 4.2.5.5a$$

$$R(Ca) = 0.48 \pm 0.03 . \qquad 4.2.5.5b$$

The ratio of attenuation factors for 0.784 and 0.400 MeV

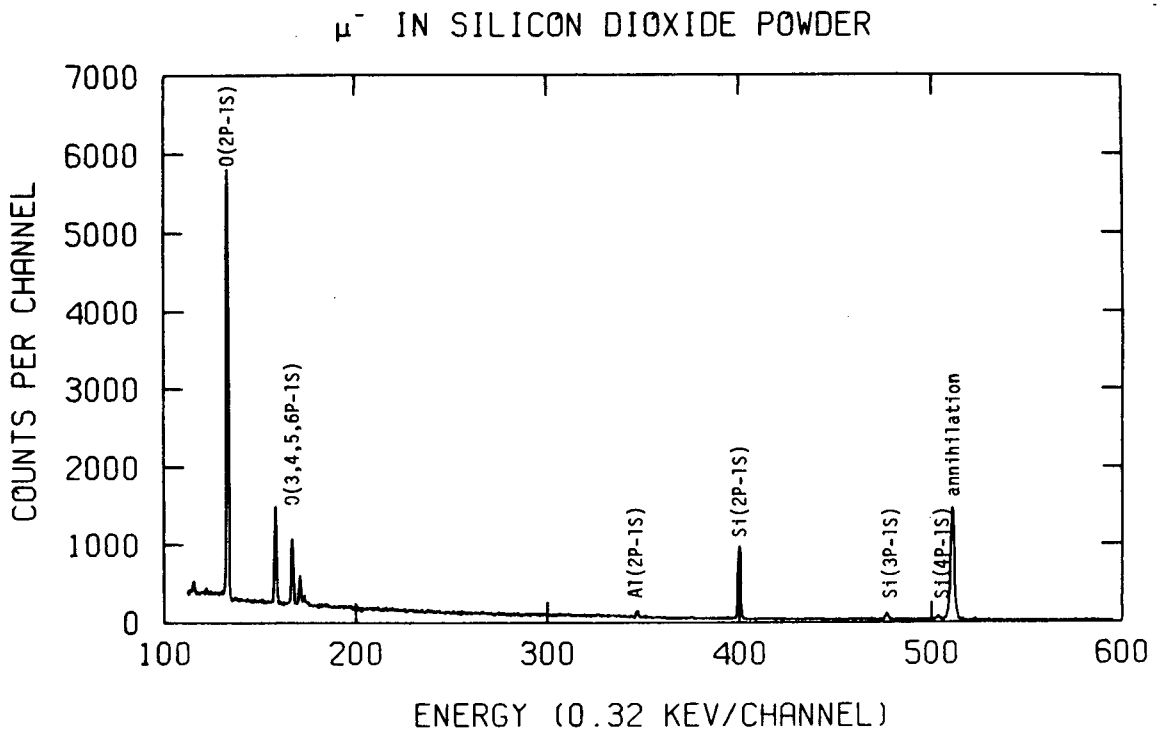

Figure 4.2.5.2. X-ray spectrum from negative muons in silicon dioxide.

radiation in aluminum, mumetal, and scintillator between target and detectors is 1.05. The ratios of photopeak efficiencies are estimated from Figure 3.2.4.2 to be 0.52 ± 0.03 (Aptec) and 0.57 ± 0.04 (Ortec). Combining this information with that of equation 4.2.5.4 and 4.2.5.5 in 4.2.5.3, the desired results are:

$$F(\text{foils})\bullet E(\text{Apt}) = (1.80 \pm 0.26) \times 10^{-4}\ , \qquad 4.2.5.6a$$

$$F(\text{foils})\bullet E(\text{Ort}) = (2.30 \pm 0.35) \times 10^{-4}\ . \qquad 4.2.5.6b$$

All numbers required for a determination of the sensitivity of

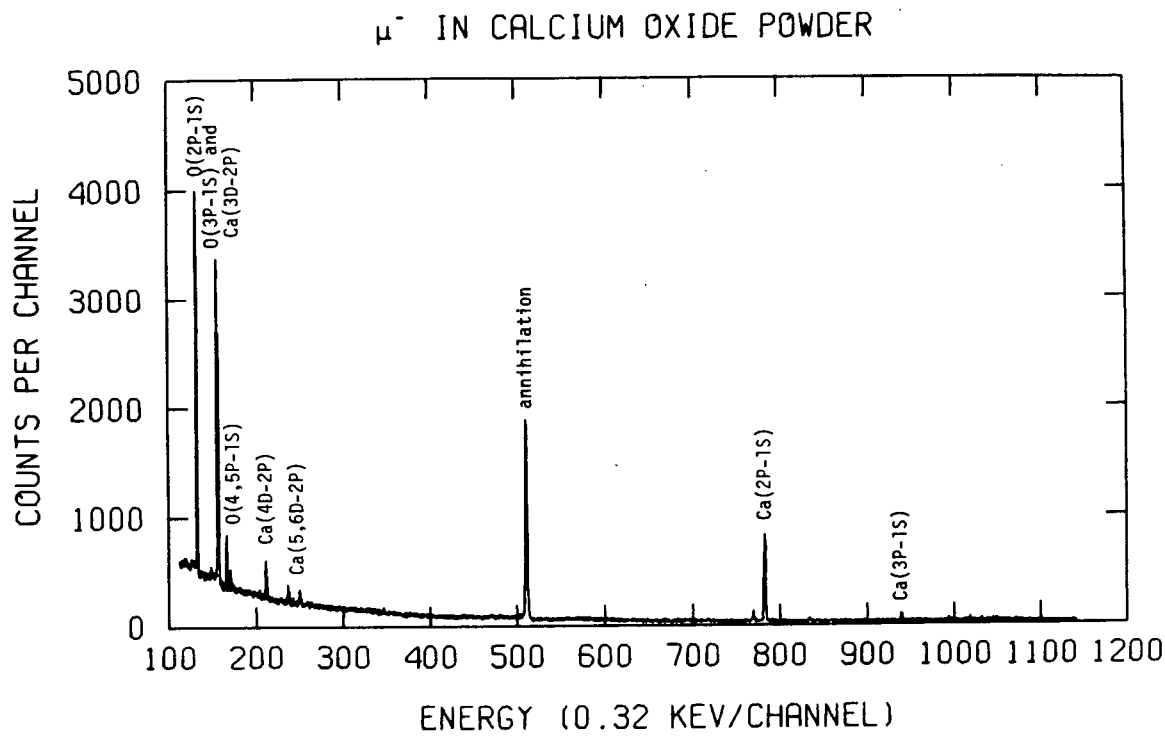

Figure 4.2.5.3. X-ray spectrum from negative muons in calcium oxide.

the experiment are now in hand; the evaluation will be carried out in the next section.

4.2.6. Detectable Events in Terms of the Coupling Constant G

Because of the differences of the two detectors, two values for equation 4.2.2 will be determined, P(Apt) and P(Ort). Apologies are extended for the proliferation of F's and P's in this chapter. The author has attempted to make the labelling unambiguous, but that does not mean it is not confusing; the

plethora of processes which must be pondered calls for the inclusion of a collossal collection of fractions and probabilities.

Numbers for the factors on the right hand side of equation 4.2.2 can be found in the expressions 4.2.1.1, 4.2.2.1, 4.2.2.3 (a lower limit), 4.2.3.5, 4.2.4.3, and 4.2.5.6. They imply that

$$P(Apt) > (1.33 \pm 0.20) \times 10^{-11}(G/G_F)^2 \text{ and} \qquad 4.2.6.1a$$

$$P(Ort) > (1.70 \pm 0.27) \times 10^{-11}(G/G_F)^2 \ . \qquad 4.2.6.1b$$

Data from the two separate detectors may be combined by modifying equation 4.2.1 to

$$N_o(Apt) + N_o(Ort) = P(Apt) \bullet N(Apt) + P(Ort) \bullet N(Ort) \ . \qquad 4.2.6.2$$

The value of N differs for the two since dead times were not equal. For 2.32×10^{10} incident muons and live times of 0.82 and 0.92 respectively,

$$N(Apt) = 1.90 \times 10^{10} \text{ and} \qquad 4.2.6.3a$$

$$N(Ort) = 2.13 \times 10^{10} \ . \qquad 4.2.6.3b$$

The right hand side of 4.2.6.2 then gives

$$N_o(Apt) + N_o(Ort) > (0.61 \pm 0.09) \bullet (G/G_F)^2, \qquad 4.2.6.4$$

which expresses the minimum number of detectable events, in

terms of the coupling constant G for muonium conversion to antimuonium. It is straightforward to use equation 4.2.6.4 in conjunction with limits on N_o as derived in section 4.1 to determine an upper limit for G. This will be undertaken in the next chapter.

5. CONCLUSION

"Nature shows us only surfaces, but she is a thousand fathoms deep."

-Ralph Waldo Emerson

The fourth chapter described quantitatively the steps required for the observation of the calcium muonic X-ray signature of muonium conversion to antimuonium in the TRIUMF experiment. In this concluding chapter a limit for conversion will be extracted, representing a considerable improvement over previous limits. In addition, the results of the fourth chapter will be scrutinized in an attempt to evaluate present techniques and suggest improvements thereof.

5.1. The Limit on the Muonium-Antimuonium Coupling Constant

In section 4.1 it was shown that the number of X-ray events observed which could have resulted from muonium conversion is consistent with zero, and that the one standard deviation limit of the sum of events from both detectors is 463. It can thus be said that

$$N_o = N_o(\text{Apt}) + N_o(\text{Ort}) < 926 \quad (95\%\ \text{C.L.}), \qquad 5.1.1$$

where a 95% confidence limit for the usual assumption of gaussian statistics corresponds very closely to two standard deviations. From equation 4.2.6.4, then,

$$(G/G_F)^2 < 1.51 \times 10^3, \text{ or} \qquad 5.1.2$$

$$G/G_F < 38.8 \ . \qquad 5.1.3$$

The uncertainty of 15% in 4.2.6.4 is halved by taking the square root; including this, the final result of the experiment is

$$G < 42\ G_F \quad (95\%\ \text{C.L.}) \qquad 5.1.4$$

which, using the value of G_F, is about 6×10^{-48} erg•cm^3.

It is possible to define the limit in more meaningful experimental terms. A muon in a system initially formed as muonium, evolving in a field-free vacuum where conversion is most likely ($\Delta = 0$), will decay as antimuonium into a negative electron with branching ratio R, equal to the right hand side of equation 2.1.3.5 with the value of δ determined from G by equation 2.1.1.7. The stated limit for G implies a value for R of less than 0.04.

The experimental result is an improvement of more than one order of magnitude on the limit $G < 610G_F$ ($R < 0.47$) determined by a search for a final state consisting of two negative muons from the collision of energetic electrons (Barber et al., 1969). It also represents an improvement of over two orders of magnitude on the limit $G < 5800G_F$ ($R < 0.50$) set using an argon

gas target at one atmosphere (Amato et al., 1968); that experiment is the only other one which measures G by searching for muonium conversion.

It was mentioned in section 4.1 that in preparation for the TRIUMF experiment an argon gas target was installed for early checks of the apparatus and detection systems. The procedure and analysis were similar to the old muonium-antimuonium effort, utilizing gas at one atmosphere and room temperature, and searching for an argon muonic 2P-1S X-ray at 644 keV. In the old experiment, a muonium formation probability of unity was assumed, whereas a value of 0.63±0.07 (Mikula et al., 1979) is used here. An upper limit of 1066 counts (95% confidence limit) is obtained for a possible argon muonic photpeak in the data of Figure 4.1.3, which implies a limit of

$$G < 190\ G_F \quad (95\%\ \text{C.L.}), \qquad 5.1.5$$

or $R < 0.32$, independent of the silica result.

In the sense that the present powder target experiment allows a substantial improvement in the limit of the coupling constant, it was undoubtedly successful. To have impact on present questions about the real nature of leptonic electroweak interactions will require an improvement of a further two (at least) orders of magnitude, which may or may not be within the realm of present technology. In the opinion of the author, the limit must be reduced to less than $0.01\ G_F$ before it can be said that muonium conversion can provide an effective test of some unified theories.

5.2. Feasibility of an Improved Experiment

Certainly some factors determining the experimental sensitivity can be improved upon. It is the intent of this final section to point to the most promising methods for further reduction of the limit on G, within the framework of known procedures and available equipment.

When assessing the value of various improvements, it is helpful to understand the dependence of the limit on experimental parameters. In section 4.2.3 it was pointed out that increasing the amount of data, that is, the number of incident muons, lowers the limit only as the fourth root of the increase; the same is true for any experimental change which increases both the signal probability P and the background rate by similar factors. The use of more and/or higher efficiency germanium detectors (to increase E) without more extensive background suppression falls into the same category. An experimental change which increases P by some factor without changing the background rate will reduce the limit on G by the square root of the factor.

Taking optimistic improvements of factors of two in F(foils), one and a half in F(Mu), ten in F(gap), and three in $P(\overline{Mu})$, a reduction in the limit of G by a factor of ten might be possible. This is not sufficient in itself to allow a test of theory.

If the experiment is not restricted to detection of muonic X-rays, but uses instead fast electrons from the high energy

part of the Michel spectrum for negative muon decays to signal a conversion event, several things change:

1. $P(\overline{Mu})$ can increase one order of magnitude to $2.5 \times 10^{-5} (G/G_F)^2$ as shown by equation 2.1.3.5.

2. P(capt) does not enter into equation 4.2.2 for P.

3. The detection efficiency E could be increased substantially by large solid angle detection of the curvature of electrons in a magnetic field. It is difficult at this juncture to estimate background levels which would be encountered, but an increase in E by two or more orders of magnitude is not beyond reason. It is probable that, with the magnetic field required, $P(\overline{Mu})$ would decrease by one half in light of the explanations of section 2.1.4, but that should be more than offset by the gain in detection efficiency.

Taking only these gains into account, P might be improved by a factor of 10^3, and G might be limited to a value less than G_F. However, it is only speculation, and a greater increase in sensitivity could be the product of clever experimentation.

The technique crucial to the success of the present experiment, that of using thin layers of fine powder to produce a useful fraction of muonium in vacuum, is at least encouraging. There is ample room for development and refinement of the idea. Most importantly, for conversion experiments and also for some investigations of the atomic structure of muonium in vacuum, a reliable measurement of the probability of muonium escaping the silica layer plus an accurate estimate of the rate at which it is expelled are of high priority.

If sufficient sensitivity can be realized by any means

whatsoever, be they similar to those of this experiment or radically different, the conversion of muonium to antimuonium could provide a clue to the nature of the fundamental interactions.

A1. MUONIUM-ANTIMUONIUM CONVERSION VIA THE FOUR FERMION CURRENT-CURRENT INTERACTION

In this appendix a value for the muonium-antimuonium conversion matrix element will be calculated assuming a vector minus axial vector (V-A) current containing the muon (ψ_μ) and electron (ψ_e) fields. This lepton flavor changing neutral current, when coupled to itself, violates an additive muon number but preserves a multiplicative one (as defined in the first chapter). The Hamiltonian density takes the form (Feinberg and Weinberg, 1961b)

$$H(x) = 2^{-(1/2)}\, G\bullet[\,\bar{\psi}_\mu(x)O^\lambda\psi_e(x)\bar{\psi}_\mu(x)O_\lambda\psi_e(x) + \text{H.C.}\,]\,, \qquad \text{A1.1}$$

where G is the effective coupling constant, $O^\lambda = \gamma^\lambda(1 - \gamma^5)$ is the V-A form for the coupling, and H.C. stands for the Hermitian conjugate. G is to be compared to the Fermi coupling constant $G_F = 1.4 \times 10^{-49}$ erg•cm^3 ($1.03 \times 10^{-5}\, m_p^{-2}$, m_p being the proton mass). O^λ and the field operators $\psi(x)$ are defined to conform with the conventions and normalizations of Bjorken and Drell (1964) (except that $\hbar = c = 1$), and the representation of the Dirac matrices which will be used explicitly is:

$$\gamma^0 = \begin{bmatrix} I & 0 \\ 0 & -I \end{bmatrix} \qquad \{\gamma^i\} = \vec{\gamma} = \begin{bmatrix} 0 & \vec{\sigma} \\ -\vec{\sigma} & 0 \end{bmatrix}$$

$$\sigma^1 = \begin{bmatrix} 0 & 1 \\ 1 & 0 \end{bmatrix} \qquad \sigma^2 = \begin{bmatrix} 0 & -i \\ i & 0 \end{bmatrix} \qquad \sigma^3 = \begin{bmatrix} 1 & 0 \\ 0 & -1 \end{bmatrix}$$

$$\gamma^5 = i\gamma^0\gamma^1\gamma^2\gamma^3 = \gamma_5 = \begin{bmatrix} 0 & I \\ I & 0 \end{bmatrix} \qquad \text{A1.2}$$

Note also that $a \cdot b = a^\mu b_\mu = a^0 b_0 - \hat{a} \cdot \vec{b}$.

The field operators satisfying the Dirac equation are (for $\ell = \mu$ or e)

$$\Psi_\ell(x) = (2\pi)^{-(3/2)} \sum_{\pm r} \int d^3p \, (m_\ell/E)^{(1/2)} [b_\ell(p,r) u_\ell(p,r) \exp(-ip\cdot x) + d_\ell^\dagger(p,r) v_\ell(p,r) \exp(+ip\cdot x)] , \qquad \text{A1.3a}$$

$$\bar{\Psi}_\ell(x) = \Psi_\ell^\dagger(x)\gamma^0 = (2\pi)^{-(3/2)} \sum_{\pm r} \int d^3p \, (m_\ell/E)^{(1/2)} [b_\ell^\dagger(p,r) \bar{u}_\ell(p,r) \exp(+ip\cdot x) + d_\ell(p,r) \bar{v}_\ell(p,r) \exp(-ip\cdot x)] . \qquad \text{A1.3b}$$

Here, b_ℓ ($b_\ell^\dagger$) and d_ℓ ($d_\ell^\dagger$) are the usual anticommuting fermion and antifermion annihilation (creation) operators, respectively. The Dirac spinors are given by (see, for example, Commins, 1973; note that his normalization differs)

$$u_\ell(p,s) = \{(E + m_\ell)/2m_\ell\}^{(1/2)} \begin{bmatrix} \eta \\ \dfrac{\vec{\sigma}\cdot\vec{p}}{E + m_\ell}\,\eta \end{bmatrix} , \qquad \text{A1.4a}$$

$$v_\ell(p,s) = \{(E + m_\ell)/2m_\ell\}^{(1/2)} \begin{bmatrix} \dfrac{\vec{\sigma}\cdot\vec{p}}{E + m_\ell}\,\eta \\ \eta \end{bmatrix} , \qquad \text{A1.4b}$$

where η is a two component Pauli spinor satisfying

$$\vec{\sigma}\cdot\hat{s}\,\eta = \eta \quad \text{and} \quad \eta\eta^{+} = 1/2\,(I + \vec{\sigma}\cdot\hat{s}) . \qquad \text{A1.5}$$

Here $\hat{s}$ is the spin polarization unit vector in the rest frame of the particle. For $\hat{s} = (0,0,1)$, $\eta = \phi$ for $u(p,s)$ and χ for $v(p,s)$, where ϕ and χ are the basis vectors

$$\phi = \begin{bmatrix} 1 \\ 0 \end{bmatrix} , \quad \chi = \begin{bmatrix} 0 \\ 1 \end{bmatrix} . \qquad \text{A1.6}$$

For $\hat{s} = (0,0,-1)$, the roles of ϕ and χ are reversed. Making the non-relativistic approximation, the small components of the Dirac spinors can be ignored and E approaches m_ℓ in the normalization coefficients.

The goal is to evaluate the energy δ, defined by the expression

$$\delta/2 = \langle \overline{Mu}(\vec{p}'+\vec{q}',r',s') |\, H(x)\, | Mu(\vec{p}+\vec{q},r,s) \rangle , \qquad \text{A1.7}$$

where $|Mu(\vec{p}+\vec{q},r,s)>$ and $|\overline{Mu}(\vec{p}'+\vec{q}',r',s')>$ are particular spin states of the muon and electron in a 1S atomic state, with $\vec{p}$ ($\vec{p}'$) and $\vec{q}$ ($\vec{q}'$) the μ^+ (μ^-) and e^- (e^+) momenta respectively. The muonium and antimuonium states are constructed in occupation number space by weighting the occupation states with the 1S momentum wave function. For example,

$$|Mu(\vec{K},r,s)> = \int d^3k\, \psi(\vec{k})\, d^\dagger_\mu((m_\mu/M)\vec{K} + \vec{k},r) \bullet b^\dagger_e((m_e/M)\vec{K} - \vec{k},s)\, |0> , \qquad \text{Al.8}$$

where

$$\vec{K} = \vec{p} + \vec{q} , \quad \vec{k} = (m_e\vec{p} - m_\mu\vec{q})/M , \quad \text{and} \quad M = m_\mu + m_e . \qquad \text{Al.9}$$

Constructed in this way, the states are normalized to delta functions in $\vec{K}$, r, and s; the $\psi(\vec{k})$ are momentum space wave functions and should not be confused with the field operators in H(x).

Evaluating equation Al.7, using Al.1 with expansions such as Al.3 and Al.8, and applying the anticommutation relations for the creation and annihilation operators, it can be shown that

$$\delta/2 = (2\pi)^{-6}\iint d^3k\, d^3k'\psi^*(\vec{k}')\psi(\vec{k})\, \exp(-i(K-K')\bullet x) \bullet 2^{(1/2)}\, G \bullet B(r,s,r',s') , \qquad \text{Al.10}$$

where

$$B(r,s,r',s') = \bar{u}_\mu(p',r')O^\lambda v_e(q',s')\bar{v}_\mu(p,r)O_\lambda u_e(q,s)$$

$$- \bar{u}_{\mu}(p',r')O^{\lambda}u_{e}(q,s)\bar{v}_{\mu}(p,r)O_{\lambda}v_{e}(q',s') \ .$$

B can be evaluated using the explicit representation, by inserting values for r, s, r', and s'. The results can be succintly written as

$$B(r,s,r',s') = 4(-1)^{(r+s)/2}\delta_{r,r'}\delta_{s,s'} \ . \qquad \text{A1.11}$$

Then, at t = 0 in the rest frame of muonium ($\vec{K} = 0$),

$$\delta/2 = 2^{-(1/2)}G\bullet 8(-1)^{(r+s)/2}\delta_{r,r'}\delta_{s,s'} (2\pi)^{-3}\iint d^3k\ d^3k'\psi^{*}(\vec{k}')\psi(\vec{k}) \qquad \text{A1.12}$$

after integration over the total final momentum K. Expanding the final momentum space wave functions in terms of coordinate space wave functions $\psi(x)$ (again, not to be confused with the field operators)

$$\psi(\vec{k}) = \langle\vec{k}\,|\psi\rangle = \int d^3x\ \langle\vec{k}\,|\,\vec{x}\rangle\langle\vec{x}\,|\psi\rangle = (2\pi)^{-(3/2)}\int d^3x\ \exp(-i\vec{k}\bullet\vec{x})\,\psi(\vec{x}) \ , \qquad \text{A1.13}$$

and the expression for δ becomes

$$\delta/2 = 2^{-(1/2)}G\bullet 8(-1)^{(r+s)/2}\delta_{r,r'}\delta_{s,s'} \iint d^3x\ d^3x'\psi^{*}(\vec{x}')\psi(\vec{x})\delta(\vec{x}')\delta(\vec{x}) \ , \text{ or}$$

$$\delta/2 = 2^{-(1/2)}G\bullet 8(-1)^{(r+s)/2}\delta_{r,r'}\delta_{s,s'}\bullet(\pi a_0^3)^{-1} \qquad \text{A1.14}$$

for the 1S wave function, where a_0 is the Bohr radius. The delta functions denote the spin selection rules for transitions

between particular initial and final spin states. All quantities of interest contain δ^2, possibly averaged over initial values of r and s, so the sign factor can be disregarded. Inserting numerical values,

$$\delta = 2.1 \times 10^{-12} \, (G/G_F) \text{ eV}. \qquad \text{A1.15}$$

A2. MOTION OF MUONIUM ATOMS IN SPHERICAL SILICA PARTICLES

In this appendix expressions will be derived to predict the rate at which an ensemble of muonium atoms, formed in fine silica powder, can escape the powder particles and move in an interstitial vacuum. The starting point for the following calculations is an expression for the rate at which particles appear at an absorbing interface per unit area, per unit time (Chandrasekhar, 1943),

$$R(t) = -D(\hat{n} \bullet \vec{\nabla} W)_{W=0} \qquad \text{A2.1}$$

where $\hat{n}$ is a unit vector normal to the surface and

$$W(\vec{r})d\vec{r} = (4\pi Dt)^{-(3/2)}\exp(-|\vec{r}|^2/4Dt)\, d\vec{r} \qquad \text{A2.2}$$

is the probability per unit area of finding a particle between $\vec{r}$ and $\vec{r}+d\vec{r}$ after movement by random walk from $\vec{r} = 0$ at $t = 0$. The boundary condition $W = 0$ applies to equation A2.1 at an absorbing interface. The diffusion coefficient is defined here as

$$D = n\langle y^2\rangle/6 \qquad \text{A2.3a}$$

for a particle undergoing n independent displacements of mean square distance $\langle y^2\rangle$ per unit time. An equivalent definition in

terms of the mean speed c and the mean free path s is

$$D = cs/3 \ . \qquad \text{A2.3b}$$

The words "absorbing interface" indicate that a particle reaching that surface will pass through it with zero probability of re-entry, presupposing a mechanism like a work function inhibiting the possibility.

Consider a sphere of radius a, whose surface is the absorbing interface, and find $R(t;\vec{x})$ for a particle starting its random motion at $\vec{x}$ at t = 0 (see Figure A2.1). Then W = 0 when

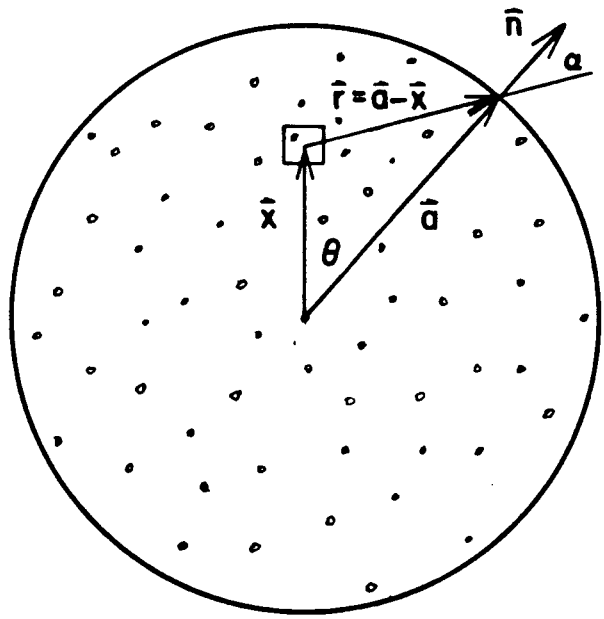

Figure A2.1. Geometry for muonium emission from a sphere.

$\vec{r} = \vec{a}-\vec{x}$, and

$$R(t;\vec{x}) = (\eta Dt)^{-(3/2)}/16t \int ds(\vec{a})\ \hat{n}(\vec{a})\bullet(\vec{a} - \vec{x}) \bullet\exp(-|\vec{a} - \vec{x}|^2/4Dt) \ . \qquad \text{A2.4}$$

The surface integration can be performed by noting that

$$\begin{aligned} ds(\vec{a}) &= a^2 \sin\theta \, d\theta \, d\phi \ , \\ |\vec{a} - \vec{x}|^2 &= a^2 + x^2 - 2ax\cos\theta \ , \text{ and} \\ \hat{n}(\vec{a})\bullet(\vec{a} - \vec{x}) &= |\vec{a} - \vec{x}| \cos\alpha = a - x\cos\theta \ . \end{aligned} \qquad \text{A2.5}$$

Carrying out the surface integration yields

$$\begin{aligned} R(t;\vec{x}) = (\eta/2)\ a^2 D(\eta Dt)^{-(3/2)} &\exp(-(a^2+x^2)/4Dt) \\ \bullet[x^{-1}(1 + 2Dt/a^2)&\sinh(ax/2Dt) \\ - a^{-1}&\cosh(ax/2Dt)] \ . \end{aligned} \qquad \text{A2.6}$$

Now assume that the particle ensemble is initially distributed uniformly throughout the sphere with a constant density of $1/V = 3/4\eta a^3$, in order to preserve the probabilistic normalization of equation A2.2. Then, integrating over the volume of the sphere,

$$R(t) = 3a^{-3}\int_0^a dx\ x^2 R(t;\vec{x}) \ , \qquad \text{A2.7}$$

which is the rate at which particles appear at the surface of the sphere, given a uniform distribution at t = 0. This may be evaluated using the exponential form for the hyperbolic functions, although the procedure becomes quite tedious. The substitution $z = -(x\pm a)/2(Dt)^{(1/2)}$ in integrations involving $\exp(\pm ax/2Dt)$, along with the knowledge that

$$\int_{-a}^{o} dx\ x^n \exp(-x^2) = (-1)^n \int_{o}^{a} dx\ x^n \exp(-x^2)\ ,$$

leads to an integrand in A2.7 proportional to $\exp(-z^2)$ times terms constant, linear, and quadratic in z. Fortunately, the coefficient of the constant term vanishes for all t. The quadratic term may be integrated by parts, giving a further linear term in the integrand plus a contribution proportional to $t^{(1/2)}\exp(-a^2/Dt)$. The linear term can then be evaluated, and the result obtained is

$$R(t) = (\pi)^{-(1/2)}\ (3/2t)(Dt/a^2)^{(1/2)} \left[1 - 2(Dt/a^2) + (1+2(Dt/a^2))\exp(-a^2/Dt)\right] . \qquad \text{A2.8}$$

As time approaches zero, R(t) grows as $t^{-1/2}$, which is a result of the non-zero particle density at the surface of the sphere at t = 0 and the assumption of a perfectly absorbing interface. As t grows without limit, R(t) behaves as $t^{-5/2}$.

It is now possible to calculate the probability that a particle has passed through the surface by time t (assuming that it will not decay). Evaluating

$$P(t) = \int_{o}^{t} dt'\ R(t') \qquad \text{A2.9}$$

gives the desired result:

$$P(t) = 1 - \mathrm{erf}[(Dt/a^2)^{-(1/2)}] - (\pi)^{-(1/2)}(Dt/a^2)^{(1/2)} \bullet \bullet \left[3 - 2Dt/a^2 - (1-2Dt/a^2)\exp(-(Dt/a^2)^{-1})\right] . \qquad \text{A2.10}$$

The error function erf(x) has the usual definition:

$$\mathrm{erf}(x) = 2(\pi)^{-(1/2)} \int_0^x dt\ \exp(-t^2) \ . \qquad \text{A2.11}$$

Another useful result includes the decay of a particle of mean lifetime λ^{-1}, so that the probability of it passing through the surface before decaying is (see also Brandt and Paulin, 1968; note that their formula contains a typographical error)

$$\begin{aligned} P &= \int_0^\infty dt\ R(t)\ \exp(-\lambda t) \\ &= (3/2)\ [1 - \beta^2 + (1 + \beta)^2 \exp(-2/\beta)] \ , \end{aligned} \qquad \text{A2.12}$$

where $\beta = (D/\lambda a^2)^{1/2}$.

Formula A2.10 has been used in the analysis of a muonium spin rotation experiment in a silica powder sample (Marshall et al., 1978). The silica particles, whose radii could be independently inferred, were surrounded with oxygen at various concentrations. The muonium polarization was relaxed by spin exchange at a rate which depended on the concentration (Fleming et al., 1980).

When this rate was high compared to the rate at which muonium appeared at the surface of the silica particles, the time dependence of the muonium polarization was assumed to have the form

$$A(t) = A(0)\ (1 - P(t)) \ . \qquad \text{A2.13}$$

In other words, the relaxation process was controlled by the rate at which the muonium atoms could get to the voids between

particles, where the polarization was then destroyed in a comparatively short time. That the data supported the model proved the likelihood that muonium was reaching the voids between silica particles before decay.

A further result of the experiment was the close similarity of the dependence of the relaxation rate on the oxygen concentration, given by the rate constant k, to that in a target consisting of oxygen in an argon gas moderator (with no silica present). In the low concentration regime, where the relaxation rate was determined by the oxygen concentration rather than the motion of muonium inside the silica spheres, a rate constant $k = (2.55 \pm 0.13) \times 10^{-10}$ $cm^3 \bullet mol^{-1} \bullet s^{-1}$ was measured, in agreement with $k = (2.52 \pm 0.18) \times 10^{-10}$ $cm^3 \bullet mol^{-1} \bullet s^{-1}$ from an argon-oxygen target at one atmosphere. For spin exchange, the rate constant can be written as $k = \sigma\langle v \rangle$, where σ is a geometrical cross section and $\langle v \rangle$ is the mean relative speed. Since the mean thermal velocity of muonium is 16.8 times that of oxygen, this equality of rate constants strongly supports the hypothesis that muonium is moving thermally within the voids, rather than attaching itself at or near the powder surface and depolarizing there.

The diffusion parameter obtained for muonium in the silica powder particles, assuming the validity of the foregoing model, was

$$D = (2.2 \pm 0.4) \times 10^{-7} \ cm^2 \bullet s^{-1} \ . \qquad \text{A2.14}$$

It must be stressed that this may not be applicable to silica in general, nor even to powders with differing particle sizes.

There are several points which must be considered:

1. There may exist fissures in the particles through which muonium could escape more quickly than by diffusion.

2. The radius assumed in the calculations is derived from measurements of the specific surface area, and may not be uniform.

3. The temperature of the grain in which muonium is moving may have been sharply elevated by the energy of the incident muon deposited there during the slowing process (Kiefl et al., 1981). Because of the model dependent nature of the analysis, the value extracted for the diffusion parameter D, which is certainly a function of temperature, would likely depend on the size of the grain.

Scanning electron micrographs do show the approximate sphericity of the particles, and a reasonably uniform size distribution consistent with the radius assumed (Cabot Corporation, unpublished technical report). The micrographs also show the tendency of the particles to form chain-like aggregates, which mechanically entangle to form agglomerates. While this has little consequence for the motion of muonium within the particles, it could play a part in the thermal motion after muonium reaches the voids, the subject of appendix A3.

A3. MOTION OF MUONIUM ATOMS IN FINE POWDER LAYERS

The purpose of this appendix is to estimate the rate at which an ensemble of thermal muonium atoms may escape a thin powder layer. The procedure is essentially identical to that of the previous appendix, with only the geometry and the parameter D requiring modification.

Consider a homogenous layer of thickness d, bounded on both sides by an absorbing surface, as in Figure A3.1. Equations

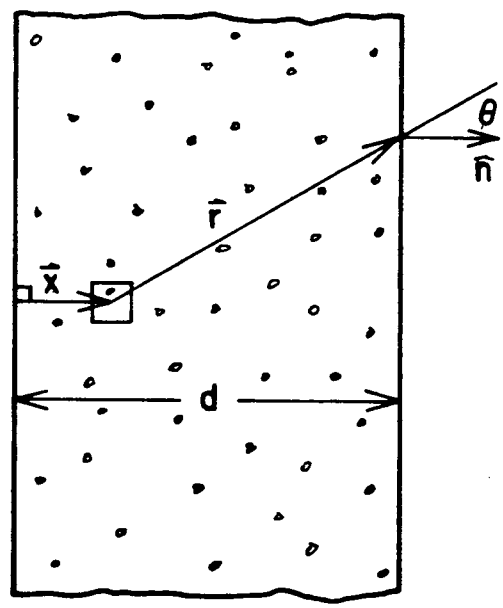

Figure A3.1. Geometry for muonium emission from a layer.

A2.1 and A2.2 apply, and the expression for $R(t;\vec{x})$ becomes,

after integration over the surfaces (assumed infinite in area),

$$R(t;\vec{x}) = (2t)^{-1}(4\pi Dt)^{-(1/2)}[x\bullet\exp(-x^2/4Dt) + (d-x)\bullet\exp(-(d-x)^2/4Dt)] \ . \qquad \text{A3.1}$$

For an incident particle distribution of 1/d per unit thickness at t = 0, the rate of emission can be integrated over x to give the effective rate from the entire volume:

$$R(t) = \int dx\ d^{-1}R(t;\vec{x}) = (4\pi Dt)^{-(1/2)}\ d^{-1}D\ [1 - \exp(-d^2/4Dt)] \ . \qquad \text{A3.2}$$

The chosen normalization permits the calculation of the probability that a particle, decaying at a rate of λ s^{-1}, will reach one particular surface of the layer:

$$P = (1/2)\int_0^\infty dt\ \exp(-\lambda t)R(t) = (1/2)(\lambda d^2/D)^{-(1/2)}\ [1 - \exp(-(\lambda d^2/D)^{1/2})] \ , \qquad \text{A3.3}$$

where the factor of 1/2 comes from the neglect of the second surface.

In order to estimate this value numerically, some reasonable assumptions must be made for the value of D. Using the expression A2.3b, and the formula (Kittel, 1969) for the mean free path s of a point particle (a muonium atom) moving freely in a uniform random collection of n cm^{-3} stationary spheres (silica particles) of radius r,

$$s = (\pi r^2 n)^{-1} \ , \qquad \text{A3.4}$$

it is found that

$$D = c(3\pi r^2 n)^{-1} \quad . \qquad \text{A3.5}$$

The average number density n can be written in terms of the density of silicon dioxide, ρ, and the density of the silica powder used in the layer, ρ', as

$$n = 3\rho'/4\pi r^3\rho \quad , \qquad \text{A3.6}$$

so that

$$D = (4cr/9)(\rho/\rho') \quad . \qquad \text{A3.7}$$

The mean thermal velocity c is 7.37×10^5 cm•s^{-1} for muonium at room temperature. The density of silica powder used in the experiment was $\rho' = 0.032$ g•cm^{-3}, whereas for bulk silica it is $\rho = 2.2$ g•cm^{-3}. A particle radius of 3.5×10^{-7} cm then leads to an estimate of

$$D = 7.9 \text{ cm}^2\text{•s}^{-1} \quad , \qquad \text{A3.8}$$

which is more than seven orders of magnitude greater than the constant of A2.14 for muonium inside a silica particle.

The agglomeration of chain-like aggregates of the powder spheres make the assumption of uniformity of the layer a little tenuous. Without that assumption, a calculation using the approach which has been taken becomes much more formidable, and at some point must rely on a detailed knowledge of the powder

structure. It is important to realize, though, that unless the agglomeration were to result in very dense regions of the layer extending for distances comparable in magnitude to its thickness, the effect is to increase the rate at which muonium is emitted. The reason for this statement is that the probability for escape from a small agglomerate (of typical dimension $<< (D/\lambda)^{(1/2)}$ with D the appropriate diffusion parameter) is close to one; after leaving that agglomerate, the mean square distance between collisions is much longer than in a uniform layer, and the probability of reaching the surface is correspondingly higher. In that case, the numbers derived from the methods used here will be valid as a lower limit, and as such are good enough for the purposes of the fourth chapter. The expressions are used in section 4.2.2 to find the probability of escape of a muonium atom from one surface of a silica powder layer.

BIBLIOGRAPHY

Amato, J.J., P. Crane, V.W. Hughes, J.E. Rothberg, and P.A. Thompson, 1968, Phys. Rev. Lett. 21, 1709.

Arnold, K.-P., P.O. Egan, M. Gladisch, W. Jacobs, H. Orth, J. Vetter, and P. Zimmerman, 1979b, in SIN Newsletter No. 12, ed. G.H. Eaton, 4.

Arnold, K.P., P.O. Egan, M. Gladisch, D. Herlach, V.W. Hughes, W. Jacobs, H. Metz, H. Orth, G. zu Pulitz, J. Vetter, W. Wahl, and M. Wigand, 1979a, in SIN Newsletter No. 11, ed. G.H. Eaton, 48.

Bailin, D., 1977, Weak Interactions, Sussex University Press.

Barber, W.C., B. Gittelman, D.C. Cheng, and G.K. O'Neill, 1969, Phys. Rev. Lett. 22, 902.

Barish, S.J., Y. Cho, M. Derrick, L.G. Hyman, J. Rest, P. Schreiner, R. Singer, R.P. Smith, H. Yuta, D. Koetke, V.E. Barues, D.D. Carmony, and A.F. Garfinkel, 1974, Phys. Rev. Lett. 33, 448.

Barnett, B.A., C.Y. Chang, G.B. Yodh, J.B. Carroll, M. Eckhause, C.S. Hsieh, J.R. Kane, and C.B. Spence, 1975, Phys. Rev. A 11, 39.

Barnett, B.A., C.Y. Chang, P. Steinberg, G.B. Yodh, H.D. Orr, J.B. Carroll, M. Eckhause, J.R. Kane, C.B. Spence, and C.S. Hsieh, 1977, Phys. Rev. A 15, 2246.

Beer, W., P.R. Bolton, P.O. Egan, V.W. Hughes, D.C. Lu, F.G. Mariam, P.A. Souder, J. Vetter, M. Gladisch, G. zu Pulitz, U. Moser, L.J. Teig, R.H. Holmes, P.H. Steinberg, J.R. Kane, and R. Hartmann, 1979, abstract submitted to 8th Int. Conf. on High Energy Physics and Nuclear Structure, Vancouver, Canada.

Bernstein, J., 1974, Rev. Mod. Phys. 46, 7.

Bertin, A., F. Ferrari, I. Massa, M. Piccinini, G. Vannini, and A. Vitale, 1978, Phys. Lett. 68A, 201.

Bjorken, J.D., and S. Weinberg, 1977, Phys. Rev. Lett. 38, 622.

Bjorken, J.D., and S.D. Drell, 1964, Relativistic Quantum Mechanics, Mcgraw-Hill.

Bouchiat, C., 1977, Proc. 7th Int. Conf. on High Energy Physics and Nuclear Structure, Exper. Suppl. 31, 353.

Bowen, T., K.R. Kendall, K.J. Nield, and A.E. Pifer, unpublished, University of Arizona Internal Report.

Brandt, W., and R. Paulin, 1968, Phys. Rev. Lett. 21, 193.

Brewer, J.H., K.M. Crowe, F.N. Gygax, and A. Schenck, 1975, Muon Physics, Vol. III, eds. C.S. Wu and V.W. Hughes, Academic Press, New York, Chapter 7.

Bunting, R.L., and J.J Kraushaar, 1974, Nucl. Instr. and Meth. 118, 565.

Cabibbo, N., and R. Gatto, 1960, Phys. Rev. Lett. 5, 114.

Cabot Corporation, technical report, Cab-O-Sil Properties and Functions, available from Cabot Corporation, 125 High Street, Boston, MA 02110, USA.

Chandrasekhar, S., 1943, Rev. Mod. Phys. 15, 1.

Cheng, T.-P., and L.-F. Li, 1977, Phys. Rev. D 16, 1425.

Clark, G.S., unpublished, PHARUN: A Program for Transferring PHA Data.

Commins, E.D., 1973, Weak Interactions, McGraw-Hill.

Crawford, J.F., M. Daum, G.H. Eaton, R. Frosch, H. Hirschmann, R. Horisberger, J.W. McCulloch, E. Steiner, R. Hausammann, R. Hess, and D. Werren, 1980, Phys. Rev. C 22, 1184.

Danby, G., J.M. Gaillaird, K. Goulianos, L.M. Lederman, N. Mistry, M. Schwartz, and J. Steinberger, 1962, Phys. Rev. Lett. 9, 36.

Daniel, H., 1979, Z. Phys. A 291, 29.

Daum, M., G.H. Eaton, R. Frosch, H. Hirschmann, J.M. McCulloch, R.C. Minehart, and E. Steiner, 1979, Phys. Rev. D 20, 2692.

Derman, E., 1978, Phys. Lett. 78B, 497.

Derman, E., 1979, Phys. Rev. D 19, 317; see also Derman, E., and H.-S. Tsao, 1979, Phys. Rev. D 20, 1207.

Eichten, T., H. Deden, F.J. Hasert, W. Krenz, J. Von Krogh, D. Lanske, J. Morfin, H. Weerts, G.H. Bertrand-Coremans, J. Sacton, W. Van Doninck, P. Vilain, D.C. Cundy, D. Haidt, M. Jaffre, G. Kalbfleisch, S. Natali, P. Musset, J.B.M. Pattison, D.H. Perkins, A. Pullia, A. Rousset, W. Venus, H.W. Wachsmuth, V. Brisson, B. Degrange, M. Haguenauer, L. Kluberg, U. Nguyen-Khac, P. Petiau, E. Bellotti, S. Bonetti, D. Cavalli, C. Conta, E. Fiorini, C. Franzinetti, M. Rollier, B. Aubert, L.M. Chounet, P. Heusse, A.M. Lutz, J.P. Vialle, F.W. Bullock, M.J. Esten, T.W. Jones, J. McKenzie, G. Myatt, and J.L. Pinfold, 1973, Phys. Lett. 46B, 281.

Engfer, R., H. Schneuwly, J.L. Vuilleumier, H.K. Walter, and

A. Zehnder, 1974, Atomic Data and Nuclear Data Tables 14, 509.

Feinberg, G., and S. Weinberg, 1961a, Phys. Rev. Lett. 6, 381.

Feinberg, G., and S. Weinberg, 1961b, Phys. Rev. 123, 1439.

Fermi, E., 1934, Z. Phys. 88, 161.

Fleming, D.G., R.J. Mikula, and D.M. Garner, 1980, J. Chem. Phys. 73, 2751.

Gamow, G., and E. Teller, 1936, Phys. Rev. 49, 895.

Garner, D.M., 1979, Ph.D Thesis, University of British Columbia, unpublished.

Garrett, M.W., 1967, J. Appl. Phys. 38, 2563.

Glashow, S.L., J. Iliopoulos, and L. Maiani, 1970, Phys. Rev. D 2, 1285.

Hasert, F.J., H. Faissner, W. Krenz, J. Von Krogh, D. Lanske, J. Morfin, K. Schultze, H. Weerts, G.H. Bertrand-Coremans, J. Lemonne, J. Sacton, W. Van Doninck, P. Vilain, C. Baltay, D.C. Cundy, D. Haidt, M. Jaffre, P. Musset, A. Pullia, S. Natali, J.B.M. Pattison, D.H. Perkins, A. Rousset, W. Venus, H.W. Wachsmuth, V. Brisson, B. Degrange, M. Haguenauer, L. Kluberg, U. Nguyen-Khac, P. Petiau, E. Bellotti, S. Bonetti, D. Cavalli, C. Conta, E. Fiorini, M. Rollier, B. Aubert, L.M. Chounet, P. Heusse, A. Lagarrigue, A.M. Lutz, J.P. Vialle, F.W. Bullock, M.J. Esten, T. Jones, J. McKenzie, A.G. Michette, G. Myatt, J. Pinfold, and W.D. Scott, 1973, Phys. Lett. 46B, 121.

Higgs, P.W., 1964, Phys. Lett. 12, 132 and Phys. Rev. Lett. 13, 508.

Hofer, H., K. Borer, P. Jenni, P. Le Coultre, P.G. Seiler, and P. Wolff, 1972, CERN Proposal PHIII-72/20, unpublished.

Hughes, V.W., Proc. Erice School on Exotic Atoms, 1979, eds. G. Fiorentini and G. Torelli, Plenum Press.

James, F., and M. Roos, 1971, MINUIT, Cern Computer Program Library Documentation, unpublished.

Kendall, K.R., 1972, Ph.D. Thesis, University of Arizona.

Kibble, T.W.B., 1967, Phys. Rev. 155, 1554.

Kiefl, R.F., J.B. Warren, G.M. Marshall, C.J. Oram, J.H. Brewer, D.J. Judd, and L.D. Spires, 1979, Hyperfine Interactions 6, 185.

Kiefl, R.F., 1981, Proc. 2nd Int. Topical Conference on Muon

Spin Rotation, to be published in Hyperfine Interactions.

Kittel, C., 1969, Thermal Physics, J. Wiley and Sons.

Konopinski, E.J., and H.M. Mahmoud, 1953, Phys. Rev. 92, 1045.

Mann, A., and H. Primakoff, 1977, Phys. Rev. D 15, 655.

Margenau, H., 1939, Rev. Mod. Phys. 11, 1.

Marion, J.B., 1968, Nuclear Data A4, 301.

Marshall, G.M., J.B. Warren, D.M. Garner, G.S. Clark, J.H. Brewer, and D.G. Fleming, 1978, Phys. Lett. 65A, 351; see also Marshall, G.M., 1977, M.Sc. Thesis, University of British Columbia, unpublished.

Mikula, R.J., D.M. Garner, D.G. Fleming, G.M. Marshall, and J.H. Brewer, 1979, Hyperfine Interactions 6, 379.

Morgan, D.L., 1967, Ph.D. Thesis, Yale University.

Nishijima, K., 1957, Phys. Rev. 108, 907.

Oram, C.J., J.B. Warren, G.M. Marshall, J. Doornbos, and D. Ottewell, 1980, TRIUMF Report TRI-80-1. See also Oram, C.J., J.B. Warren, G.M. Marshall, And J. Doornbos, 1981, Nucl. Instr. and Meth. 179, 95.

Particle Data Group, 1976, Review of Particle Properties, Rev. Mod. Phys. 48, S1.

Perl, M.L., G.S. Abrams, A.M. Boyarski, M. Breidenbach, D.D. Briggs, F. Bulos, W. Chinowsky, J.T. Dakin, G.J. Feldman, C.E. Friedberg, D. Fryberger, G. Goldhaber, G. Hanson, F.B. Heile, B. Jean-Marie, J.A. Kadyk, R.R. Larsen, A.M. Litke, D. Liike, B.A. Lulu, V. Lueth, D. Lyon, C.C. Morehouse, J.M. Paterson, F.M. Pierre, T.P. Pun, P.A. Rapidis, B. Richter, B. Sadoulet, R.F. Schwitters, W. Tanenbaum, G.H. Trilling, F. Vanucci, J.S. Whitaker, F.C. Winkelman, and J.E. Wiss, 1975, Phys. Rev. Lett. 35, 1489.

Perl, M.L., 1978, Nature 275, 273.

Pifer, A.E., T. Bowen, and K.R. Kendall, 1976, Nucl. Instr. and Meth. 135, 39.

Pontecorvo, B., 1958, Zhur. Eksp. i Teoret. Fiz. 33, 549 (1957); see Sov. Phys. JETP 6(33), 429 (1958) for translation.

Reines, F., H.W. Sobel, and E. Pasierb, 1980, Phys. Rev. Lett. 45, 1307.

Reist, H.-W., D.E. Casperson, A.B. Denison, P.O. Egan, V.W. Hughes, F.G. Mariam, G. Zu Pulitz, P.A. Souder, P.A. Thompson, and J. Vetter, 1978, Nucl. Instr. and Meth. 153,

61.

Salam, A., 1968, "Elementary Particle Physics", ed. by N. Svartholm, Almqvist and Wiksells, Stockholm, p. 367.

Schneuwly, H., 1979, Proc. Erice School on Exotic Atoms, eds. G. Fiorentini and G. Torelli, Plenum Press.

Schwinger, J., 1957, Ann. Phys. 2, 407.

Tawara, H., and A. Russek, 1973, Rev. Mod. Phys. 45, 178.

Taylor, J.C., 1976, Gauge Theories of Weak Interactions, Cambridge University Press.

Trower, W.P., 1966, Range-Energy and dE/dx Plots of Charged Particles in Matter, UCRL-2426, Vol. II.

Weinberg, S., 1967, Phys. Rev. Lett. 19, 1264.

Weinberg, S., 1972, Phys. Rev. D 5, 1962.

Weinberg, S., 1974, Rev. Mod. Phys. 46, 255.

Weinberg, S., 1977, Proc. 7th Int. Conf. on High Energy Physics and Nuclear Structure, Exper. Suppl. 31, 339.

Willis, S.E., V.W. Hughes, P. Nemethy, R.L. Burman, D.R.F. Cochran, J.S. Frank, R.P. Redwine, J. Duclos, H. Kaspar, C.K. Hargrove, and U. Moser, 1980, Phys. Rev. Lett. 44, 522. Errata, 1980, Phys. Rev. Lett. 45, 1370.

Wu, C.S., E. Ambler, R.W. Hayward, D.D. Hoppes, and R.P. Hudson, 1957, Phys. Rev. 105, 1413.

Yang, C.N., and R.L. Mills, 1954, Phys. Rev. 96, 191.